# UNIVERSITÉ DU QUÉBEC

THÈSE PRÉSENTÉE À

L'UNIVERSITÉ DU QUÉBEC À CHICOUTIMI

COMME EXIGENCE PARTIELLE

DU DOCTORAT EN INGÉNIERIE

par

## AZAM NEKAHI

ÉTUDE SPECTROSCOPIQUE DE L'ARC À LA

SURFACE DE LA GLACE

SPECTROSCOPIC INVESTIGATION OF ARC OVER

AN ICE SURFACE

Septembre 2011

# ABSTRACT

Ice accumulation on insulators of overhead transmission lines and substations has been recognized as a major problem which may cause insulator flashover and power outages. This phenomenon starts with corona discharge activity and continues with the formation of partial arcs which may result in flashover. Due to the complexity of the process, resulting from surface interaction of discharge with the water film on the ice surface, is not yet fully understood. As for any other type of discharge, the knowledge of some parameters such as temperature and concentration of different species is necessary in order to describe the mechanisms involved. Moreover, to develop mathematical models for discharge propagation, an estimation of discharge channel conductivity is necessary. The current flows through this conductive channel and supplies the energy needed to sustain the ionization activity inside the channel. The conductivity of discharge channel is directly related to its temperature, which illustrates the need for discharge temperature measurements. Up to now, for an arc over an ice surface the temperature has been assumed to have a constant value of 5,000 K, but without any experimental support. The existence of Local Thermodynamic Equilibrium (LTE) is another important aspect for proposing theories and models, but this has not yet been verified for flashover on ice-covered insulators. The verification of LTE condition requires information about temperature and concentration of different species, electron density and ionization level.

The objective of this research is to augment our knowledge of flashover on ice-covered insulators by measuring and calculating several important discharge column parameters. Measurement of rotational and excitation temperatures, and electron density during arc propagation are the first steps. The effect of discharge current, voltage type

and polarity on the variation of the mentioned arc parameters should be also studied. Based on these data, the LTE condition could be examined.

Spectroscopic plasma diagnostic is a non-destructive test method used to achieve the stated objectives. The emitted light from an arc over an ice surface was transmitted to a spectrometer. The time-resolved recorded spectra of arc were used to study the nature and concentration of ionized species. The gas and electron temperatures and electron densities were also measured using Boltzmann and Stark broadening methods.

Measured rotational temperatures were found to vary from 4,000 K to 6,500 K, while the current increased from 200 mA to 700 mA during the discharge propagation. It was observed that under similar experimental conditions, the arc current intensity of DC+ arcs were hotter than that of DC-. Moreover, arc temperatures under AC voltage were lower than those of DC+, and close to that of DC-. The excitation temperature was measured at about 9,000 K and does not vary significantly with discharge current. As current increases, electron densities increased as well. For currents ranging from 200 mA to 700 mA, electron densities increased from 1 to 2 $\times 10^{17}$ cm$^{-3}$. Electron densities increased up to $2.5 \times 10^{17}$ cm$^{-3}$ at the later stages of arc development, when flashover occurs. Differences between the rotational and excitation temperatures showed that the arc was not in a state of thermal equilibrium.

# RÉSUMÉ

L'accumulation de glace sur les isolateurs de lignes de transport d'énergie électrique et de leurs postes est reconnue comme un problème majeur qui peut causer le contournement des isolateurs et dans certaines conditions l'interruption de courant. Ce phénomène commence par des activités de décharge de couronne, s'ensuit la formation d'arcs partiels qui peut se développer en arcs de contournement. Dû à la complexité de ce processus, qui résulte de l'interaction des décharges avec le film d'eau formé à la surface de la glace, le phénomène de contournement n'est pas encore entièrement compris. Pour une meilleure connaissance des mécanismes en jeu dans l'arc de contournement et d'autres types de décharge le précédant, il sera nécessaire de développer certaines connaissances concernant des paramètres comme la température et la concentration d'autres espèces d'ions. De plus, afin de développer des modèles mathématiques pour la propagation de décharges, une estimation de la conductivité de canal de décharge est nécessaire. Le courant circulant dans ce canal conducteur fournit l'énergie nécessaire aux activités d'ionisation à l'intérieur de ce canal. La conductivité de ce dernier est une fonction directe de sa température, ce qui illustre le besoin de mesurer la température de ces décharges. Jusqu'à présent, pour un arc apparaissant le long d'une surface de glace, on a arbitrairement donné à cette température a une valeur de 5000 K, mais sans preuve expérimentale. L'existence d'équilibre thermodynamique local (ETL) est un autre aspect important pour proposer des théories et des modèles, mais ceci n'a pas été vérifié pour l'arc de contournement sur les isolateurs recouverts de glace. La vérification de condition d'ETL exige des informations sur la température et la concentration de diverses espèces ioniques, ainsi que sur la densité d'électron et sur le degré d'ionisation.

L'objectif principal de cette recherche est d'approfondir nos connaissances du contournement des isolateurs recouverts de glace en mesurant et en calculant plusieurs paramètres importants dans le canal de décharge. La mesure des températures rotationnelles et d'excitation, et de la densité d'électrons pendant la propagation d'arc est préalablement nécessaire. De plus, l'effet du courant de décharge, du type de tension et de sa polarité sur la variation des paramètres d'arc ci-haut mentionnés devrait être étudié. Sur les bases de ces données, la condition d'ETL pourrait être examinée.

Le diagnostic spectroscopique de plasma est une méthode de test non destructive qui a été utilisée pour atteindre les objectifs mentionnés. La lumière émise d'un arc sur une surface de glace a été transmise à un spectromètre. Les spectres obtenus ont été utilisés pour étudier la nature et la concentration d'espèces d'ions. Les températures du gaz et des électrons, ainsi que leur densité, ont été également mesurées à l'aide de méthodes appropriées.

Les températures rotationnelles mesurées se situaient entre 4000 et 6500 K, alors que l'intensité de courant a augmenté de 200 à 700 mA pendant la propagation des décharges. Il a été observé que dans les mêmes conditions expérimentales, les températures des arcs en courant continu positif étaient plus élevée que celle des arcs en courant continu négatif. De plus, les températures d'arc en courant alternatif étaient plus faible que celles en courant continu positif et prohes de celles en courant continu négatif. La température d'excitation mesurée se situait à environ 9000 K et ne variait pas significativement en fonction du courant de décharge. La densité d'électron augmentait avec l'augmentation du courant. Pour les courants variant de 200 à 700 mA, les densités d'électron ont augmenté de 1 à 2 $\times 10^{17}$ cm$^{-3}$. Les densités d'électron étaient supérieures à $2.5 \times 10^{17}$ cm$^{-3}$ avant l'apparition de l'arc de contournement. Les différences entre les

températures rotationnelles et d'excitation ont montré que l'arc n'était pas dans un état d'équilibre thermique.

# ACKNOWLEDGMENTS

I would like to express my gratitude to my supervisor, Professor Masoud Farzaneh, whose expertise, understanding, and patience, added considerably to my graduate experience. I appreciate his vast knowledge and skill in many areas.

Many thanks go in particular to Dr. W.A. Chisholm for his valuable advice and discussion.

I would like to extend my thanks to Marc André Perron, Xavier Bouchard, Pierre Camirand, and Claude D'Amours at CIGELE Laboratory for their technical support and to Denis Masson and Désirée Lezou for their help with administrative tasks.

I am very grateful to Jean Talbot for his precious efforts and editorial help for making this thesis legible.

Most importantly, I would like to thank all my friends who helped me get through the years of my study.

This thesis is dedicated to my parents, who taught me the value of education. to my mother so far away who has inspired me profoundly. To my father who has constantly encouraged me to reach my dreams. I am deeply indebted to them for their continued support and unwavering faith in me.

I am grateful to my husband, Shahab for his constant love and strength throughout the years. Without him, and his ability to raise my spirits when I was most discouraged, I could never made it this far. Above all and the most needed, he provided me encouragement and support in various ways. Shahab, you were the wind beneath my

wing and of course to my little Najin, who was like a star guiding me through the nights during my intense work.

# TABLE OF CONTENTS

# LIST OF FIGURES

# LIST OF TABLES

14

# CHAPTER 1

# INTRODUCTION

# CHAPTER 1

# INTRODUCTION

## 1.1 Overview

In cold climate regions, ice accretion on outdoor insulators may cause a drastic reduction of their electrical insulation strength, sometimes resulting in flashovers and power outages [1]. Incidents caused by flashover on ice-covered insulators have been reported by various authors from different countries [2- 4].

The electric field along an insulator is non-uniform. In the high stress areas of the insulator, partial discharges and arcs can lead to ice shedding. This will cause some part of the insulator string to become ice free; these ice-free zones are referred to as air gaps. The formation of a water film on the ice surface is the first step of this process. This film can be formed by a rise in ambient temperature, sunshine, condensation, the heating effect of electrical discharge, or leakage current. Because of the high conductivity of the water film, leakage resistance is decreased and voltage drops are observed across the air gaps. The high electric field will initiate corona discharges, leading to the development of local arcs at this area. This will cause an increase in leakage current and consequent ice melting. If the leakage current continues to increase over a short period, a white arc will appear, which will accelerate ice melting and cause further increase in leakage current.

When the length of arc reaches about 60% of inter-electrode distance, the speed of arc propagation will increase rapidly, leading to flashover of the whole insulator string [2].

Considerable efforts have been made to develop dynamic and static mathematical models for studying the propagation of the arc over an ice surface [5, 6] and predicting the critical flashover voltage of ice- or snow-covered insulators.

The formation of a flashover arc on an ice surface is a complex process and is not fully understood. Many researchers have tried to characterize arcing by determining the arc constants using a relationship between arc voltage and current. However, very little has been done in terms of determining arc temperature, which is an important component of flashover modeling [7].

In order to simulate arc propagation, initial values of different circuit elements in each stage of propagation are required. In the existing dynamic models, the exact values of the different variables, such as arc length and temperature, and surface condition, are required for simulating the arc current. Otherwise, the prediction of arc current during propagation cannot be carried out [7]. Concerning arc temperature, it has been assumed, without any experimental support, to have a constant value of 4,550 K during white arc propagation.

Also, rotational temperature, which is close to gas temperature [8], should be determined and compared to the electronic temperature in order to verify the existence of Local Thermodynamic Equilibrium (LTE) [9].

Moreover, no data are available to calculate the electron density of arc on an ice surface, which is an important parameter for understanding the flashover mechanisms as well for evaluating the existence of LTE.

17

Spectroscopic plasma diagnostic methods provide some important advantages of interest to researchers for a long time. This technique enables to obtain a large amount of information about plasma without disturbing it. In addition, it is applicable to transient as well as to stationary states [10, 11].

Luminous emissions from arcs and plasmas often have complex spectral structures. Line spectra, particularly if time-resolved, can yield much information not only on the nature and concentration of ionized species, but also on the gas and electron temperatures, and electron density [12]. The spectroscopic investigation of discharge can also provide insights on the physics of ice surface discharge.

The main purpose of this project is to carry out a spectroscopic analysis of arcs formed on the surface of ice to determine their rotational and excitation temperatures, and also their electron densities. The results will be used to verify the existence of LTE in the discharge channel.

## 1.2 Research objectives

The main objective of this thesis is the spectroscopic investigation of arcs formed over an ice surface. This comprises the two following stages: identifying the different lines in the arc spectra, and calculating arc temperatures and electron densities.

The specific objectives are:

- **Identifying the lines and bands specific to various atoms and molecules**

Detailed analyses of the spectra allow identifying different atomic lines and molecular bands from background gases, as well as excited species from polluted ice.

18

- **Developing a method for the measurement of gas and excitation temperatures of arcs formed over an ice surface**

Optical emission spectroscopy is an applicable method for the measurement of excitation and rotational temperatures of this type of discharge.

- **Developing a method for electron density measurement of arcs formed over an ice surface**

Some spectral lines are broadened under the effect of the electric field resulting from the concentration of free-electrons. The Stark broadening method can be used to obtain the electron density of the arc channel.

- **Investigating the variation of gas and excitation temperatures, and electron densities of arcs over an ice surface at different current levels during arc propagation**

Time-resolved spectra will be recorded and analyzed to obtain the gas and excitation temperatures, and electron densities. When combined with synchronized electrical measurements these data should yield the overall variation of the measured quantities with the discharge current during arc propagation.

- **Examining the existence of LTE in the discharge channel**

Based on the results of the temperature and electron density measurements of different species, the existence of thermodynamic equilibrium will be examined.

## 1.3 Statement of originality and contribution to knowledge

To the best of our knowledge no experimental work has ever been performed to obtain the temperatures and electron densities of arcs formed over an ice surface.This investigation is the first using a spectrometer to record the light emitted from discharge activities over an ice surface. Moreover, employing a CCD (gateable charge-coupled device) detector head on the output of the spectrometer and synchronizing the spectra with electrical measurements (current and voltage) yielded the time-resolved spectra during arc propagation from the initial stage to flashover.

Besides the originality of the methodology, this work is the first research which determined the gas and excitation temperatures, as well as the electron densities of discharges over ice based on an experimental method. It is also a pioneering work for the examination of the thermodynamic state of this type of discharge. Based on the new findings, this fundamental work will provide valuable information for the improvement of dynamic models of arc propagation.

## 1.4 Methodology

The spectroscopic method was chosen to achieve the afore-mentioned objectives. Light emitted from the arc is brought to the spectrometer by means of a 10-meter fiber-optic cable. Because of the practical problems associated with capturing the light emitted by the arc, a simplified test setup was chosen. First, an ice bulk was formed in a Plexiglas mould by freezing several distilled water layers in a cold chamber to achieve a flat

surface. This procedure yields a polycrystalline ice structure with semi-transparent appearance. The final layer was formed using salty water, the salt content being adjusted to reach a specified level of conductivity. Then, a 6 mm air gap was made at one end of the setup. The overall dimensions of the mould were 100 cm × 15 cm × 5 cm.

Voltage and current measurements were also performed and synchronized with recorded spectra through a data acquisition system (DAQ). The following analyses were carried out on the experimental results:

### 1.4.1 Rotational temperature measurements

Rotational temperatures were measured using OH (A-X) emission bands. The variation of rotational temperatures, which is similar to that of gas temperatures with discharge current, was studied. In addition, the $N_2^+$ $1^{st}$ negative system was also used to measure the rotational temperatures of AC and DC applied voltages.

### 1.4.2 Excitation temperature measurements

Excitation temperatures of the arc column were determined using copper and oxygen lines and employing the method of relative line intensities. Deviations from LTE were taken care of using the Burton and Blade correction factor.

### 1.4.3 Electron density measurements

Electron densities were estimated by analyzing the Balmer line $H_\alpha$ profile, broadened by the Stark effect.

The above analyses were also carried out by studying the effects of voltage polarity.

## 1.5 Structure of the thesis

This thesis is structured as follows:

Chapter 1 presents general information about problematic, objectives, originality and general methodology.

Chapter 2 is dedicated to the review of literature.

Chapter 3 introduces the experimental equipment and the methodology.

Chapter 4 presents the experimental results.

Chapter 5 discusses in detail the experimental results presented in Chapter 4.

Finally, Chapter 6 concludes this work and provides recommendations for future studies.

# CHAPTER 2

# LITERATURE REVIEW

# CHAPTER 2

# LITERATURE REVIEW

## 2.1 Introduction

A large number of experimental investigations and theoretical studies on the subject of ice accretion on outdoor insulators have been carried out in several laboratories [13-17]. A good survey of the related literature is found in [18]. Spectroscopic plasma diagnostic methods have been used to obtain information such as temperatures of different species, electron densities, and to examine the local thermodynamic equilibrium of plasma [11, 19 and 20].

The first part of this chapter reviews spectroscopic plasma diagnostic techniques. Spectroscopic temperature measurement techniques are reviewed in the second part, including rotational and excitation temperature measurements. The next section describes the application of spectroscopic methods to measure electron densities in plasma. Studies of temperature and electron density measurements in lightning and other types of electric discharges are also reviewed. In addition, the conditions and established criteria used to verify the existence of local thermodynamic equilibrium are described.

## 2.2 Plasma

Plasma is often referred to as the fourth state of matter. As temperature increases, molecules become more energetic and transform in the following sequence: solid, liquid, gas and plasma. In the latter stages, molecules in the gas dissociate to form a gas of atoms and then a gas of free-moving charged particles, electrons and positive ions. This state is called the plasma state [21]. It is characterized by a mixture of electrons, ions, and neutral particles moving in random directions.

Normal state gases are electrical insulators. This is because they contain no free charged particles, only neutral molecules. If electric field of sufficient intensities is applied, they become conductive and the complex phenomena which then occur are called gas discharges.

For the various types of ionized gases, the quantities $\alpha = n/ (n+n_o)$ and degree of ionization should be characterized. $n_o$ is the number of neutral molecules and $n$ is the number of electrons. This value varies in practice between very low values of the order of $10^{-10}$ to 1. We can classify ionized gases into two groups:

Weakly ionized gases, $\alpha < 10^{-4}$

Strongly ionized gases $\alpha > 10^{-4}$

When the degree of ionization is equal to unity, the density of neutral molecules is zero; the gas is then said to be completely ionized, or to constitute plasma. [22]

Plasma is electrically conductive due to the presence of free charge, and its electrical conductivities are larger than those of such metals as gold and copper. Plasma can occur naturally or be manmade. Plasma rarely occurs naturally, some phenomena such as solar corona, solar wind and lightning can however create plasma.

25

Because plasmas can occur over a wide range of pressures, it is customary to classify them in terms of electron densities. Most plasmas of practical significance have electron temperatures of 1 eV to 20 eV with densities in the range of $10^6$ to $10^{18}$ $cm^{-3}$.

Plasma is a region not influenced by its boundaries. As in any gas, the temperature is defined by the average kinetic energy of the particle, molecule, atom, neutral or charge. Thus, plasma will typically exhibit multiple temperatures unless sufficient collisions occur between particles to equilibrate. However, because the mass of an electron is much less than the mass of a heavy particle, many collisions are required for this to occur.[21]

Electrical discharge is one of the most common ways to create and maintain plasma. The energy from the electric field is accumulated between collisions by the electron, which subsequently transfers a portion of this energy to the heavy neutral particle, through collision. Even with a high collision frequency, the electron temperature and heavy particle temperature will generally be different.

## 2.3  Spectroscopic plasma diagnostics

Spectroscopic plasma diagnostics offers some important advantages that have long attracted researchers. It yields large amounts of simultaneous information about the plasma (concentration of various species of particles, temperatures) without disturbing it. In addition, spectroscopic plasma diagnostics can be applied to both transient and stationary states. [10].

Luminous emissions from arcs and plasmas often have complex spectral structures. Line spectra, particularly if time-resolved, can yield much information not

only on the nature and concentration of the species present in the discharge medium, but also on the gas and electron temperatures and electron densities. [12].

Non-thermal plasmas are characterized by a non-equilibrium distribution of energy between different species. The various temperatures describe distinct aspects of the physical state of the system:

*Electron temperature* is the temperature that describes, through Maxwell's Law, the kinetic energy distribution of the free electrons.

*Gas temperature* describes in a similar way the kinetic energy distribution of the gas atoms.

*Excitation temperature* is the temperature that describes, through Boltzmann's Law, the relative population distribution of atoms or molecules over their energy levels. We distinguish between electronic excitation temperature, vibrational temperature, and rotational temperature.

*Ionization temperature* is related to the ionization equilibrium described by the Saha-Eggert equation [23].

## 2.3.1 Mechanism of emission and absorption of spectra

Table 2.1 classifies the various types of spectra observed in plasma according to the particles which emit them and the degree of freedom they set into action. The atoms and ions emit a spectrum of lines from infrared to the far ultraviolet, resulting from electron excitation. At the time of electronic transition, the energy of an atom varies according to the following equation:

$$E_u - E_e = h\nu = \frac{hc}{\lambda}$$

(2.1)

Where $h$ is Planck's constant and the emitted radiation of frequency $\nu$ is characteristic of the emitting atom for which we know the energy levels $E_u$ (Figure 2.1).

**Table 2.1. Spectra observed in plasma [10]**

| Particles | Degree of freedom | Type of spectrum | Spectral region |
|---|---|---|---|
| Atom or Ion | Electronic excitation | Line | U.V.-visible-I.R. |
| | Ionization | Continuum | U.V.-visible-I.R. |
| | Translation | Line profiles | |
| Electrons | Recombination | Continuum | U.V.-visible |
| | Free-free transitions | Continuum | I.R. |
| Molecules | Rotation | Line | Far infrared |
| | Vibration-rotation | Band | I.R. |
| | Electronic excitation | Band systems | U.V.-visible-I.R. |

The electron changing the orbit remains bound to the atom; this is called the "bound-bound" transition. The recombination of the electron and the ion corresponds to a "free-bound" transition, which gives a continuous spectrum observed in the visible and the ultraviolet.
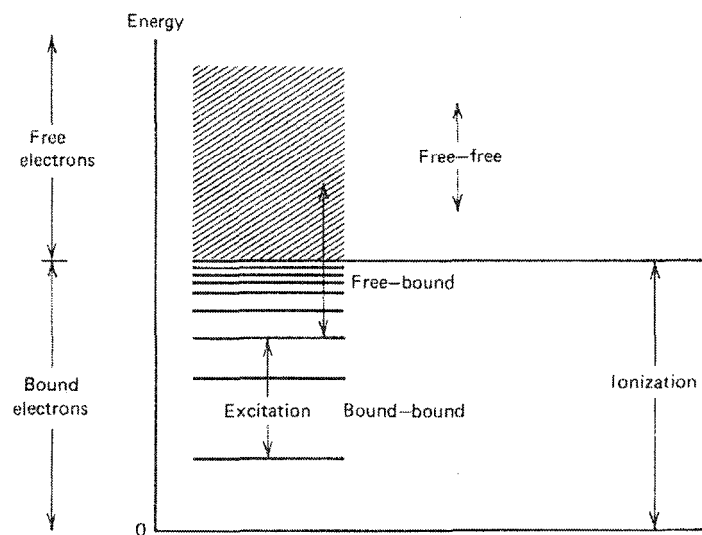
**Figure 2.1. Excitation levels of an atom or an ion [10]**

We may also consider "free-free" transitions of free-ion electron systems for which the electrons are free before and after (Figure 2.1). Such transitions give a continuous spectrum observed in the infrared and which occurs during electron-atoms collision as well.

The diatomic molecules emit much more complex spectra. The energy diagram for CN (Figure 2.2) shows that electronic excitation occurs at energies greater than 1 eV only, whereas vibration excitation occurs at energies of some tenths of an electron volt, and rotational excitation at much lower energies still. In the far infrared, a line spectrum due to pure rotation is observed, this corresponds with transition in which only the rotational energy of the molecule changes.

In the near infrared the spectrum consists of vibration-rotation bands. With a high-resolution spectrometer, such vibration bands may be resolved into lines of rotation,

29

the intensities of which are related to their rotational temperatures. Finally, in the visible and ultraviolet bands, we obtain systems of electronic excitation bands [10].
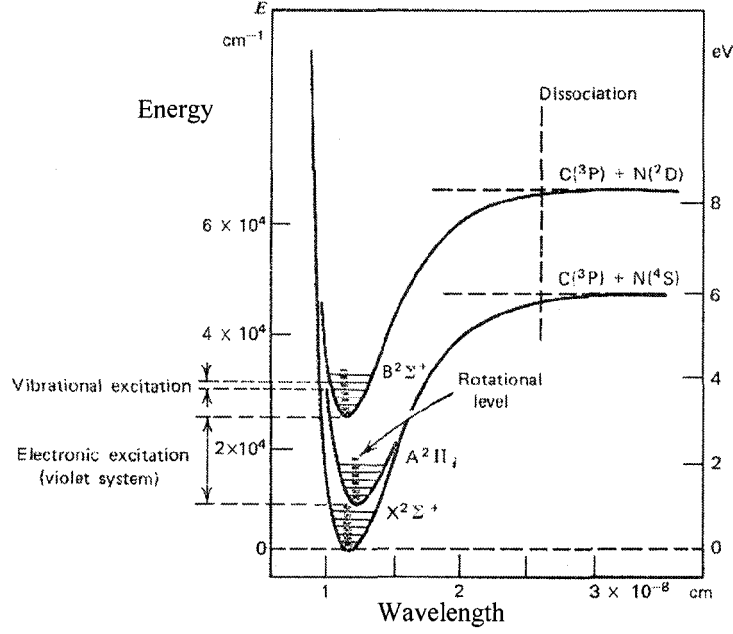


**Figure 2.2. Energy curves for a diatomic molecule (CN) and schematic spectrum of the violet and red systems [10].**

## 2.3.2 Different types of emission spectra

### 2.3.2.1 Line spectra

In optically thin plasma, the emission coefficient corresponding to a line frequency emitted by an atom, which undergoes a transition from a higher-level $u$ to a lower level $l$, is given by:

$$\varepsilon_v = \frac{h v}{4\pi} A_{ul} N_u \qquad (2.2)$$

30

$N_u$ is expressed as a function of density $N$ of neutral atoms. The observed line is not infinitely narrow but always has a certain width $\Delta v; \varepsilon_v$ can be related to the spectral emission coefficient $\varepsilon(v')$ by [10]:

$$\varepsilon_v = \int_{\Delta v} \varepsilon(v')dv' \qquad (2.3)$$

### 2.3.2.2 Continuum spectra

In general, continuous plasma emissions are due to the superimposition of several continued spectra caused by different mechanisms:

a)     Free-free radiation

This corresponds to the emission of a photon when an electron subjected to the electric field of an ion or an atom passes through a free state to another free state of lower kinetic energy.

b)     Radiation due to recombination (free bound radiation)

This results from the capture of a free electron by an ion; the inverse phenomenon is photo ionization.

c)     Continuum due to negative ions

This is emitted, as in the case of recombination, during the attachment of a free electron to an atom or molecule.

d)     Pseudo-continuum of lines

This is due to the overlapping of neighboring lines broadened through Stark effect.

31

### 2.3.2.3 Line profiles

The lines emitted by atoms or ions are not infinitely narrow, but always show a certain profile which depends upon the environment in which the emitter is placed; in plasma, the natural broadening being always very small is negligible compared to other types of broadening: statistical Doppler effect, collisional effect, and pressure effect.

### 2.3.2.4 Band spectra

When the temperature of plasma does not exceed 15,000 K, its spectrum can include molecular bands, the examination of which may yield the temperatures of rotation, vibration or electronic excitation of molecules [10].

## 2.4 Spectroscopic temperature measurement techniques

Temperature is considered one of the most important parameters for plasma state characterization. Accurate temperature measurements lead to better understanding of the plasma processes, i.e. vaporization, dissociation, excitation and ionization [24]. In the literature dealing with plasma gas, temperature measurements are usually made using emission spectroscopy of excited plasma gas species [25]. Besides the qualitative determination of chemical composition of plasma from emission and absorption line identification, the measurement of electron and ion, or atom temperatures is the oldest application of spectroscopic methods to plasma and gaseous electrical discharge physics [26].

Non-thermal plasmas are characterized by a non-equilibrium distribution of energy between different species. Hence, the various temperatures each describe a distinct aspect of the physical state of the system [27]: the electron temperature ($T_e$) is determined by the kinetic energy of the electrons, the rotational temperature ($T_{rot}$) is relevant to all processes in which molecules, radicals, and their dissociation products are involved, and the excitation temperature ($T_{exc}$) describes the population of the various energy levels [28].

## 2.4.1 Rotational temperature measurement

Molecular spectra can successfully give information in the temperature range of 2,000–8,000 K, where atomic spectra are not strong enough to ensure good sensitivity [29].

It can be assumed that the rotational temperature is close to the gas temperature, because rotational relaxation is fast at atmospheric pressure [8]; but the often-used assumption that $T_{rotational}$ and $T_{vibrational}$ are approximately equal to the electron temperature is not always valid in non-equilibrium plasmas [12].

The OH ($A^2\Sigma$–$X^2\Pi$) transition is one of the most intense systems emitted by low-temperature air plasmas containing even a small amount (~1 %) of $H_2$ or $H_2O$. The rotational temperature can be derived by fitting the entire band, or more simply from the relative intensities of two groups of rotational lines corresponding to the R and P branches of the OH (A–X) (0, 0) vibrational band. These branches present distinct peaks at about 307 nm and 309 nm, respectively [8]. This technique provides a sensitive thermometer, because the relative intensity of the two peaks varies rapidly with the

rotational temperature. Another advantage of the technique is that it does not require absolute or relative intensity calibration because the response of usual detection systems is nearly constant over the small spectral range of interest [8].

Generally the value of the rotational temperature of the OH radicals is close to the gas temperature. The OH band diagnostic applies to a wide temperature range and even to non-equilibrium plasmas [30].

Bands of NO, OH, and $O_2$ dominate the spectrum at temperatures below ~5,000K. The second positive system of $N_2$ (C–B), the first negative system of $N_2^+$ (B–X), and atomic lines of O and N appear at higher temperatures [8].

For low-temperature plasmas in humid air, the emission spectrum of the OH (A–X) transition around 300 nm provides a convenient way to measure the rotational temperature. At higher temperatures, or in the presence of an electric field, the OH transition is overlapped by strong emissions from $N_2$ (C–B) (second positive system). In this case, the rotational temperature can be measured from $N_2$ (C–B) rotational lines [8].

The rotational lines of the $N_2^+$ first negative system ($B^2\Sigma^+$-$X^2\Sigma^+$), particularly those of the (0-0) band, have often been used to determine rotational and vibrational temperatures in plasma [31, 32].

The group of rotational lines of the $N_2^+$ first negative system in the region of 380 nm to 392 nm is well isolated from lines of other transitions. Their lines are sensitive function of rotational temperature, but they appear at higher temperatures [8].

The intensity $I_{nm}$ of a spectral line corresponds to a transition between two levels ($n \rightarrow m$), derived from [33]:

$$I_{nm} = \frac{K_{nm}}{Z(T)} \exp(-\frac{E_n}{kT})$$ (2.4)

Where $k$ is the Boltzmann constant, $K_{nm}$ is a constant for a given transition $(n \rightarrow m)$, $Z$ $(T)$, the partition function of the particle, and $E_n$, the energy of the state $n$.

When $I_{nm}$ is known for a given temperature $T_{ref}$ ($I_{nm\ ref}$ is used as reference), one can read [33]:

$$I_{nm} = I_{nm_{ref}} \frac{Z(T_{ref})}{Z(T)} \exp(-\frac{E_n(T_{ref} - T)}{T_{ref}T}) \tag{2.5}$$

In their work, Dieke and Crosswhite [34] provided the wavelengths of the different branches, the energy of the upper level of each transition, and the normalized intensity $I_{nm\text{-}ref}$ of each line of the rotational band OH (A-X) for a reference temperature of $T_{ref} = 3000K$. The term $Z$ (3000)/$Z$ (T) is the same for all rotational lines issued to the upper vibrational level $n$. From that viewpoint, this term is normalized to one in the evaluation of Equation (2.5) [35]. SPECAIR software [36] can be used to calculate the theoretical spectra of each rotational temperature, considering the slit function of the spectroscopic system.

## 2.4.2 Excitation temperature measurement

The spectral lines are due to the quantization of energy levels in atoms, ions, molecules or particles, resulting from transitions from one energy level to another, accompanied by the release or absorption of photons. Rest wavelengths of the lines can be accurately derived from quantum mechanical calculations or laboratory measurements. From the intensities of lines of the same atom, ion or molecule, and detailed calculations of the transition probabilities, it is possible to determine the density and temperature of the region in which it arises [37].

In many cases, it is necessary to distinguish between kinetic temperatures of electrons, ions, and atoms, say, $T_e$, $T_z$ and $T_a$. These temperatures may differ from each other even if the individual velocity distributions are close to Maxwellians, because electron-electron energy transfer rates are much larger than electron-ion collision rates, as are ion-ion rates [37].

Most of the spectroscopic temperature measurements primarily yield $T_e$. They are based on:

- Relative line intensities either of the same atom or ion of neighbouring ionization stages or of successive isoelectronic ions;

- Relative continuum intensities, on ratios of line and continuum intensities;

- Relative and absolute intensities from optically thick plasmas;

- Time histories of emission from transient plasmas [37].

Several techniques are based on this concept. In the Boltzmann method [38], the absolute intensity of a spectral line involved in the transition from an upper level $q$ to a lower level $p$ is:

$$I_{qp} = \frac{d}{4\pi} A_{qp} n \frac{g_q}{Z} exp(-\varepsilon_q / kT) h v_{qp} \qquad (2.6)$$

Where $d$ is the depth of emission source, $A_{qp}$ is the transition probability of $q$ to $p$, n is the population of the $i^{th}$ excited state, $g_q$ is the known statistical weight or degeneracy of the excited state, $Z$ is the partition function, $\varepsilon_q$ is the excitation energy, $k$ is the Boltzmann constant, $T$ is the absolute temperature, $h$ is the Planck constant, and $v_{qp}$ is the frequency of the spectral line emitted in the transition from $q$ to $p$. Taking the logarithm of both sides of this rearranged equation, we have:

$$\ln(\frac{I_{pq}}{g_q A_{qp} v_{qp}}) = \ln(\frac{n}{z}) - \frac{\varepsilon_q}{KT} \tag{2.7}$$

If we plot the left hand side of this equation versus the excitation energy ($\varepsilon_q$), a linear relationship with a slope of (-1/KT) is obtained, often referred to as the Boltzmann plot [37].

In the modified Boltzmann method [37], the temperature can be derived from the slope of the plot between $\log(\frac{\varepsilon_q I_{qp}}{g_q A_{qp}})$ and $\varepsilon_q$.

Another variation of the Boltzmann method uses the intensity ratio of two lines [37]. If the lines are labelled $a$, $b$, respectively, and subscripts p and q are omitted for the sake of convenience, we obtain:

$$\frac{I_a}{I_b} = \frac{(gA)_a}{(gA)_b} \frac{v_a}{v_b} exp[-(\varepsilon_a - \varepsilon_b)/kT] \tag{2.8}$$

Rearranging this equation, we obtain:

$$T = \frac{5040(V_a - V_b)}{\log((gA)_a/(gA)_b) - \log(\lambda_a/\lambda_b) - \log(I_a/I_b)} \tag{2.9}$$

- $V$ is the excitation potential (eV)

- $A$ is the (relative) transmission probability

- $g$ is the statistical weight

- $\lambda$ is the wavelength

- $I$ is the (relative) intensity

The subscripts $a$, $b$ refer to the lines $a$ and $b$, respectively.

In this method, both lines should belong to the spectrum emitted by the neutral atom or the ion of an element. Furthermore, the difference between the excitation potentials $V_a$ and $V_b$ should be sufficiently large.

The measurement of arc properties by atomic emission spectroscopy relies on the existence of a local thermodynamic equilibrium (LTE). Another method that may be used down to ambient temperatures is laser-scattering temperature measurement, essentially independent of LTE [39].

Another variation of the Boltzmann method considers two different spectral lines, the absolute temperature being determined from the relative intensities of these two lines with known relative transition probability, as follows [37]:

$$T = \frac{(E_m - E_n)/k}{\ln\left(\dfrac{I_{nr}}{I_{mp}} \dfrac{g_p}{g_r} \dfrac{f_{pm}}{f_{rn}} \dfrac{\lambda_{nr}^3}{\lambda_{mp}^3}\right)} \tag{2.10}$$

- $E_m$ is the excitation potential of the m$^{th}$ level (eV)

- k is the Boltzmann constant

- $I_{mp}$ is the intensity of transition from level $m$ to level $p$

- $g_p$ is the statistical weight of the $p^{th}$ level

- $f$ is the absorption oscillator strength for a particular transition

- $\lambda$ is the wavelength (nm)

The criteria for selecting lines in the emission spectrum can be determined by performing an error analysis on (2.10):

$$\frac{\Delta T}{T} = \frac{\ln[(1 + \Delta R/R)/(1 + \Delta F/F)]}{(E_m - E_n)/\Delta T - \ln[(1 + \Delta R/R)/(1 + \Delta F/F)]} \tag{2.11}$$

- $1/R$ is the intensity ratio $I_{nr}/I_{mp}$

- $1/F$ the ratio of oscillator $f_{pm}/f_{nr}$

38

The range of error can thus be minimized by choosing a large $E_m$–$E_n$. It could be also minimized by choosing strong lines of approximately equal intensity [37].

When the local thermodynamic equilibrium deviates, the non-equilibrium parameter $b$ (defined as the ratio of the actual to calculated LTE level populations) may be used [40]. Using this method proposed by Burton and Blades [40], the actual populations can be calculated, allowing theoretical Boltzmann plots to be constructed. Hence, the intensity of a spectral line resulting from transition from level $m$ to $n$ is:

$$I = \frac{1}{4\pi}\frac{hc}{\lambda_{mn}} A_{mn} g_m \frac{b_{atom}^m n_i}{z_{int}(T)} e^{-(E_m / kT)} \qquad (2.12)$$

Where $A_{mn}$ is the transition probability, $\lambda_{mn}$ is the wavelength between the upper level $m$ and lower level $n$, $g_m$ is the statistical weight, and $E_m$ is the energy of the upper level; $n_i$ is the total number density of chemical species $I$, $z_{int}(T_{exc})$ is the internal partition function calculated at temperature $T_{exc}$, and $b_{atom}^m$ is a non-equilibrium parameter that can be evaluated for the considered atom as [40]:

$$b_{atom}^m = 1 + \frac{6.55 \times 10^{13} E_\infty (E_\infty - E_m)^{2.607}}{n_e T^{0.107}} \qquad (2.13)$$

where $E_\infty$ is the ionization energy (eV) and $n_e$ is the electron density expressed in cm$^{-3}$.

## 2.5 Spectroscopic density measurement techniques

Depending on various plasma conditions, such as size, composition, densities and temperatures, electron densities can be measured using a number of techniques. Langmuir probes provided the first means to infer local values of electron density, mostly

39

at relatively low densities. Thomas scattering of laser light has become a method of choice for localized electron density measurements over a range of about $10^{11}$ to $10^{21}$ cm$^{-3}$ [26].

The purely spectroscopic density determinations are based on the interpretation of measurement of at least one of the following quantities: spectral line widths or profiles, absolute continuum intensities, absolute line intensities, or relative line intensities. In general, this interpretation depends on some knowledge of the temperature. Generally, an iterative procedure also using the methods of temperature determination is called for. In practice, this iterative method is replaced by comparing measured and synthetic spectra, the latter being calculated for sets of assumed plasma conditions until a satisfactory fit is obtained [26].

### Densities from spectral line widths and profiles

Under favorable circumstances the widths, shifts and profiles of suitable spectral lines are very insensitive to both electron and ion temperatures [26].

One of the common electron density measurement methods consists in making use of the Stark effect. This effect involves the interaction between radiating atoms or ions and electrons or ions [12], and therefore depends on charged particle densities. In fact, the effect depends primarily on the densities of charged particles and is only a weak function of temperature [41]. Stark widths and profiles of many spectral lines are found in Griem [42].

The most important experimental considerations for choosing spectral lines for plasma density measurements are their strengths and separation from neighboring lines; and also the wavelength range, i.e., the relative ease of obtaining sufficient resolution and

signal. On the theoretical side, it is important that broadening mechanisms other than the Stark effect are ruled out, or at least accounted for. Doppler broadening can be calculated if the atom or ion kinetic temperatures are known. Instrumental broadening should be measured separately. Both effects are best accounted for by including them in any simulated spectra. If this is not possible, they should be allowed for in error estimates [26].

The principal advantages of using synthetic spectra for comparisons with measured data before inferring electron densities are the possibility of fitting entire profiles, rather than only comparing measured and calculated line widths, and the ease of accounting for variations of plasma conditions along the line of sight [26]. It is preferable to use optically thin lines with high intensities that are highly sensitive to Stark effects. A good example in this category is the $H_\beta$ line of hydrogen. At temperatures near 1 eV, can be applied to electron densities from $10^{14}$ to $10^{17}$ cm$^{-3}$. At 10 eV, only densities above $10^{15}$ cm$^{-3}$ can be determined reliably due to grater Doppler broadening. Above $N_e = 10^{17}$ cm$^{-3}$, it is preferable to use the less sensitive $H_\alpha$ line, because the $H_\beta$ line becomes too broad for a clean separation from the underlying continuum and from the $H_\gamma$ line [26].

Since the Stark profiles are only weak functions of temperature, measured values can be used to determine electron densities in situations where the temperature is only approximately known, or even when the existence of a unique temperature is questionable e.g. when LTE is not achieved [43].

The Lorentzian function is used to describe Stark broadening and is expressed as follows:

$$S(\lambda;\lambda_0,\gamma) = \frac{1}{\pi}\left[\frac{\gamma/2}{(\gamma/2)^2 + (\lambda-\lambda_0)^2}\right]$$

(2.14)

- $S(\lambda;\lambda_0,\gamma)$ is the light intensity

- $\lambda_0$ is the central wavelength of the line

- $\gamma$ is the scale parameter which specifies the FWHM (Full Width at Half Maximum).

Electron densities can be obtained directly from the profile widths [26] or by fitting the data to theoretical line profiles [44]. Because of theoretical developments, the half-width measurement of Stark-broadened lines now ranks as one of the most accurate and convenient methods for determining electron densities [45]. In principle, one must match the measured line profiles and the calculated Stark profiles properly within a range of electron densities. The correct density corresponds to the best-fit Stark profile [46]. However, a more reliable and still simple method is the standard procedure for deriving electron densities from measured line widths [46, 47].

In laboratory-created plasma, the Balmer-$\alpha$ ($H_\alpha$) line of hydrogen, due to transitions between principal quantum number n=3 and 2 levels, often is a prominent line [48]. The line shape strongly depends on the density of charged particles surrounding the emitter. Due to the decomposition of water vapor during discharge activities on the ice surface, hydrogen is present in the arc column, and the $H_\alpha$ line of the Balmer series is considerably Stark-broadened so that electron density may be determined by comparing the measured profiles with theoretical profiles [26].

## 2.6 Arc discharge temperature and electron density measurement

There are a lot of different methods for studying electrical discharge phenomena. They can be divided into two main categories: optical and electrical measurements. In this study only the "Spectroscopic analysis" method is described.

The pioneering works of Uman [19] and Orville [11] are good references for measuring the temperatures and electron densities of lightning using the spectroscopic method. Uman and Orville [19] measured the electron (ion) densities in three different lightning strokes by observing the Stark-broadening of the $H_\alpha$ lines in lightning spectra. They concluded that the electron density in the stroke when the maximum integrated intensity from $H_\alpha$ was being recorded was between $1\times10^{17}$ and $5\times10^{17}$ cm$^{-3}$. Orville [11] employed the ratio of intensities of emission lines to calculate the temperature of a ~10 m section of return-stroke channel. The peak temperatures were in the 28,000-31,000 K range. He used the Stark-broadened half-width of the $H_\alpha$ line and calculated an electron density in the order of $8\times10^{17}$ cm$^{-3}$ in the first 5 $\mu$sec, decreasing to $1-1.5\times10^{17}$ cm$^{-3}$ at 25 $\mu$s. They also performed the same study on long air gaps [49], [54].

Les Renardières Group [50], [51] applied spectroscopic analysis to obtain time-resolved information on the physical process occurring at different stages of breakdown of long gaps using two spectrometers and a streak camera. They observed the different spectral distributions between leader coronas and leader channel phenomena. The leader coronas were predominantly in the ultraviolet region, about 300 nm, while the leader channel was in the red, between 500 nm and 700 nm [50].

They observed different lines of neutral and ionized nitrogen and oxygen and also

the atomic hydrogen lines $H_\alpha$ and $H_\beta$ in their recorded spectra of leader channels [52].

They derived gas and electron temperatures and ionization degrees in the leader channels

and compared their results with Orville [49] and Vassy [53]. Figure 2.3 shows their

results [52].
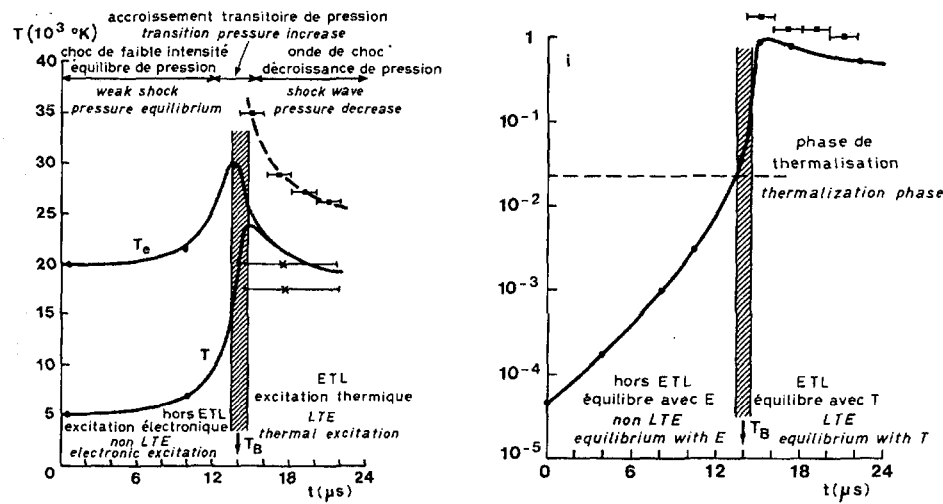


**Figure 2.3. Gas and electron temperature and ionization degree in the leader channel, comparison of Les Renardières Group [52] results with Orville [49] and Vassy [53]**

Uman et al. [54] investigated a four-meter spark in air, using streak photography

and spectroscopy. They observed that primary radiating species in the leader is singly

ionized nitrogen (N II) and estimated the leader temperature to be in the order of

20,000K.

Staack et al. [55] experimented with DC glow discharges in atmospheric pressure

helium, argon, hydrogen, nitrogen and air. They measured the rotational temperatures

using the $\Delta$vib +2 transitions of the $N_2$ $2^{nd}$ positive system for the various discharge gases

relative to discharge current. The gas temperatures for a 3.5 mA normal glow discharge

44

were around 420 K , 680 K, 750 K, 890 K and 1,320 K in helium, argon, hydrogen, nitrogen and air, respectively. They also used atomic transitions to determine the electronic excitation temperatures for different upper-state energies on Boltzmann plots which indicated a non-thermal discharge [56].

Shinobu et al. [57] preformed a spectroscopic study of 150 W plasma in water. The Balmer atomic hydrogen lines ($H_\alpha$ and $H_\beta$), OH (A-X) (0, 0) band at 309 nm, O (777 nm) and O (845 nm) were detected as strong emissions. In addition to $H_\gamma$, peaks of O I and O II were also detected as weak emissions. The Na line (589 nm) also appeared as an impurity in the spectra. They measured electron temperatures from the ratio of the emission intensities of $H_\alpha$ and $H_\beta$ and rotational temperatures of OH radicals was obtained from OH $A^2\Sigma-X^2\Pi$ (0, 0) band emissions [57].

Nieto-Salazar et al. [58] carried out spectroscopic studies of positive streamers in water. The light emitted by streamers showed the UV OH band, atomic lines of OI, $H_\alpha$ and a strong continuum from 350 nm to 500 nm. Rotational temperatures were calculated from OH bands to be in the range of 3,000 K to 4,000 K, and the electron densities were measured from Stark broadenings of $H_\alpha$ and OI (777nm) to be in the order of $10^{17}$ $cm^{-3}$.

Gas temperatures, electron densities and electron temperatures of excited plasma were measured by optical emission spectroscopy by Xi-Ming Zhu et al. [59]. The gas temperatures were obtained from the rotational temperatures of the hydroxyl molecule (A $2\Sigma+$, v = 0) and the electron densities were measured by the Stark broadening of the hydrogen Balmer $\beta$ line. The electron temperatures were estimated based on the measured excitation temperatures of Argon 4p and 5p levels [59].

## 2.7 Thermodynamic study of plasma

The condition of the arc plasma can be regarded as a state of thermal equilibrium when all definitions of temperature give the same numerical values. In non-equilibrium sources, different definitions will, in general, lead to different values of the parameter.

The various temperatures each describe a distinct aspect of the physical state of the system [27]:

Electron temperatures, which are determined by the kinetic energy of the electrons; gas temperatures, which are defined by the kinetic energy of the neutral atoms; excitation temperatures, which describe the population of the various energy levels; and ionization temperatures, which govern the ionization equilibrium.

### 2.7.1 Thermal equilibrium in the arc

For gases to be in complete thermal equilibrium, the various gas components, i.e. neutral particles, charge carries, and photons, must be in equilibrium mutually and with respect to the surroundings. Complete thermal equilibrium (C.T.E) prevails in an enclosure whose walls and interior have a uniform temperature with respect to radiation and internal energy.

A gaseous system in C.T.E is characterized by the following conditions:

1. The velocity distributions of all kinds of free particles (molecules, atoms, ions and electrons) at all energy levels satisfy Maxwell's law.

2. For each separate kind of particle the relative population of energy levels conforms to Boltzmann's distribution law.

3. Ionization of atoms, molecules and particles is described with Saha's equation.

4. Radiation density is consistent with Plank's Law [16].


### 2.7.1.1 Maxwell's Law

In thermal equilibrium conditions, the speeds of particles are distributed according to the Maxwell's function.

$$f(v)dv = (\frac{m}{2\pi KT})^{3/2}(e^{\frac{-mv^2}{2KT}})4\pi v^2 dv \qquad (2.15)$$

Where $v$ is the frequency of the photon emitted in the transition, $T$ is temperature, and $f(v)$ is the fraction with speeds between $(v, v + dv)$ [60].


### 2.7.1.2 Plank's Law

The black body is an ideal body of uniform temperature T (K) that perfectly absorbs all incidental radiation, and emits isotropically unpolarized thermal radiation according to Planck's Law. It is customary to indicate with $B_\lambda$ (T):

In wavelength units, the emission is:

$$B_\lambda(T) = \frac{2hC^2}{\lambda^5}\frac{1}{e^{\frac{-hC}{kT\lambda}} - 1} \qquad erg.cm^{-2}s^{-1}cm^{-1}\,s \qquad (2.16)$$

Where $B_\lambda(T)$ is the specific intensity energy per unit area per unit time per unit bandwidth, $h$ is Plank's constant, $h = 6.57 \times 10^{-27}$ erg.s$^{-1}$, k is Boltzmann's constant, $\lambda$ is wavelength, and T is temperature in Kelvin.

47
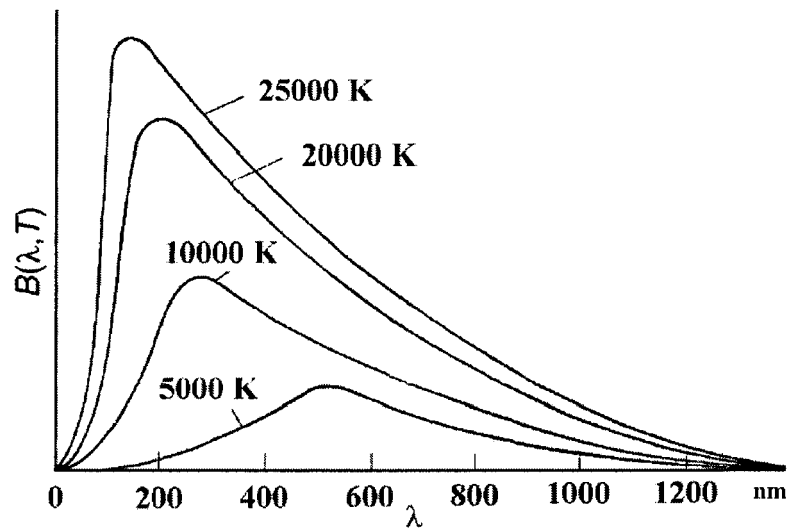
**Figure 2.4. Plank's distribution [61]**

Equilibrium between light quanta and material particles in an arc column is not expected to be reached owing to the absence of walls with the same temperature as the arc gas, and hence the radiation density is not expected in general to satisfy Planck's Law. But with increasing concentrations of emitting and absorbing particles the intensity in the center of the spectral line asymptotically approaches the intensity of blackbody radiation at the same temperature and wavelength. Under such conditions, the radiation density distribution may thus be assumed, to a good approximation, to be consistent with the upper limit of Planck's Law [61]. Furthermore, the energy loss from the arc by radiation amounts to only a few percent of the total energy supply. For this reason a state of partial thermal equilibrium can exist [27].

### 2.7.1.3 Saha's equation

The basic concept of thermal ionization introduced by Saha is the application of the mass action law to ionization equilibria. For each component (labeled $i$) of a composite gas we can consider on equilibrium of the form:

neutral atom $\Leftrightarrow$ ion + electron

The equilibrium constant $K_{nj} = \dfrac{n_{ij} n_e}{n_{aj}}$ can be calculated as a function of temperature. The resulting equation $K_{nj} = S_{nj}(T)$ is known as Saha's relationship, where $n_{ij}$ and $n_{aj}$ are the densities and concentrations of the ions and neutral atoms of the component labeled $j$, and $n_e$ is the electron density.

The dependence of the ionization constant $S_{nj}$ on temperature is expressed by Saha's equation:

$$\frac{n_{ij} n_e}{n_{aj}} = S_{nj} = \frac{(2\pi mkT)^{3/2}}{h^3} \frac{2Z_{ij}}{Z_{aj}} \exp(-\varepsilon_{ij}/kT) \tag{2.17}$$

Where $m$ is the electronic mass, $k$, the Boltzmann constant, $h$, the Plank constant, $Z$, the partition function, and $\varepsilon$, the ionization energy. The factor 2 that immediately precedes the ratio of partition function is the statistical weight of a free electron [27].

### 2.7.1.4 Boltzmann's Law

If a gaseous body in an enclosure is in thermal equilibrium with the walls, the population of energy levels for each separate kind of particle follows as Boltzmann distribution, namely:

$$\frac{n_q}{n_o} = \frac{g_q}{g_o} e^{-\varepsilon/kT} \qquad (2.18)$$

Where $n_q$ is the density or concentration of particles in the excited state q, $n_o$ is the density of ground state atoms, $g_q$ and $g_o$ are the statistical weights of the corresponding levels, $\varepsilon_q$ is the excitation energy of the state q, k is the Boltzmann constant, and T, the absolute temperature.

The statistical weight of a particular state is the probability of populating a state under identical conditions. Under those conditions we have "detailed balancing", i.e. in equilibrium the total number of particles leaving a certain quantum state per second equals the number arriving in that state per second, and the number leaving by a particular path equals the number arriving by the reverse path [27].

### 2.7.1.5  Partition function

To drive the equation we write, instead of Boltzmann's equation:

$$n_0 : n_1 : n_2 : ...n_j = g_0 : g_1 \exp(-\varepsilon_1 / kT) : g_2 \exp(\varepsilon_2 / kT) : ...g_j \exp(-\varepsilon_j / kT) \qquad (2.19)$$

Where the energy of levels 1, 2... j is taken from ground level zero. Now, since:

$$\sum_{m=0}^{m=j} n_m = n \qquad (2.20)$$

We have:

$$\frac{n_q}{n} = \frac{g_q \exp(-\varepsilon_q / kT)}{\sum_{0}^{j} g_m \exp(-\varepsilon_m / kT)} \qquad (2.21)$$

If we put $Z = \sum_0^j g_m \exp(-\varepsilon_m / kT)$, which is called the *partition function* (or the

sum over states) of the particular atom, the summation will include all possible energy

levels of the relevant particle [27].

The importance of the partition function Z is that in Maxwell-Boltzmann and

classical statistics, all the thermodynamic properties of a system can be expressed in

terms of Z and its partial derivatives [62].

To distinguish the quantities n and Z of neutral atoms and singly charged ions, the

g of ions is distinguished from that of atoms. Accordingly, for atoms we write:

$$n_{aq} = n_a \frac{g_q}{Z_a} \exp(-\varepsilon_q / kT) \qquad (2.22)$$

A similar equation holds for ions. The practical form of expression is:

$$n_{aq} = n_a \frac{g_q}{Z_a} 10^{-5040V_q/T} \qquad (2.23)$$

Where $V_q$ is the excitation potential expressed in electron volts.

The above equation is often conveniently employed in its logarithmic form, as in

[16].

$$\log n_{aq} = \log n_a + \log g_q - \frac{5040}{T} V_q - \log Z_a \qquad (2.24)$$


## 2.8 Thermodynamic equilibrium

When an arbitrary system is isolated and left alone, its properties will in general

change with time. If initially there are temperature differences between parts of the

51

system, after a sufficiently long time the temperature even out at all points, and then the system is in *thermal equilibrium.*

If there are variations in pressure or elastic stresses within the system, parts of the system may move, or expand, or contact. Eventually this motions, expansions, or contractions will cease, and then the system is in what is called *mechanical equilibrium.*

Finally, suppose the system contains substances that can react chemically. After a sufficiently long time has elapsed, all possible chemical reactions will have taken place, and the system is then said to be in *chemical equilibrium.*

A system, which is in thermal, mechanical, and chemical equilibrium, is said to be in *thermodynamic equilibrium* [62].

## 2.8.1 Thermodynamic properties

### 2.8.1.1 Mass density

Considering a gas at thermodynamic equilibrium consisting of different species *i*, with mass $m_i$ and density $N_i$, the mass density will be [60]:

$$\rho = \sum_i N_i . m_i \qquad (2.25)$$

### 2.8.1.2 Enthalpy

In thermodynamics and molecular chemistry, the enthalpy, or heat content, (denoted as H or $\Delta$H) is a quotient, or description, of the thermodynamic potential of a

system, which can be used to calculate the useful work obtainable from a closed thermodynamic system under constant pressure. By definition:

H=U+pV                                                      (2.26)

Where U is the internal energy, p is the pressure and V is the volume [63].

### 2.8.1.3 Heat Capacity at constant pressure

The variation of enthalpy with temperature at constant pressure is also an extensive property called Heat Capacity at constant pressure and denoted by $C_p$ [63]:

$$C_p = \left( \frac{\partial H}{\partial T} \right)_p$$                                   (2.27)

## 2.8.2 Composition and thermodynamic properties of two-temperature plasma

Up to now it has been assumed that ions, neutral particles, and electrons have Maxwellian distributions, and that collisions between these particles are numerous enough to allow equalization of energies between the heavy and light particles. Such a hypothesis leads to a unique temperature (defined as the mean kinetic energy) for both heavy and light particles.

However, if the pressure is lowered or the electric field increased (for example near the electrodes of arcs in atmospheric pressure) and where there are large gradients (near cold walls or when a cold gas is injected into the plasma), equilibrium will no longer exist. When the energy gained by the electrons between two collisions is no longer

negligible compared with the thermal energy $kT_e$, the electron temperature $T_e$ differs from that of the heavy species $T_h$ [64].

### 2.8.3 Local Thermodynamic Equilibrium

When a gas is in thermodynamic equilibrium, it is possible to calculate the particle densities of all the species in terms of the thermodynamic state of the gas.

Partially ionized gases are rarely in complete thermodynamic equilibrium, but they may frequently be in a state of approximate Local Thermodynamic Equilibrium, or LTE. A gas is said to be in LTE when the matter particles are in equilibrium with each other, but when the photons are not in equilibrium with the matter. In most situations, a partially ionized gas is transparent in many frequency intervals, and some radiation therefore escapes from the gas, thus violating a condition necessary for complete thermodynamic equilibrium. For the matter to be in LTE, the collisional rates that populate and depopulate the various energy levels of the matter must exceed the corresponding radiative rates. For a gas in LTE, the Boltzmann and Saha relations can be used even though complete thermodynamic equilibrium does not prevail.

For collision-dominated gases the Boltzmann and Saha relations are often applicable even when other kinds of departures from complete thermo-dynamic equilibrium occur.

It is often possible for the electrons to have a temperature $T_e$ that differs from the heavy particle temperature $T_h$: Both types of particles may still have Maxwellian velocity distributions, but at different temperatures. When it is primarily collisions with electrons which produce the transitions that determine the population of some energy level or the

degree of ionization, the "temperature" that appears in the corresponding Boltzmann or Saha relation should be interpreted as the electron temperature [65].

Plasma will be termed as strongly ionized when its ionization degree is so high that the collisions of electrons with ions become as essential as those with neutral molecules. When strongly ionized, plasma often exhibits a thermodynamic equilibrium of an ionization degree corresponding to the electron temperature.

Since the behavior of equilibrium plasma is related to its temperature, knowing the temperature is important to understand the process involving such plasma, those in spark discharges [66].

The ionization process in strongly ionized plasma differs much from that in weakly ionized plasma, where molecules are ionized by electrons that have acquired their energy directly from the electric field. On the contrary, the field effect in the strongly ionized plasma seems to be smeared out: the field supplies its energy to the electron gas as a whole. Electrons become thermalized by collisions with one another, eventually acquiring a Maxwellian distribution. The gas is ionized by electrons, which have gained sufficient energy through the energy exchange with other particles rather than from the field.

It is important to understand why weakly ionized plasma is in a state of non-equilibrium, while strongly ionized plasma is generally in a state of equilibrium and easier to sustain. Weakly ionized plasma sustained by an electric field is in non-equilibrium in two respects. First, there is a considerable difference between the electrical temperature and the gas temperature (meaning by temperature the measure of mean electron energy, which is not entirely accepted). Second, the ionization degree of such

plasma is much lower than in the thermodynamic equilibrium corresponding to the actual temperature (mean energy) of electrons. [66]

The electron temperature must be high, about 1 eV = 11,600 K, otherwise the number of energetic electrons would be too small to ionize the atoms, that is, the conditions needed for producing plasma would not be met. A high electron temperature is achievable via increasing the electric field strength. The electric temperature in strongly ionized plasma is approximately the same as in weakly ionized plasma, 10,000 K, because the atoms still need to be ionized. But, owning to the high ionization degree, high conductivity and great energy release, the latter turn out to be sufficient to heat the gas up to the electron temperature [66].

### 2.8.3.1 Criteria for Local Thermodynamic Equilibrium

In optically thin plasma the processes leading to radiation are those resulting from spontaneous emissions and radiative recombinations. Griem deduced a very simple criterion of LTE: for a given unit of time, the number of transitions due to electronic collisions between the first excited state and the fundamental level is ten times greater than the number of transitions due to spontaneous emissions [10].

LTE will be realized if the electron density $N_e$ is higher than the critical density $N_e^*$, determined by the relation:

$$N_e^* = 9 \times 10^{11} (E_2 - E_1)^3 T_e \qquad \text{cm}^{-3} \qquad (2.28)$$

$E_2 - E_1$ is the difference in energy between the first exited level and the fundamental level, expressed in electron volts.

Drawin suggested a more precise criterion where the greatest difference of energy between two consecutive levels is obtained for two levels, p and q, unlike the fundamental and the first excitation level.

$$N_e^* = 6.5 \times 10^{10} \frac{g_p}{g_q} (E_p - E_q)^3 T_e^{1/2} \phi_j (\chi_{p,q}) \qquad \text{cm}^{-3} \qquad (2.29)$$

Where $(E_p - E_q)$ is in eV and $T_e$ in K. $(E_p - E_q)$ is the maximum energy difference between two consecutive p and q levels; $g_p$, $g_q$ are the statistical weights of the levels p and q; $\phi_j (\chi_{p,q})$ is a numerical factor, j=1 for neutral atoms and j=2 for the ions [10]:

$$\chi_{p,q} = (E_p - E_q)/kT_e \qquad (2.30)$$

## 2.8.3.2 Partial Local Thermodynamic Equilibrium

For hydrogen and a large number of elements, impact cross-sections decrease and transition probabilities increase as the fundamental level is approached. Consequently, if the electron density decreases, radiative de-excitations, which cause further depopulation of the excitation states and over-population of the fundamental (Figure 2.5), can no longer be neglected for levels $i$ below a certain limit level $h$ ($E_i < E_h$). The relations of LTE are still valid for levels $j$ situated above the level $h$ ($E_j > E_h$), beginning from where the number of transitions through spontaneous emissions is small compared to the number of transitions through impacts. The plasma can be said to be in "partial LTE" [10].
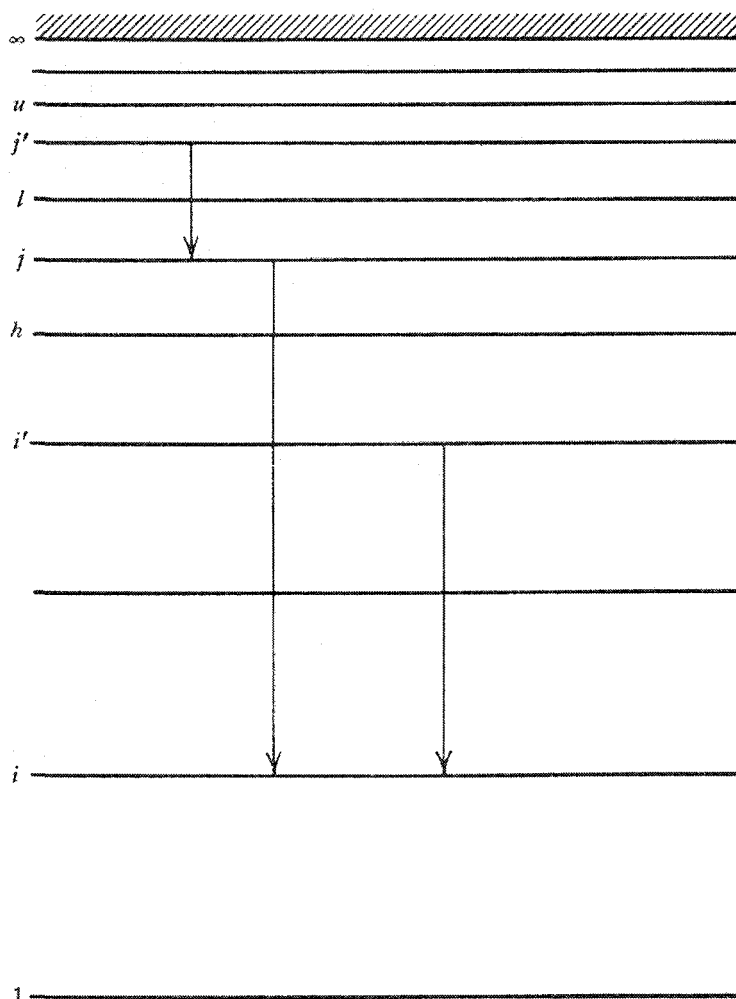
**Figure 2.5.** Scheme of levels [10]

Because the collision frequency is pressure dependent, high pressure will increase this frequency and the electrons' mean free pass between collisions will decrease. The temperature difference between electrons and heavy neutral particles is proportional to the square of the ratio of the energy an electron receives. The temperature difference between electrons and heavy neutral particles is proportional to the square of the ratio of the energy an electron receives from the electric field (E) to the pressure (P). Only in the case of small values of E/P do the temperatures of electrons and heavy particles approach

each other. This is a basic requirement for Local Thermodynamic Equilibrium (LTE) in the plasma [21]. In optically thin plasma, the processes leading to radiation are those resulting from spontaneous emissions and radiative recombination [10]. For LTE plasma the expression for line emissions is a function of electron number density and kinetic electron temperature [67].

In atmospheric pressure plasmas, the rotational temperature is close to the gas temperature owing to fast collisional relaxation. The rotational temperature ($T_{rot}$) is relevant to all processes in which molecules, radicals, and their dissociation products are involved, and the excitation temperature ($T_{exc}$) describes the population of the various energies.

As mentioned earlier Griem deduced a very simple criterion of LTE, expressing for unit time the number of transitions due to electronic collisions between the first excited state and the fundamental level as ten times larger than the number of transitions due to spontaneous emission [10].

Another criterion to verify the existence of LTE is given by Mcwhirter [45]:

$$N_e^* \geq 1.6 \times 10^{12} T_e^{1/2} \chi(p,q)^3 \quad \text{cm}^{-3} \tag{2.31}$$

Where $T_e$ is the electron temperature in K and $\chi(p,q)$ is the excitation potential of level $p$ from level $q$ in eV.

The expressions found by Wilson and Griem are in good agreement. They differ only in the constants [45]:

Griem $9.2 \times 10^{11}$

Wilson $1.3 \times 10^{12}$

Mcwhirter $1.6 \times 10^{12}$

59

## 2.9 Conclusion

To the best of our knowledge no research has been conducted on the measurement of temperature and electron density of an arc formed over an ice surface. However, for other types of discharges, i.e. lightening, these parameters have already been measured.

The review of literature showed that spectroscopy is suitable to measure the properties of electric discharges propagating over an ice surface. Emission spectroscopy is a non-destructive measurement which has been used in different applications.

Rotational temperature, which is close to the gas temperature, can be measured using an appropriate molecular band, i.e. OH (A-X) (0, 0) transition band. The excitation temperature measurement method is generally based on the ratio of line intensities of different spectral lines. However, for non-LTE conditions a correction factor should also be considered. Electron density can be measured from the broadening of a suitable spectral line due to the Stark effect. Established empirical criteria can also be used to examine the existence of local thermodynamic equilibrium from electron temperature and density measurements.

# CHAPTER 3

# METHODOLOGY AND EXPERIMENTAL PROCEDURE

# CHAPTER 3
# METHODOLOGY AND EXPERIMENTAL PROCEDURE

## 3.1 Introduction

In this chapter, the method used for measuring the temperature of arc and electron density will be described along with the experimental procedures. This chapter is divided into two sections. In the first part, the experimental equipment and facilities are introduced. In the second part, the experimental procedure and the method used to analyze the results are explained.

## 3.2 Equipment and facilities

In order to simulate flashover on an ice surface, different experimental systems should be prepared and synchronized. Besides the spectroscopic equipment, high-voltage source, voltage and current measuring instruments, and the data acquisition system (DAQ), the ice-making procedure requires special equipment.

### 3.2.1 High-voltage system

Considering the estimated voltage needed for these particular experiments, a 120kV (maximum), 240 kVA, 60 Hz single-phase test transformer with a 5% short-circuit impedance was used. The output voltage could be adjusted from 0 kV to 120 kV through a regulator, consisting of an SCR control-type feedback thyristor with a dynamic voltage drop of the source below 5% when the load current is 0.5 A. Voltage is increased either manually or automatically at a fairly constant rate of about 3.9 kV/s. Since high-voltage experiments on ice-covered insulators are carried out in an enclosed area, and the transformer is kept outside that area, the security system for this type of experiment is of vital importance. Two circuit-breakers and an accurate relay which interrupts the voltage instantaneously on demand are a part of this security system. The system may be adjusted to cut off the voltage and de-energize automatically when personnel enters any of the test areas. A high-voltage SF6 bushing conducts the applied voltage through the walls of the cold-climate room.

When needed, DC voltage is supplied using the above transformer connected to a rectifier module, comprising a half-wave rectifier and a smoothing capacitor (15.2 μF). Positive and negative DC voltages are obtained by inverting the diode direction in the rectifier. Using the automatic control, DC voltage increases at a constant rate of about 5.5kV/s.

### 3.2.2 Climate room

The climate room is equipped with an HV SF6 composite busing and a water droplet generator. The temperature can reach as low as -30 °C ± 0.2.

This climate room is a thermally insulated and measures 6 m (W) x 6 m (L) x 4 m (H).

### 3.2.3 Spectroscopic system

The spectroscopic analyses were performed using a TRIAX 320 (Jobin Yvon Co.) spectrometer (scanning range from 0 nm to 1,500 nm, dispersion of 2.64 nm/mm and spectral resolution of 0.06 nm.). These specifications are given for a 1,200 grooves/mm grating which should be multiplied by the appropriate scale factor for other groove densities. The spectrometer is equipped with two different gratings: 300 and 1,200 grooves/mm. Top view of the Triax 320 is shown in Figure 3.1.
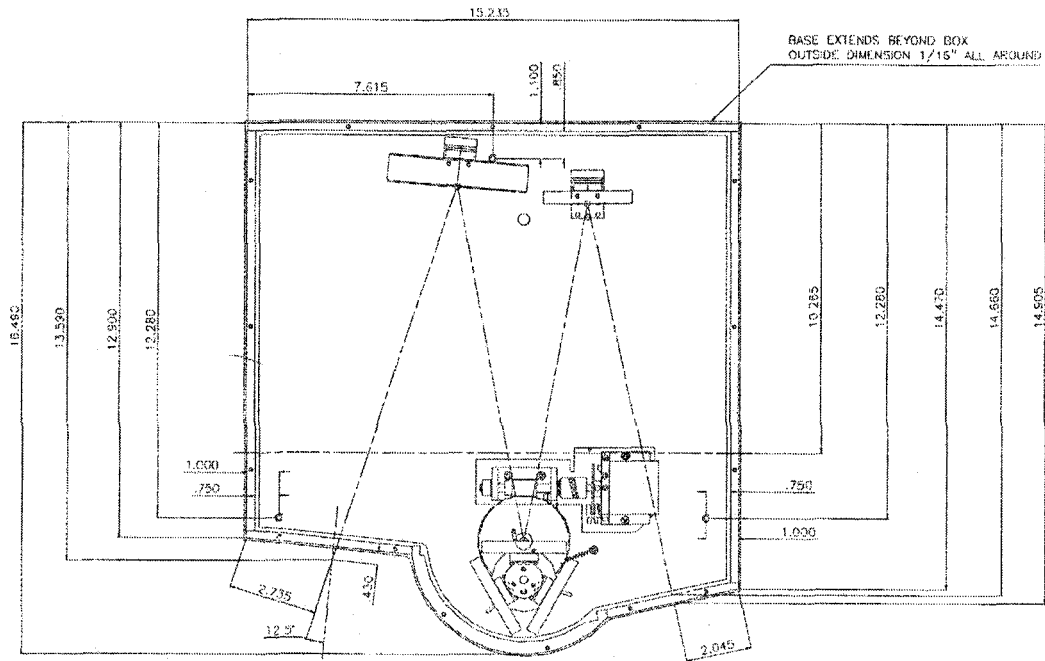
**Figure 3.1.    Triax 320 top view [68]**

The light emitted from the arc is coupled to the entrance slit of the spectrometer by means of a 10 m bundle fiber optic. An optical apparatus 220F is attached to the entrance slit of spectrometer as an adaptor.

The light detector attached to the output of the spectrometer is a gateable charge-coupled device (CCD) camera. The exposure time of the CCD could be set as low as 1ms to a maximum of 49.71 days. Once the CCD has been mounted at the spectrometer output, it should be focused and aligned. The entire operation of the CCD is controlled through a controller (Symphony) and image processing software (SynerJY).

The entire spectroscopic arrangement, including the CCD detector, is placed in a Faraday cage to protect it from electromagnetic interference. The PC is placed in a separate Faraday cage.

### 3.2.4 Data acquisition system

The synchronization between the electrical and spectroscopic measurements is established using a data acquisition (DAQ) system. It monitors the current and CCD shutter signals during the experiments. The test signals were connected to a measuring set through a conditioning box providing protection and insulation. A National Instruments DAQ card (PCI-6035E, 200 kS/s, 16-Bit, 16-Analog-Input Multifunction DAQ) and LabVIEW graphical software was used to acquire high-quality data. The AC voltage signal was attenuated by using a resistive voltage divider. Current measurements were carried out using a current transformer (Pearson™ current monitor: Model 110) with a sensitivity of 0.1 V/A and usable rise time of 20 ns.

In DC experiments, voltage measurements were performed using a resistive voltage divider. The leakage current was measured using a 10-ohm shunt resistance located in series between the ground electrode of the test setup and ground terminal of the HV system.

## 3.3 Experimental procedure

### 3.3.1 Setup

Because of the time-consuming ice accumulation process of in the climate room with nozzles, random distribution of discharge paths along ice-covered insulators, and practical problem associated with capturing the light of arc, a simple physical model was

chosen for the experiments. It consists of a Plexiglas mould, 140 cm (L)* 15 cm (W) * 5 cm (D), filled with de-ionized water at several freezing stages to obtain the flattest possible surface. The last layer was poured in three steps with freezing water with predetermined conductivity by adding pure NaCl to de-ionized water. After each step, the model was returned to the cold chamber to let the layer freeze. Finally, an air gap of about 6 cm was made at one end by cutting and removing the ice while the other end was grounded. The HV electrode is a copper hemisphere 2 cm in diameter. Figure 3.2 shows a schematic diagram of the physical setup.
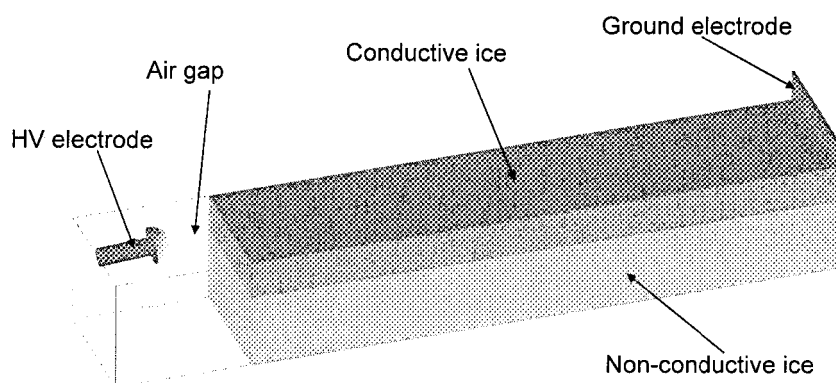


**Figure 3.2.  Ice geometry**

Optical emission spectroscopy (OES) was used to reach the mentioned objectives. A monochromator was set to receive light from a region of discharge below the air gap. Time-resolved spectra were recorded by adjusting the exposure time of a Charged Coupled Device (CCD) detector connected to the output slit of a spectrograph set to 8 ms. The time interval between two consecutive acquisitions was 27 ms. The signal from the shutter of the CCD detector, leakage current and applied voltage were recorded

simultaneously through a data acquisition system. This provided the time relation between the spectroscopic and electrical measurements.

Figure 3.3 shows a schematic of the experimental setup for optical emission spectroscopy (OES) measurements.
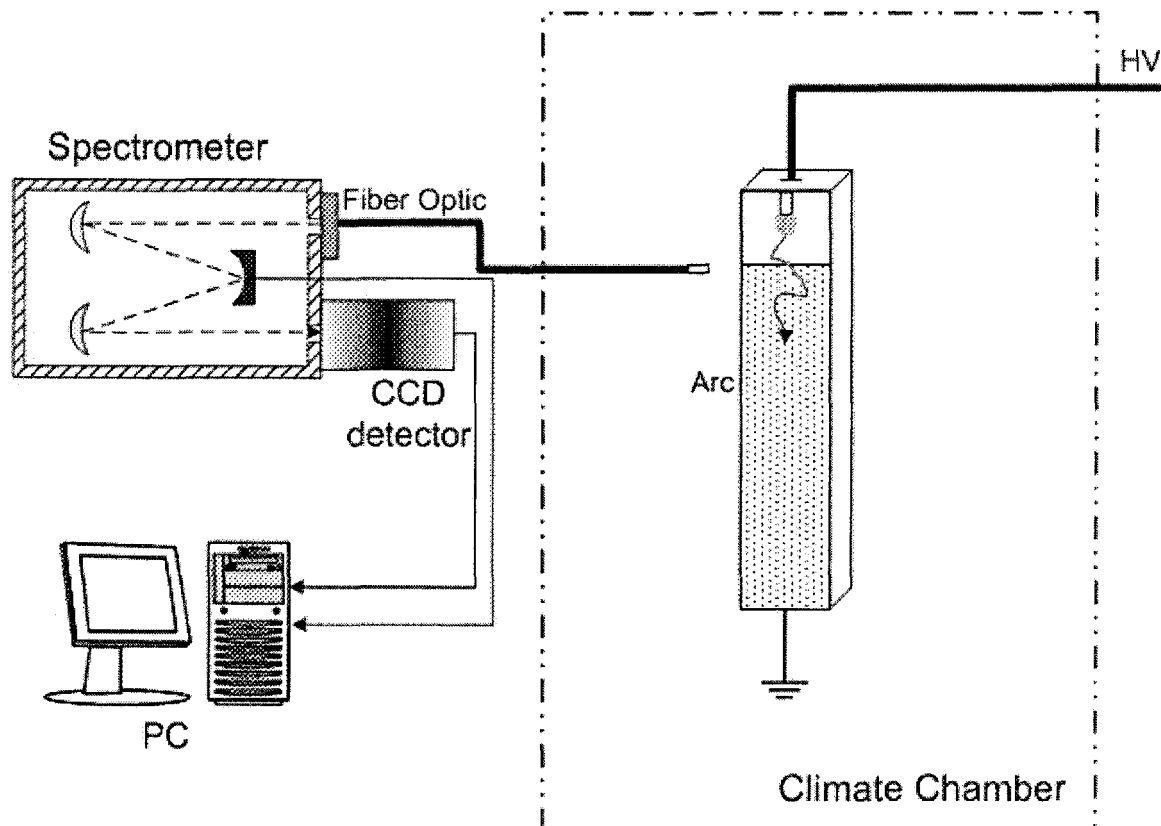


**Figure 3.3.** **Schematic diagram of the experimental setup**

## 3.3.2 Calibration

Spectroscopic temperature measurements require the knowledge of either the relative or absolute intensity of spectral features. The measured emission spectra must be corrected for the spectral response of the detection system, which includes lenses,

mirrors, monochromator, optical fiber and CCD. The detector system had to be calibrated in the spectral range of interest. Calibrations of spectral intensities were made using a tungsten lamp.

A mercury lamp was used as a source for CCD wavelength and monocramotor calibrations.

Light from a tungsten filament lamp emitted onto a Teflon surface was used as the intensity calibration source. The spectral lines from the discharge were corrected according to the known spectrum of this tungsten lamp.

### 3.3.3 Current and voltage measurements

As a general rule, the flashover process on ice-covered insulators includes the following stages: first, several violet arcs appear across the air gaps (or ice-free zones); second, one of the arcs propagates along the ice surface forming a white arc; and finally, when the white arc reaches a certain length, a flashover arc occurs eventually leading to a short-circuit [1].

Recording the current, CCD shutter signal and time-resolved spectra simultaneously through a data acquisition system enabled us to analyze different stages such as the white arc and flashover arc over the ice surface. As mentioned, synchronization between electrical (current and voltage) and spectroscopic system was achieved through the DAQ system.

Figure 3.4 and Figure 3.5 show the voltage and current measurement devices with AC and DC applied voltage. A resistive voltage divider was used to measure the voltage for both applied voltages. In AC (see Figure 3.4), current measurements were

carried out using a current transformer (Pearson™ current monitor: Model 110) with a sensitivity of 0.1 V/A and usable rise time of 20 ns.

In DC (see Figure 3.5), leakage current was measured using a 10-ohm shunt resistance between the ground electrode of the test setup and ground terminal of the HV system.
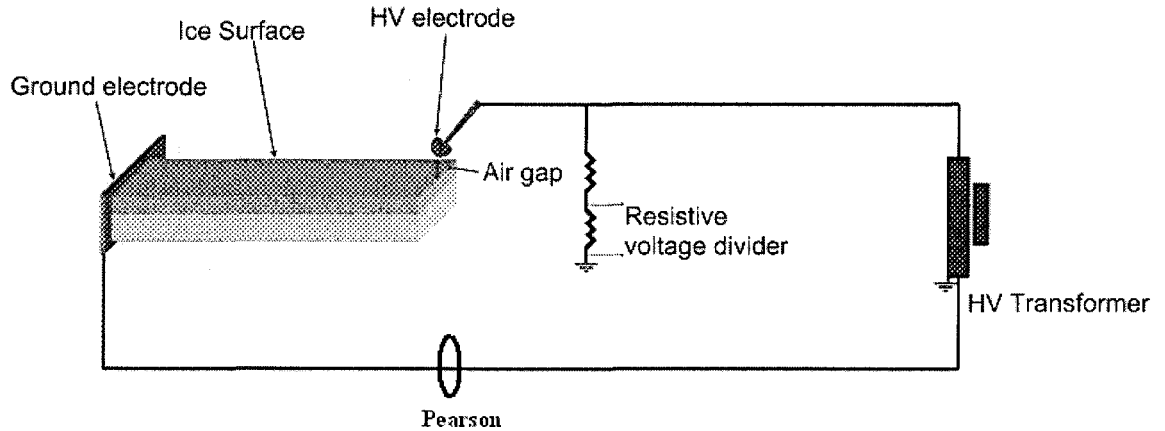


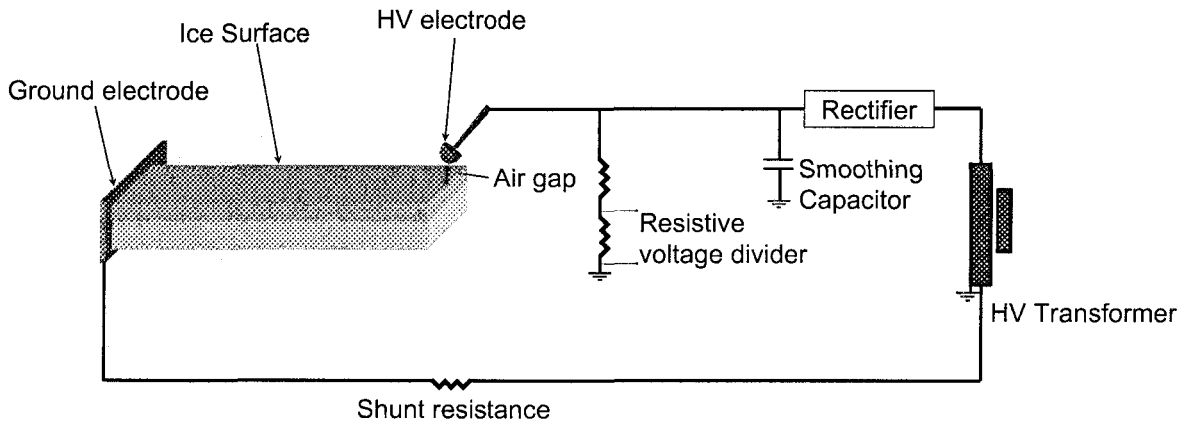**Figure 3.4.** Setup arrangement to measure AC voltage and current



**Figure 3.5.** Setup arrangement to measure DC voltage and current

### 3.3.4 Rotational temperature measurements

In this work, rotational temperature, which is equal to the gas temperature in atmospheric pressure, is measured using OH (A-X) emission bands. The rotational temperature can be obtained by fitting the entire band, or more simply from the relative intensities of two distinct peaks of OH bands at about 307 nm and 309 nm.

With the fitting method, synthetic spectra were produced using simulated OH (A-X) (0-0) emissions, normalized to P-branch peak, relative to the rotational temperature. With the experimental spectra normalized to P-branch, the rotational temperature can be derived by finding the best fit that has the same P/R branch intensity ratio, and also coincides along the whole band system.

To obtain the variation of rotational temperatures, with discharge current, relative intensities of the two peaks of OH (A-X) can be used. As mentioned in Chapter 2, relative intensity of these two peaks varies rapidly with the rotational temperatures. The relationship between the ratios of intensities of these two peaks with rotational temperatures can be simulated with SPECAIR software. Using this relationship and employing an interpolation of data, the rotational temperatures of the experimental spectra for different current levels can be derived.

In addition, the $N_2^+$ $1^{st}$ negative system can also be used to measure the rotational temperature. As the $N_2^+$ $1^{st}$ negative system could not be observed at low current levels, this method could not be used over the entire current range. Because this system appears at higher excitation levels, a spectrum from an instant when the discharge has a high current value can be selected for analysis. This experimental spectrum can be compared with the numerical spectra of the $N_2^+$ $1^{st}$ negative system ($B_2\Sigma^+$-$X_2\Sigma^+$) for a range of 380

nm to 392 nm, relative to rotational temperatures. Rotational temperatures can be derived by finding the best fit of whole region of synthetic and experimentally obtained spectra.

The rotational temperatures of positive and negative DC arcs, and AC arcs were measured and compared during arc propagation.

### 3.3.5 Excitation temperature measurements

The excitation temperature of the arc column was determined using the ratio of intensities of the spectral lines and the Boltzmann method.

Three copper lines of 510 nm, 515 nm and 521 nm, and singly ionized oxygen lines of 777 nm, 844 nm and 926 nm were used for excitation temperature measurements.

Excitation temperature was obtained by applying the Boltzmann method for the following two line intensity ratios: Cu I 510 nm /Cu I 515 nm, Cu I 510 nm/ Cu I 521 nm, OI 777 nm/OI 926 nm, OI 844 nm/OI 926 nm. It is well known that the spectral lines selected for the construction of a Boltzmann plot should satisfy certain requirements [27]. They should be strong lines having approximately equal intensities. The most important of these requirement is that the difference in excitation energy should be large enough (1-2 eV) to ensure accurate temperature measurements. This requirement is well satisfied for the selected line pairs as seen in Table 3.1.

**Table 3.1. Table Spectroscopic parameters of copper spectral lines**

| Wavelength | E upper state (eV) | E lower state (eV) |
|---|---|---|
| Cu 510.554 | 3.817 | 1.389 |
| Cu 515.324 | 6.191 | 3.786 |
| Cu 521.820 | 6.192 | 3.817 |
| O 777.34 | 10.74 | 1.389 |
| O 844.65 | 10.988 | 3.786 |
| O 926.66 | 12.0786 | 3.817 |

Temperature measurements were made by evaluating the following two-line intensity ratios: Cu I 510 nm/Cu I 515 nm, Cu I 510 nm/Cu I 521 nm, OI 777 nm/OI 926 nm, OI 844 nm/OI 926 nm, and by using the measured ratio in conjunction with the expression [27]:

$$T_{exc} = \frac{-5040(E_b - E_a)}{\log(\lambda I / gA)_b - \log(\lambda I / gA)_a} \qquad (3.1)$$

where $T_{exc}$ is the excitation temperature (K), $E$ is the upper level excitation energy (eV), $A$ the (relative) transition probability (S$^{-1}$), $g$, the statistical weight, $\lambda$, the wavelength (nm), and $I$, the (relative) intensity; the subscripts $a$ and $b$ refer to the lines $a$ and $b$ respectively.

Plotting $\log(\lambda I / gA)$ versus excitation energy ($E$) should yield a straight line (Boltzmann plot) with slope $m$, from which the excitation temperature can be calculated as:

$$T_{exc} = -5040 / m \qquad (3.2)$$

The Boltzmann plot applying for two selected lines pairs of copper yield two straight lines. The excitation temperature is calculated from the mean value of two line slopes. Using this method, the excitation temperature can be calculated for different current values. The same method can be applied to the selected oxygen line pairs.

When the local thermodynamic equilibrium deviates, the non-equilibrium parameter $b$ (defined as the ratio of the actual to calculated LTE level populations) may be used [40]. Using the method proposed by Burton and Blades [40], the actual populations can be calculated, allowing theoretical Boltzmann plots to be constructed. Hence, the intensity of a spectral line resulting from transition from level $m$ to $n$ is:

73

$$I = \frac{1}{4\pi} \frac{hc}{\lambda_{mn}} A_{mn} g_m \frac{b_{atom}^m n_i}{z_{int}(T)} e^{-(E_m/kT)} \qquad (3.3)$$

where $A_{mn}$ is the transition probability, $\lambda_{mn}$ is the wavelength between the upper

level $m$ and lower level $n$ , $g_m$ is the statistical weight and $E_m$ is the energy of upper level;

$n_i$ is the total number density of the chemical species $i$ and $z_{int}(T_{exc})$ is the internal

partition function calculated at the temperature $T_{exc}$, $b_{atom}^m$ is a non-equilibrium parameter

that can be evaluated for the considered atom as [40]:

$$b_{atom}^m = 1 + \frac{6.55 \times 10^{13} E_\infty (E_\infty - E_m)^{2.607}}{n_e T^{0.107}} \qquad (3.4)$$

where $E_\infty$ is the ionization energy(eV) and $n_e$ is the electron density expressed in

cm$^{-3}$.

Considering a given electron density and employing the ionization potential $E_\infty$

for copper (7.7264 eV) and for oxygen (13.6181 eV), the non-equilibrium parameter $b_{atom}^m$

is calculated using Equation (3.4) at each calculated excitation temperature.

This non-equilibrium parameter may be incorporated into a Boltzmann plot

as $\log(\lambda I / gAb_{atom}^m)$, to reconstruct Boltzmann plots.

### 3.3.6 Electron density measurements

Electron density is estimated from an analysis of the Balmer line $H_\alpha$ profile,

broadened by the Stark effect. As mentioned in Chapter 2, Stark profiles of $H_\alpha$ lines for

different electron densities at specific $T_e$ have been provided by Griem.

To compare experimental spectra with Griem's Stark profiles of $H_\alpha$ lines, one

should consider instrumentation broadening. Measured instrumentation functions should

also be convolved with Griem's data. If a recorded $H_\alpha$ line is placed on a background continuum, in order to use the profile for Stark-effect analysis, this background continuum should be subtracted from the original profile.

Another simple and still precise variation of this method is the application of Full-Width at Half-Maximum (FWHM) of profiles. The FWHM of Griem's profiles for different electron densities and considering instrumentation broadening can be measured. Fitting the simulation results using a function could yield a relationship between the FWHM and electron density of $H_\alpha$ line. Thus, for each experimental spectrum the FWHM of $H_\alpha$ line could be calculated by subtracting the background level of the adjacent continuum from the profile. Electron density can be calculated using evaluated relations from measured FWHM.

### 3.3.7 Local Thermodynamic Equilibrium

To verify the existence of LTE, the criteria stated by equation (2.31) could be used. When electron temperature and density are known, this expression can be assessed. It should be noted that this inequality is a necessary, but not sufficient condition for plasma to be in LTE. Another important requirement can be examined from the comparison of different temperatures, i.e. excitation and rotational temperatures. A considerable difference in the values of these temperatures could be an indication of non-LTE condition.

## 3.4 Conclusion

Optical emission spectroscopy is selected as a methodology to achieve the mentioned objectives.

A simplified physical model is used for the experiments because of the time-consuming ice accumulation process and practical problems associated with capturing the light of arc. Discharge current and shutter signal data are transmitted to a data acquisition system. This provides a relation between the electrical and spectroscopic measurements.

Rotational temperature measurement method consists of measuring the ratio of peak intensities of the OH (0, 0) R and P branches and comparing them with computer-simulated spectra.

Excitation temperatures are calculated using the intensity ratios of different copper and oxygen lines.

Wherever inequality between excitation and rotational temperatures exists, deviation from LTE has occurred. In such cases, the Burton and Blade correction factor can be used to reconstruct the Boltzmann plots.

To calculate the electron density in the discharge column, a method based on broadening of the $H_\alpha$ line considering instrumentation broadening is employed.

# CHAPTER 4

# EXPERIMENTAL RESULTS

# CHAPTER 4

# EXPERIMENTAL RESULTS

## 4.1 Introduction

Using the facilities and methodology described in Chapter 3, several experiments were performed. These experiments were oriented to achieve the stated objectives. This chapter explains the results of the tests performed. Firstly, the spectra taken from an arc over an ice surface will be described and analyzed. Next, the results of rotational and excitation temperature measurements, as well as those of electron density, will be explained.

## 4.2 Identified spectral lines and bands

Typical emission spectra of DC discharge are shown in Figure 4.1, Figure 4.2 and Figure 4.3.

In the UV-VIS emission spectrum (Figure 4.1), strong emissions from OH (A-X) vibrational bands were detected with distinct peaks of about 306 nm and 309 nm. OH radicals were formed from water vapour in ambient air. In our case, in which one end of discharge is placed over an ice surface, water also evaporated into the discharge column.

As usual with atmospheric air discharges, $N_2$ molecular band spectra are detectable. Emissions from the $N_2^+$ 1$^{st}$ negative system $(B_2\Sigma^+ - X_2\Sigma^+)$ for (0-0) and (2-1) bands were observed at 391.1 nm and 356.1 nm, respectively (Figure 4.1). The presence of $N_2^+$ indicates that the plasma has high electron temperature and a significant level of non-equilibrium [69]. An NH (A-X) molecular band is also visible at 336 nm.
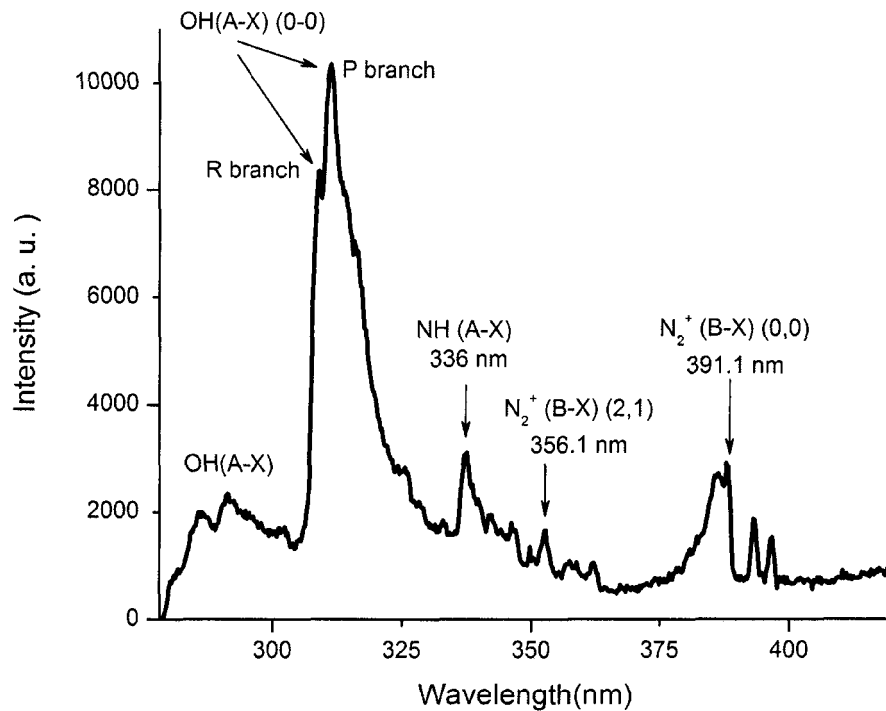


**Figure 4.1.** **Identified bands from a typical spectrum of light emitted from DC discharge for the region between 280 nm and 420 nm**

Figure 4.2 shows several lines from copper in CuI (510.5 nm), CuI (515.3 nm) and CuI (521.8 nm) and also $H_\alpha$ (656.3 nm) from hydrogen Balmer series.

During the observation of time-resolved spectra of the white arc, a high intensity line at about 590 nm was present (Figure 4.2). This line actually consists of two

neighbour lines of sodium, often called Sodium-D, at 590 nm and 590.6 nm, respectively. Because of the low excitation energy of the Sodium-D lines, which is about 2.1 eV [70], these lines could be ionized easily in the vicinity of arc contact with the ice surface.

Due to the presence of oxygen in ambient air, three singly ionized oxygen OI (777.3 nm), OI (844.6 nm) and OI (926.6 nm) lines appeared, as shown in the Figure 4.3.
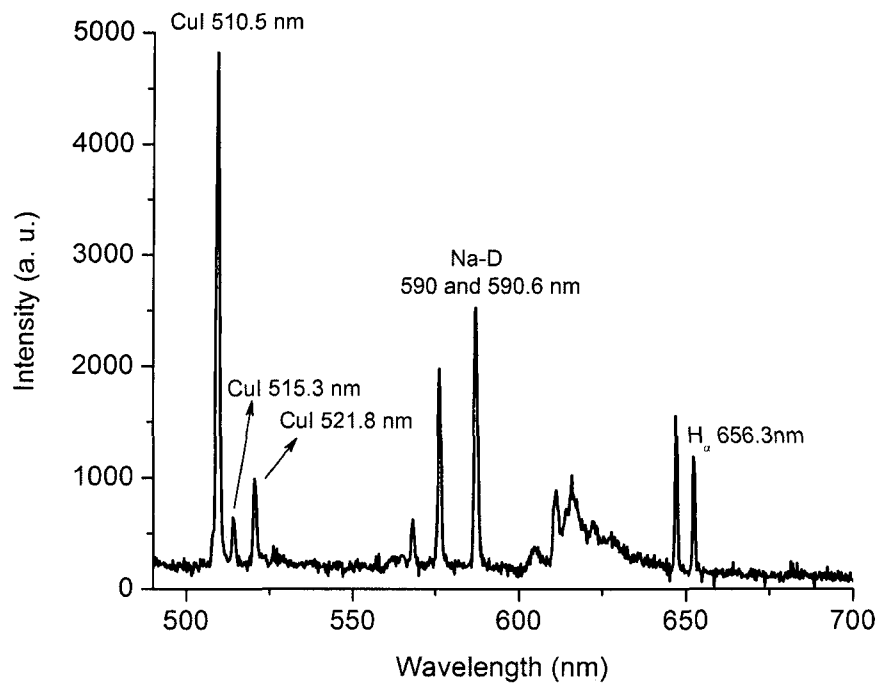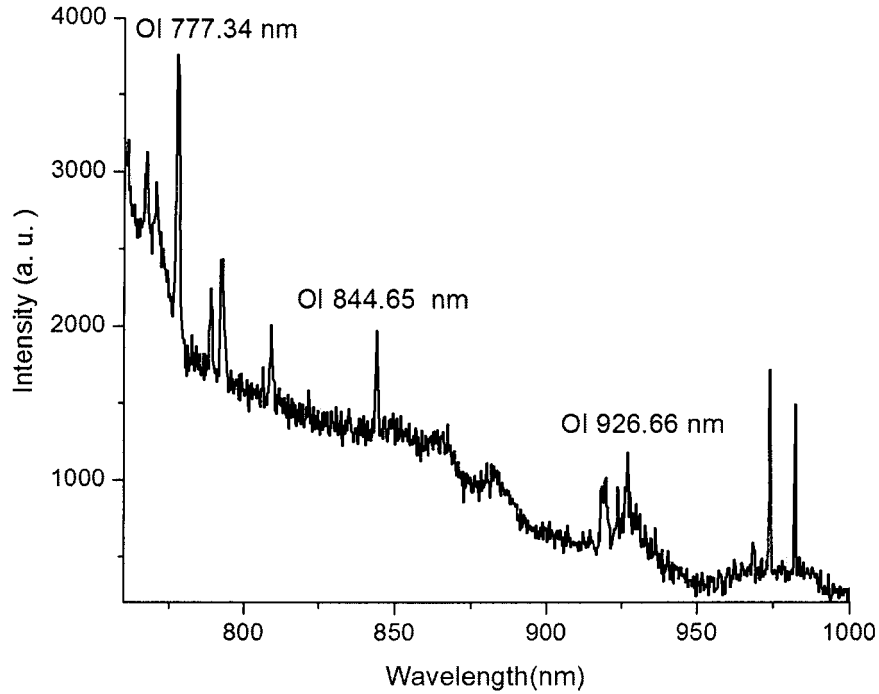


**Figure 4.2.** **Identified lines from a typical spectrum of light emitted from DC discharge for the region between 500 nm and 700 nm**

**Figure 4.3.** Identified lines from a typical spectrum of light emitted from DC discharge for the region between 750 nm and 1000 nm

## 4.3 Gas temperature measurements

### 4.3.1 AC applied voltage

Figure 4.4 shows a spectrum captured during white arc propagation using AC applied voltage. Figure 4.4 shows a spectrum taken from final jump (flashover arc). From the comparison of Figure 4.4 and Figure 4.5 the following conclusion could be made: During discharge development, due to the presence of water molecules, OH(A-X) transition is dominant Figure 4.4). This dominant band is replaced by the spectral bands of the first negative system (FNS) of $N_2^+$ and a strong emission of the atomic line of hydrogen ($H_\beta$) in the flashover spectrum (Figure 4.5).
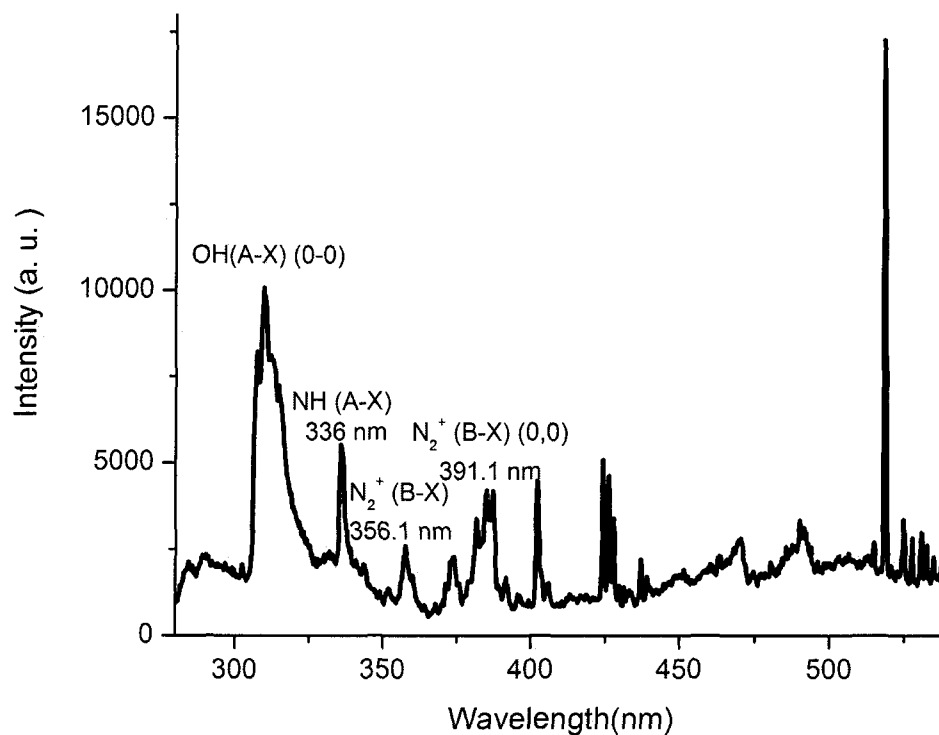
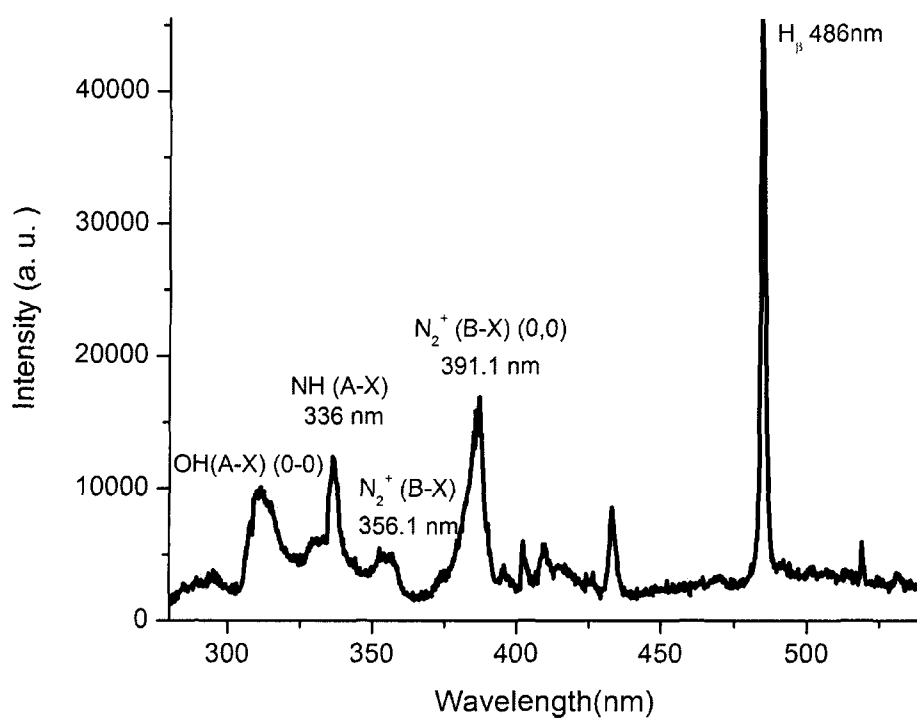**Figure 4.4.** Spectrum of a discharge during its development over the ice surface



**Figure 4.5.** Spectrum of an arc during the final jump (which leads to flashover)

82

The variations of the peak intensities of different molecular emission bands and hydrogen atomic lines are shown in Figure 4.6. The last points highlighted with filled shapes correspond to the intensity of bands and line emissions in the last captured spectrum, which to the flashover instant. It can be seen that increasing the discharge current results in an increase of the intensity of molecular emission bands. In the flashover instant, the intensity of the OH emission band remains constant, while the intensity of NH (A-X) and FNS of $N_2^+$ increases to a high value. Another interesting aspect is the hydrogen atomic line ($H_\beta$) at the instant of flashover, which appears only in the last spectrum.
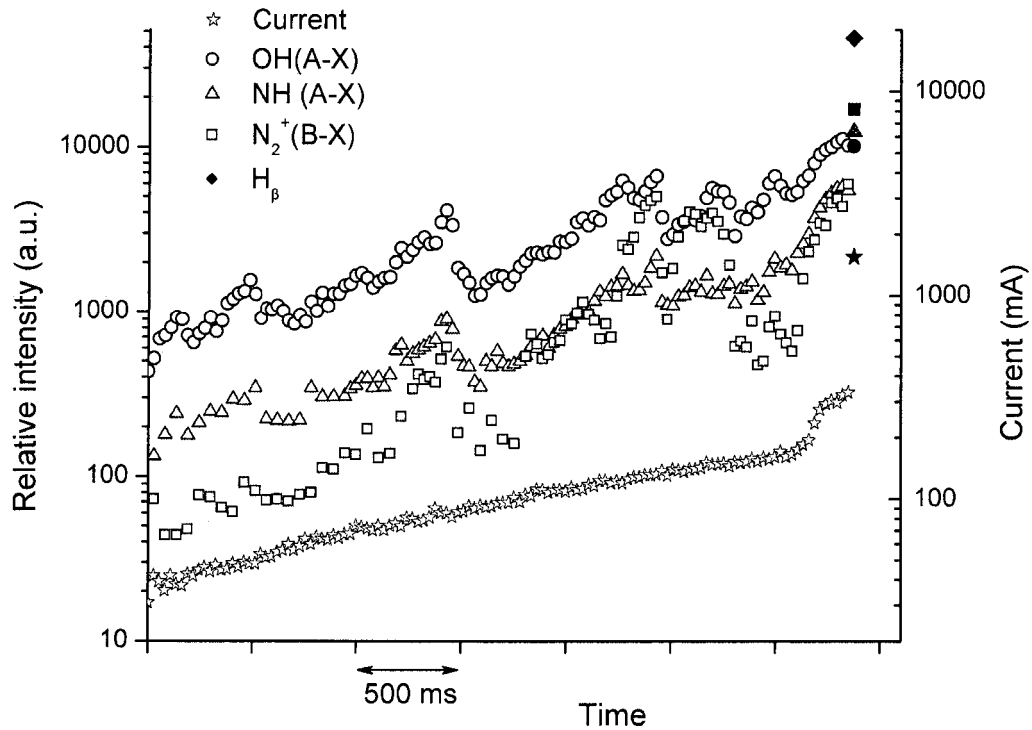


**Figure 4.6.** Emission intensity variation of peak intensities of OH (A-X) at 309 nm, NH (A-X) at 336 nm, $N_2^+$ (B-X) at 391.1 nm, and $H_\beta$ at 486 nm. Measurement points at the end emphasized with filled shapes correspond to the flashover instant. The variation of the RMS value of AC current has also been depicted.

For the discharge current shown in Figure 4.7, the spectroscopic emission method was used to measure rotational temperatures from the ratio of the P and R branches of the OH (A-X) band. Figure 4.8 shows the ratios of R/P branch peaks during arc propagation. For each spectrum, the RMS current during the opening of the CCD shutter was calculated.

Relative intensities of the two peaks of OH (A-X) vary rapidly with rotational temperatures, and this method could be used as a sensitive thermometer [8]. Figure 4.9 shows the simulation results performed with SPECAIR software [36], which yields the relationship between the ratios of intensities of these two peaks with rotational temperatures. Using the results of Figure 4.8 and employing an interpolation of data in Figure 4.9 , rotational temperatures were calculated for different currents. The results are shown in Figure 4.10.
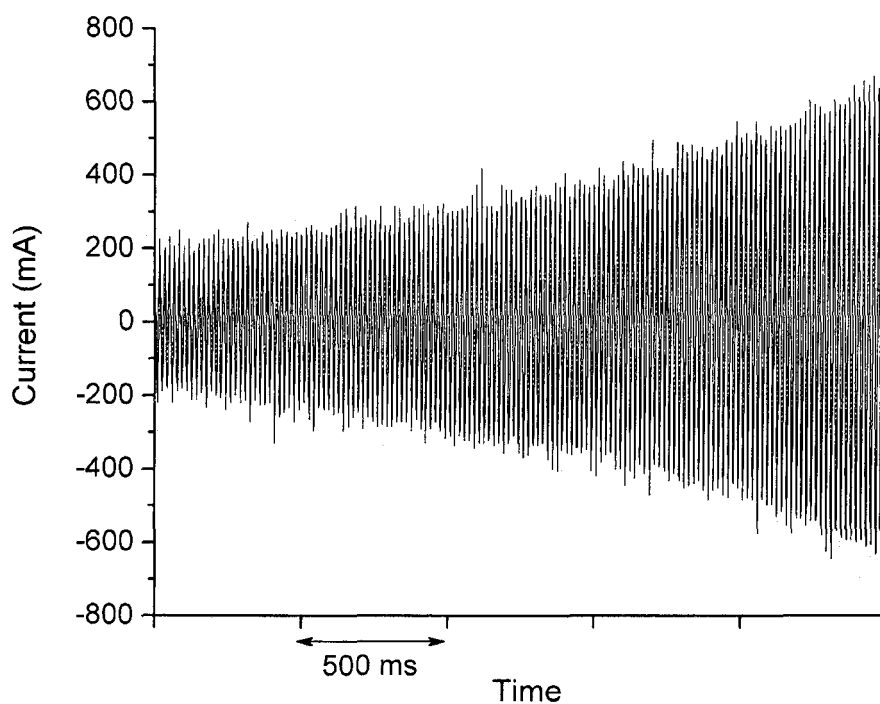


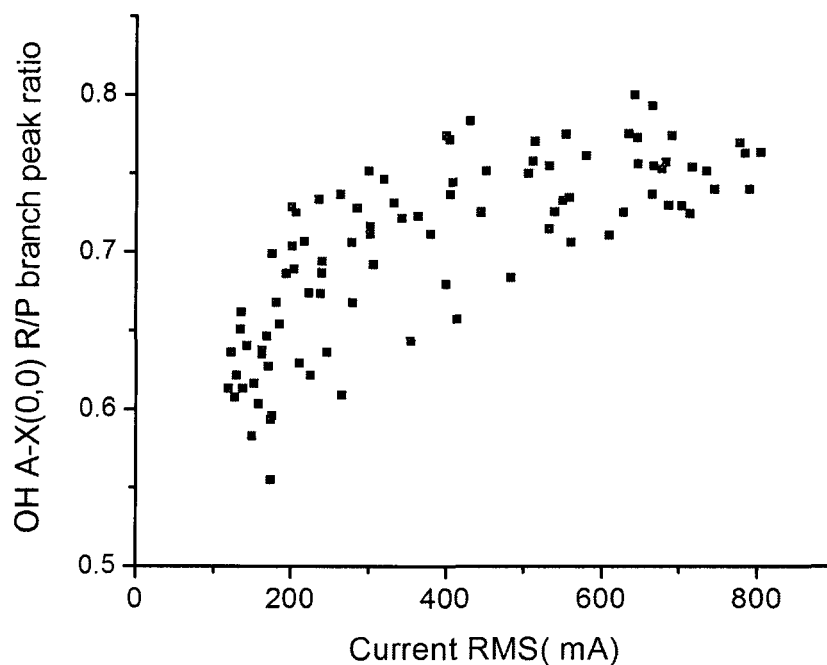**Figure 4.7.** **Current waveform profile used for rotational temperature computation.**

**Figure 4.8.** Ratios of peak intensities of the OH (0, 0) R and P branches as a function of RMS value of current during each spectrum acquisition (8ms).
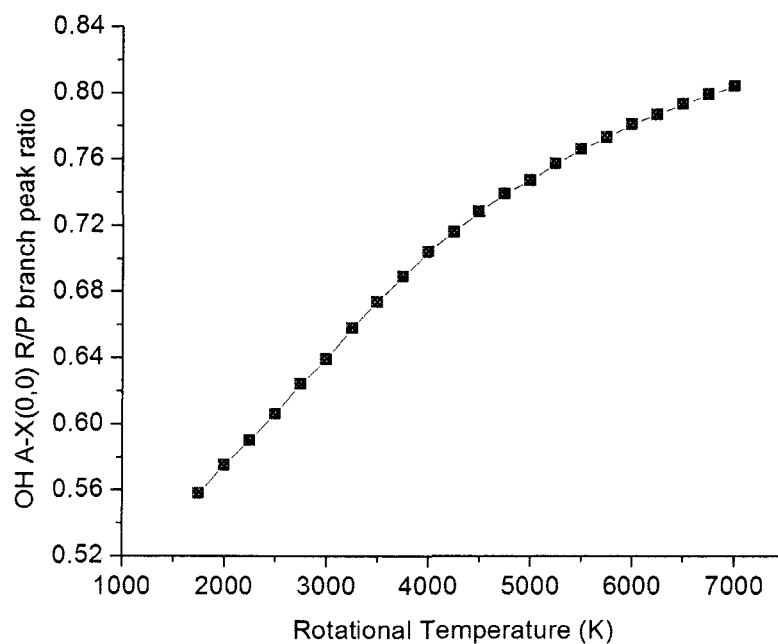


**Figure 4.9.** Simulated ratio of peak intensities of the OH (0, 0) R and P branches relative to rotational temperatures. These simulations were performed with SPECAIR [8] software.
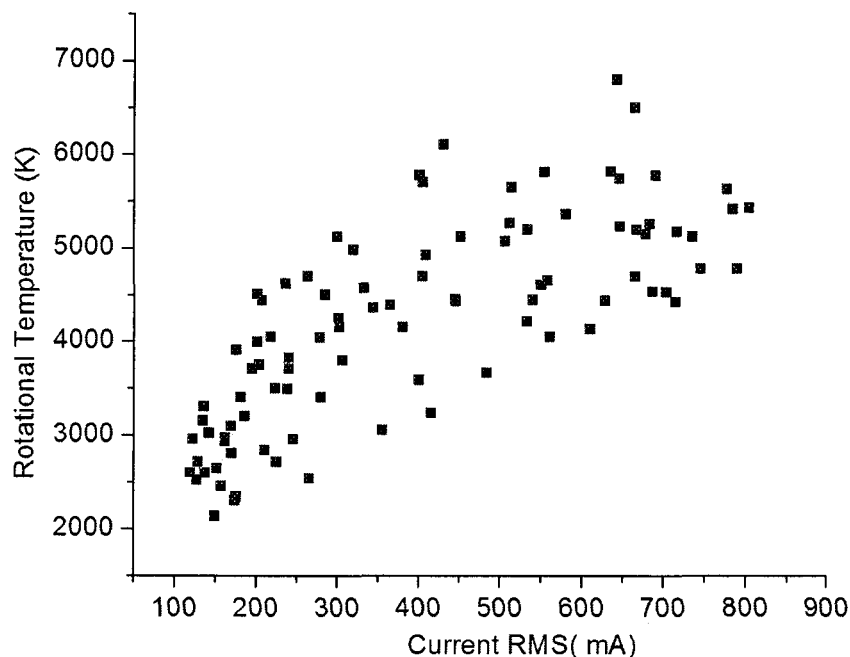
**Figure 4.10.** Evolution of gas temperatures during the AC discharge obtained from the rotational temperatures of OH emission bands calculated by ratio of peak intensities of the OH (0, 0) R and P branches.

## 4.3.2 DC applied voltage

### 4.3.2.1 DC-

Figure 4.11 shows the profile of recorded spectra during discharge development. The spectra were recorded with an exposure time of 8 ms, and the time interval between two consecutive acquisitions was 27 ms. This figure shows clearly that the intensity of OH bands increases during arc propagation, while the intensity of the $N_2^+$ $1^{st}$ negative system at 391.1 nm increases suddenly at the later stages of arc development, when the current is higher. The discharge current variation for the same experiment is also depicted in Figure 4.12.

Synthetic spectra were produced using simulated OH (A-X) (0-0) emissions, normalized to P-branch peak, relative to the rotational temperature. The dashed lines in Figure 4.13 are the theoretical spectra calculated with rotational temperatures of 4,000 K, 4,500 K, 5,000 K, and 5,500 K. In the same figure, the experimental spectra for two different current intensities are depicted with solid lines. As illustrated, rotational temperatures can be derived by finding the best fit that has the same P/R branch intensity ratio, and also coincide along the whole band system. For current values of 228 mA and 765 mA, the simulated spectra for 4,000 K and 5,500 K, respectively, could be considered as the best fit.

Figure 4.14 shows that measured temperatures using OH transition versus discharge current for a DC- discharge. The values shown are the rotational temperatures, which are approximately equal to the neutral gas temperatures, obtained from the best fit with the experimental spectra.

Because of the appearance of the $N_2^+$ $1^{st}$ negative system at higher excitation levels, a spectrum from an instant when the discharge has a high current value was selected for analysis.
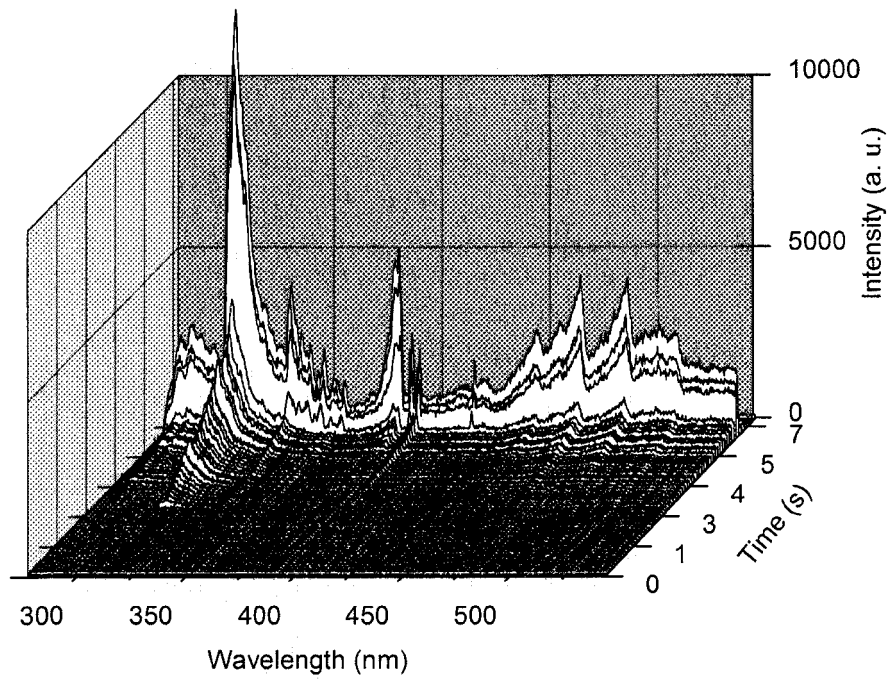
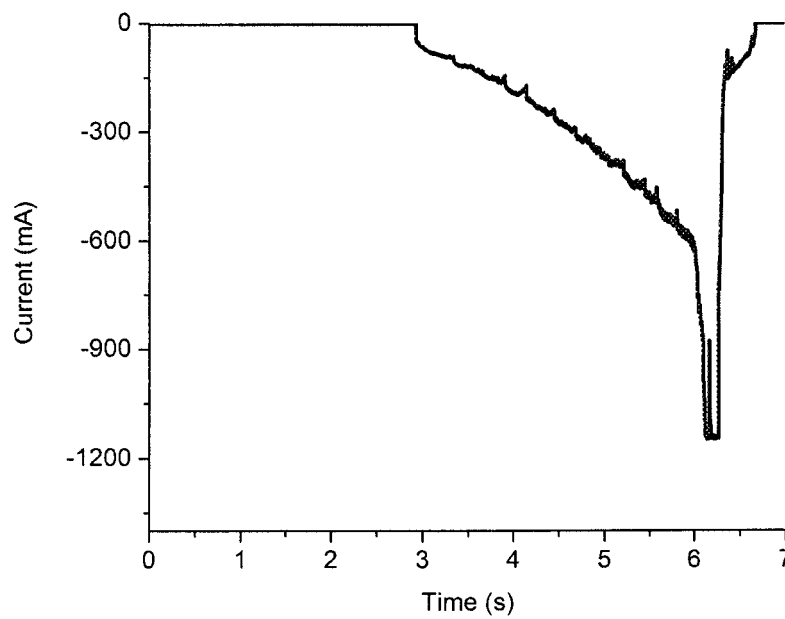**Figure 4.11.** The profile of recorded spectra during discharge development.



**Figure 4.12.** Current variation during discharge development leading to flashover.
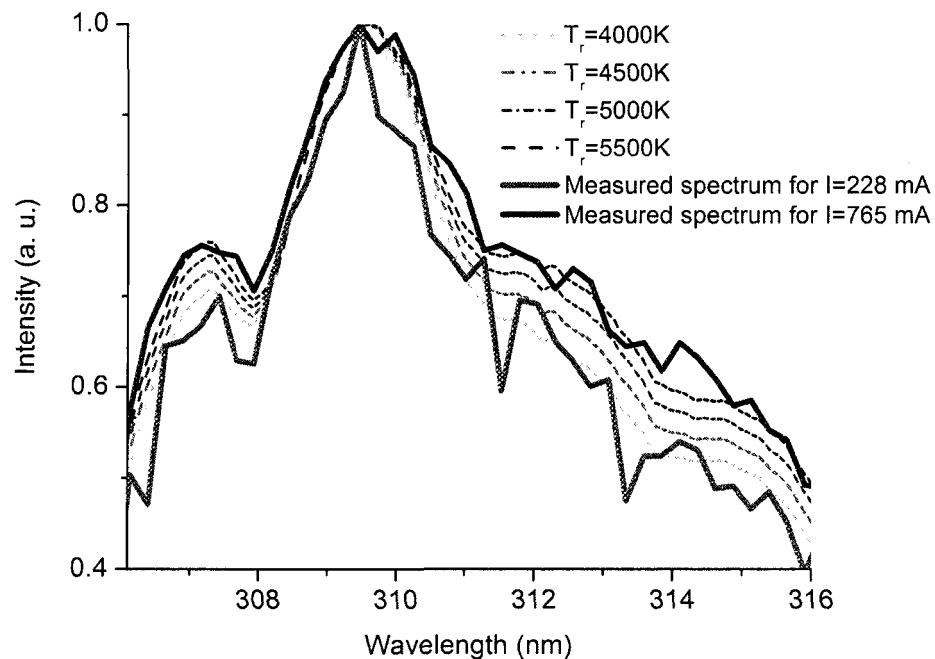
**Figure 4.13.** Experimental spectra recorded for 228 mA and 765 mA discharges, and synthetic spectra of OH A-X (0,0) emissions simulated for different rotational temperatures.
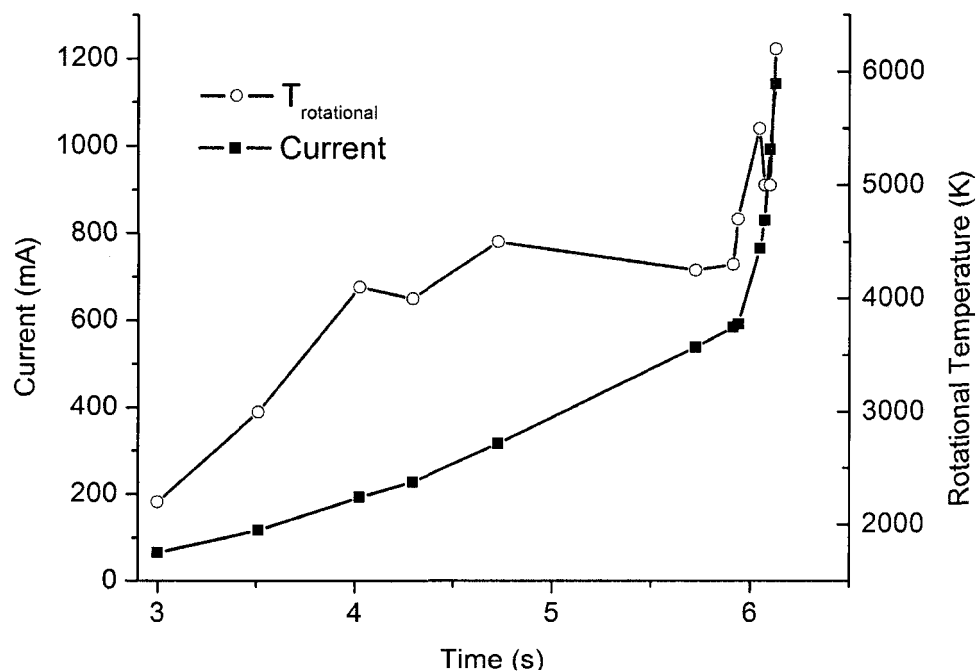


**Figure 4.14.** Rotational temperature measurements using UV-OH (A-X) for a DC-discharge over an ice surface for different discharge currents.

Figure 4.15 shows the measured spectrum for a discharge current of 1,000 mA

and the numerical spectra of the $N_2^+$ $1^{st}$ negative system ($B_2\Sigma^+$-$X_2\Sigma^+$) for the region of

380 nm to 392 nm, versus rotational temperatures. The dashed lines are the theoretical

spectra calculated with rotational temperatures of 5,000 K, 6,500 K and 8,000 K.

Rotational temperatures can be derived by finding the best fit of whole region, which

results in 6,500 K. This value is in good agreement with the results obtained by fitting the

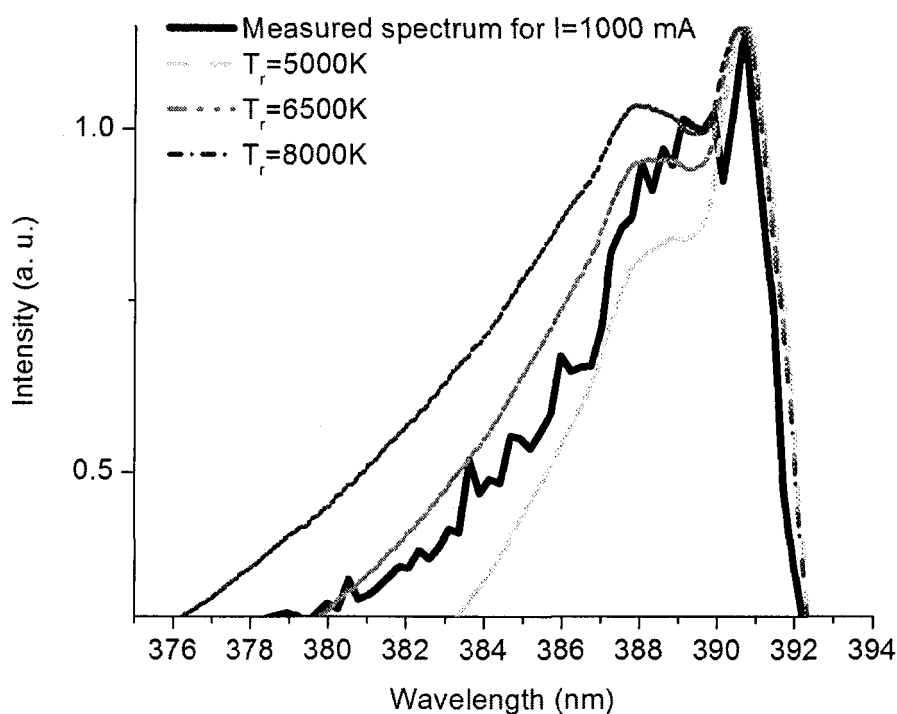OH band from which it was calculated to be about 6200 K.



**Figure 4.15.** **Experimental spectrum recorded for 1,000 mA discharge and synthetic**

**spectra of the $N_2^+$ 1st negative system simulated for different rotational temperatures.**

#### 4.3.2.2 DC+

Using the same method (Relative intensities of the two peaks of OH), the rotational temperatures of DC+ arc over the ice surface was found, as shown in Figure 4.16. These results were obtained from several experiments.
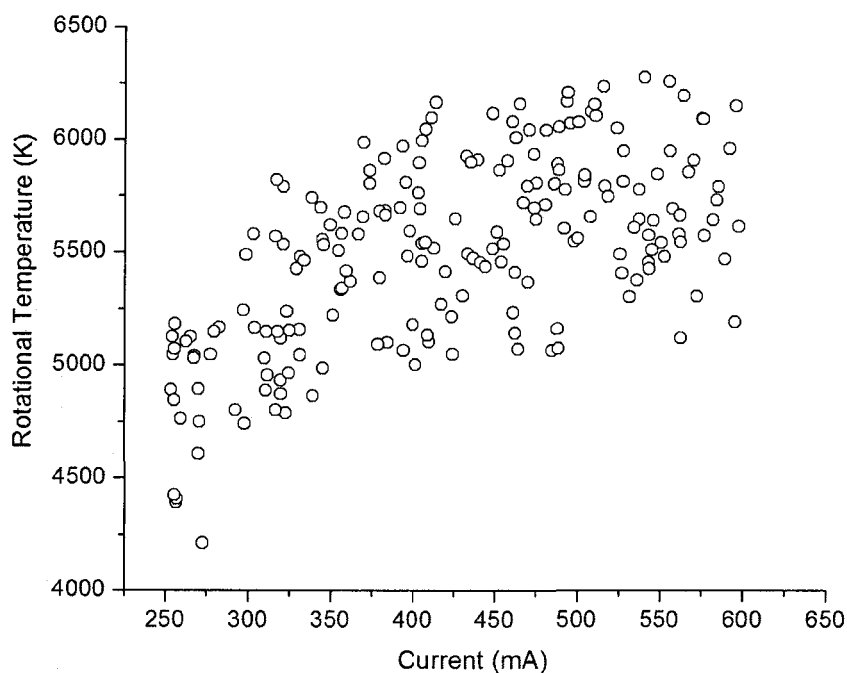


**Figure 4.16. Evolution of gas temperatures during DC+ discharge obtained from the rotational temperatures of OH emission bands calculated by ratio of peak intensities of the OH (0, 0) R and P branches.**

## 4.4 Excitation temperature

Figure 4.17 (a) shows 3D time-resolved spectra of the arc in the infrared region. Due to the presence of oxygen in ambient air, three singly ionized oxygen OI (777.3 nm), OI (844.6 nm) and OI (926.66 nm) lines are present. Figure 4.17 (b) shows the 3D time-resolved spectra of the copper lines at 510 nm, 515 nm and 521 nm.

The above three copper lines have already been used for excitation temperature measurements [71, 72 and 73]. Temperatures could also be measured from the singly ionized oxygen lines at 777 nm, 844 nm and 926 nm [24, 72 and 49].
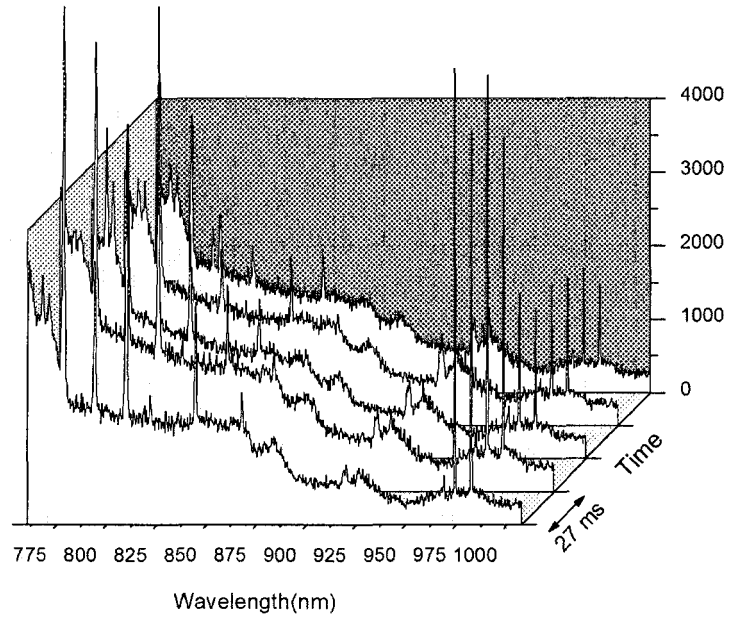


(a)
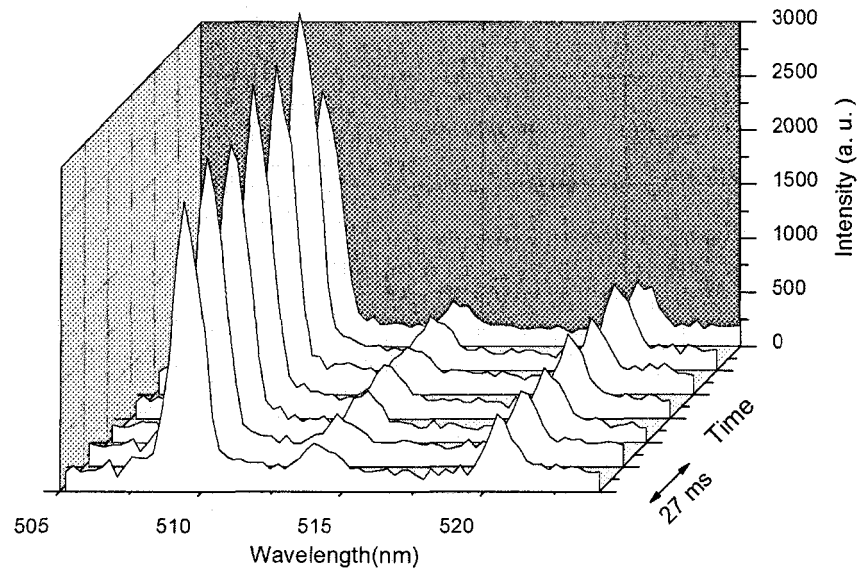


(b)

**Figure 4.17.** **Time resolved spectra of the arc over an ice surface a) between 775 nm and**

**1,000 nm b) between 505 nm and 525 nm**

92

Temperatures are determined by measuring the following two line intensity ratios:

CuI 510 nm/CuI 515 nm, CuI 510 nm/CuI 521 nm, OI 777 nm/OI 926 nm, OI 844 nm/OI

926 nm.

It is well known that the spectral lines selected for the construction of a

Boltzmann plot should satisfy certain requirements [27]. The most important of these

requirement is that the difference in excitation energies should be large enough (1-2 eV)

to ensure accurate temperature measurements. This requirement is well satisfied for the

selected line pairs, as show in Table 4.1 and Table 4.2.

The wavelengths ($\lambda$), statistical weights ($g$) of the upper levels and transition

probabilities ($A$), and the energies of the upper levels ($E_i$) of line transitions are listed in

Table 4.1 for copper lines and Table 4.2 for oxygen lines [74].

**Table 4.1. Spectroscopic parameters of copper spectral lines [74]**

| Wavelength(nm) | E Upper state(eV) | E Lower state(eV) | g | A ($10^8$ s$^{-1}$) |
|---|---|---|---|---|
| Cu 510.554 | 3.817 | 1.389 | 4 | 0.02 |
| Cu 515.324 | 6.191 | 3.786 | 4 | 0.6 |
| Cu 521.820 | 6.192 | 3.817 | 6 | 0.75 |

**Table 4.2. Spectroscopic parameters of oxygen spectral lines [74]**

| Wavelength(nm) | E Upper state(eV) | E Lower state(eV) | g | A ($10^7$ s$^{-1}$) |
|---|---|---|---|---|
| O 777.34 | 10.74 | 1.389 | 5 | 3.69 |
| O 844.65 | 10.988 | 3.786 | 5 | 3.22 |
| O 926.66 | 12.0786 | 3.817 | 9 | 4.45 |

Plotting $\log(\lambda I / gA)$ versus excitation energy ($E$) should yield a straight line (Boltzmann plot) with slope $m$, from which the excitation temperature can be calculated as:

$$T_{exc} = -5040/m \qquad (4.1)$$

Figure 4.18 shows the Boltzmann plot applying this method to two selected line pairs of copper for a 485 mA discharge current. The excitation temperature was calculated to be 5,188 K from the mean value of two line slopes. Using this method, excitation temperatures were calculated for different current values, as shown in Figure 4.19. The spectra for current values below 200 mA were not used, as low-intensity lines could not be distinguished from the background noise. The current increased to about 600mA, suddenly leading to flashover, which corresponds to a jump in current. Due to the interval between two acquisitions (27 ms), which are larger than the final jump of arc, no spectra were recorded during this period.

Figure 4.19 shows that during arc propagation, the excitation temperature is approximately $5,000 \pm 500$ K and does not vary significantly.

The same method was applied to the selected oxygen line pairs. The results are shown in Figure 4.20 and Figure 4.21. In Figure 4.21, the excitation temperature calculated from oxygen lines is about 9,000 K.
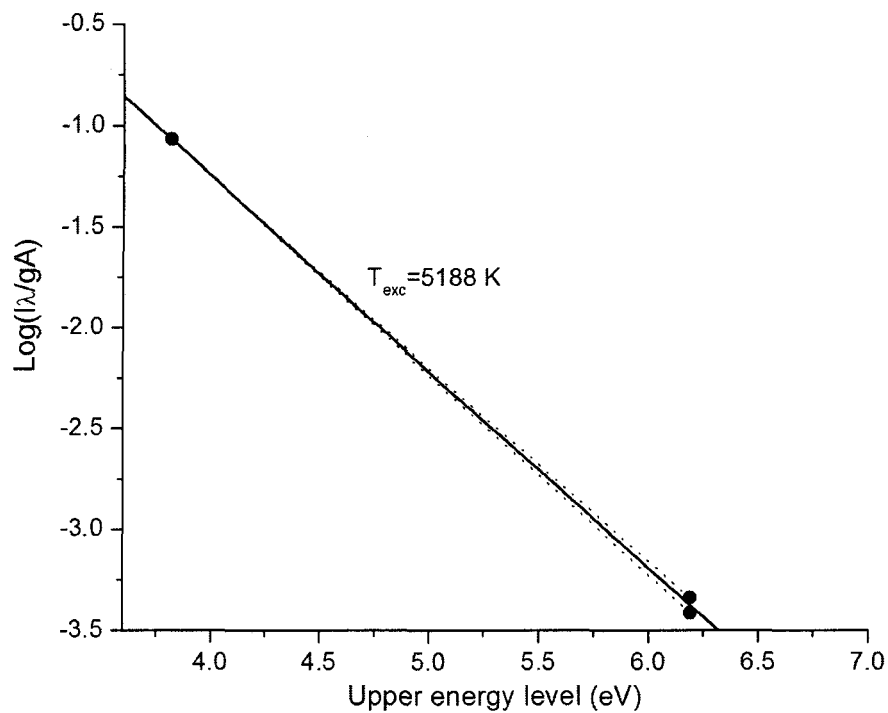
**Figure 4.18.** A typical Boltzmann plot using the copper line parameters found in Table 4.1, for a 485 mA discharge current
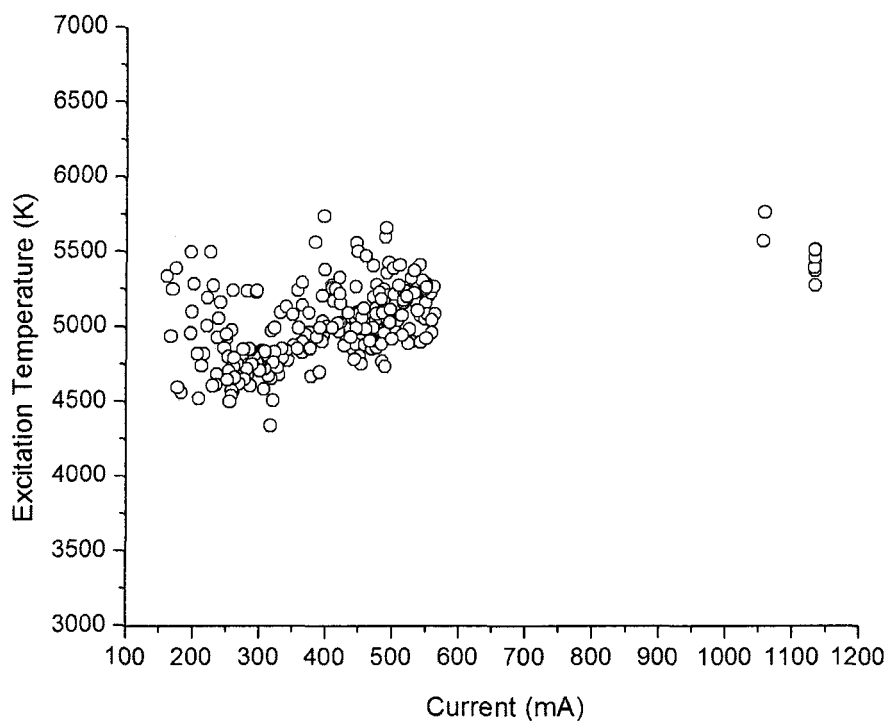


**Figure 4.19.** Excitation temperature using copper lines versus discharge current.
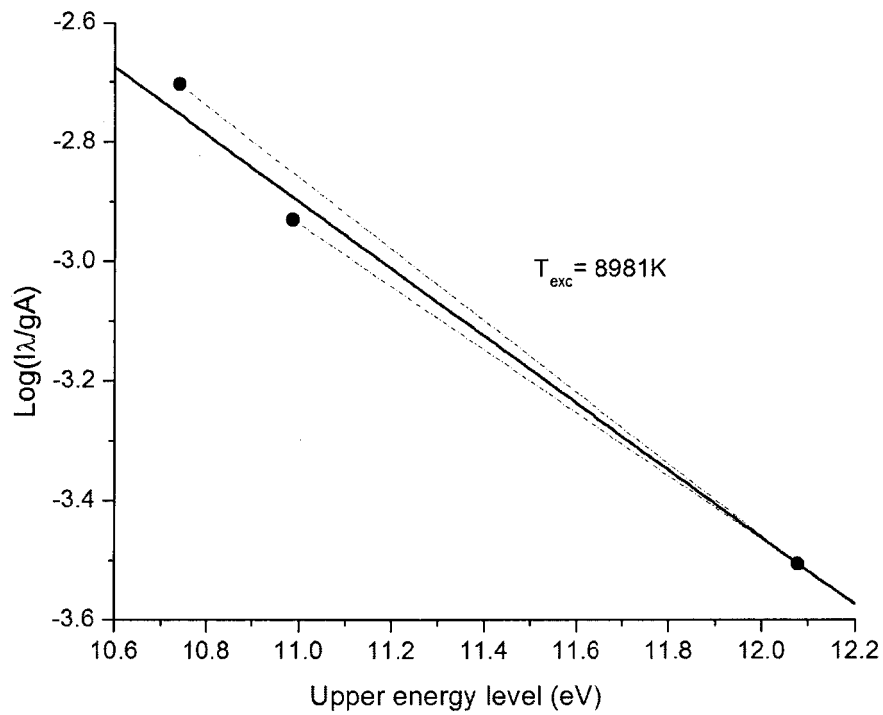
**Figure 4.20.** A typical Boltzmann plot using the parameters found in Table 4.2 for singly ionized oxygen lines, for a 449 mA discharge current
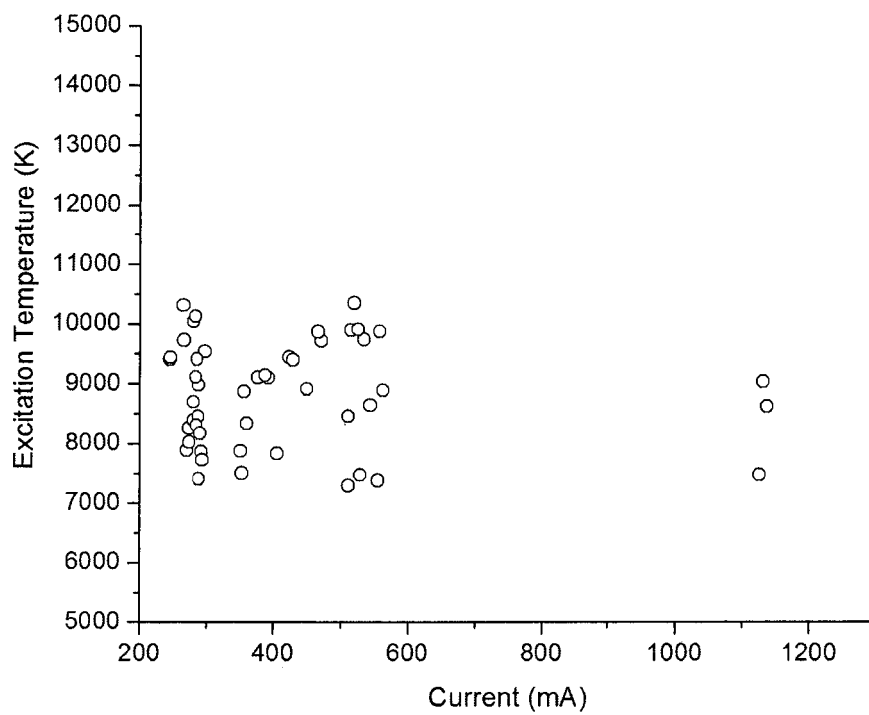


**Figure 4.21.** Oxygen excitation temperature variations relative to discharge current.

The large difference between the excitation temperatures calculated from these two elements signifies a state of non-thermal equilibrium of this kind of discharge.

As mentioned above, when the local thermodynamic equilibrium deviates, the non-equilibrium parameter $b$ may be used [40]. Using the method proposed by Burton and Blades [40], the actual populations can be calculated, allowing theoretical Boltzmann plots to be constructed. $b_{atom}^m$ for the considered atom could be evaluated as:

$$b_{atom}^m = 1 + \frac{6.55 \times 10^{13} E_\infty (E_\infty - E_m)^{2.607}}{n_e T^{0.107}} \qquad (4.2)$$

where $E_\infty$ is the ionization energy(eV) and $n_e$ is the electron density expressed in cm$^{-3}$.

Considering an electron density of $2 \times 10^{17}$ cm$^{-3}$ [75], and employing the ionization potentials $E_\infty$ for copper (7.7264 eV) and oxygen (13.6181 eV), the non-equilibrium parameter $b_{atom}^m$ can be calculated from Equation (4.2) at each calculated excitation temperature.

This non-equilibrium parameter may be incorporated into a Boltzmann plot as $\log(\lambda I / g A b_{atom}^m)$, to reconstruct Boltzmann plots. Figure 4.22 shows the reconstructed Boltzmann plot using the Burton and Blades correction parameter for copper lines, for a 485 mA discharge current.
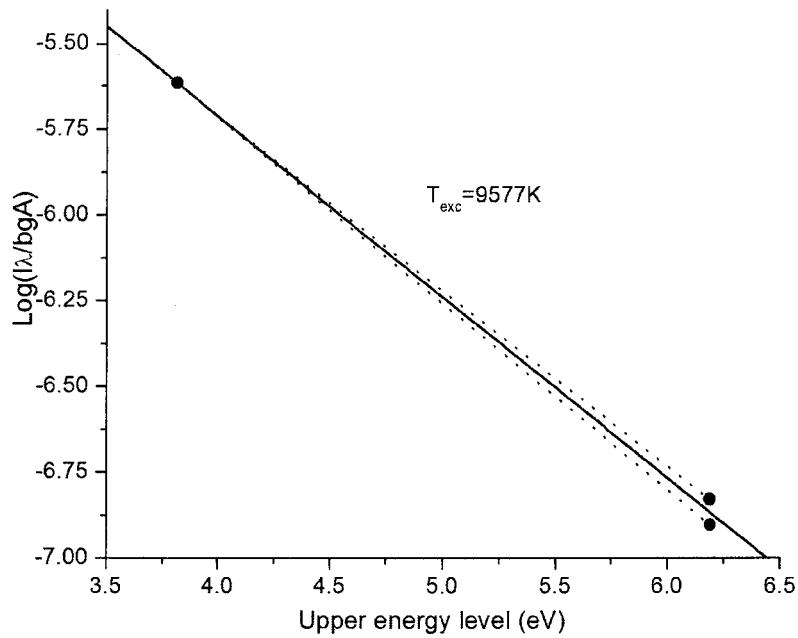
**Figure 4.22.** Reconstructed Boltzmann plot using the Burton and Blades correction

parameter for copper lines, for a 485 mA discharge current.

Figure 4.23 shows the excitation temperatures calculated from copper lines using

the Burton and Blades correction factor. It shows values of about 9500 K. Applying this

method to oxygen lines does not change the previously calculated temperature of 8981K

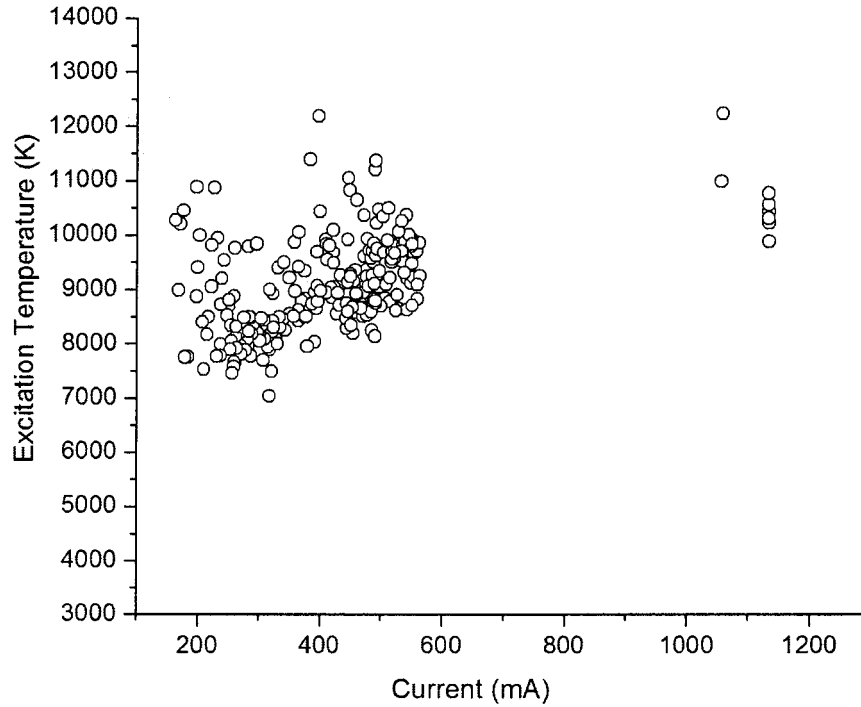for a similar 449mA discharge current.

**Figure 4.23.** **Excitation temperatures of copper using the Burton and Blades correction**

**parameter at different discharge currents.**

## 4.5 Electron density measurement

An example of time-resolved emission spectra taken during DC+ arc propagation leading to flashover is shown in Figure 4.24. The values of discharge current for the last two spectra are also indicated in the figure. It can be seen that the line intensities and continuum levels increase suddenly in the last spectrum, which is associated with flashover.

Figure 4.25 shows the arc current profile simultaneously with the CCD shutter signal. It indicates the interval in which the spectra in Figure 4.26 are acquired. These

time-resolved spectra show the $H_\alpha$ line intensity variations. It can be seen that the intensity of this line corresponds to the arc current increase.

In Figure 4.27 the dashed lines are adopted from the data provided by Griem [42]. They show normalized Stark profiles of $H_\alpha$ lines for different electron densities at $T_e$ = 10,000 K. In order to use data for each spectroscopic system, one should also consider instrumentation broadening. In Figure 4.27 solid lines represent the results of convolution of Griem data with measured instrumentation function.
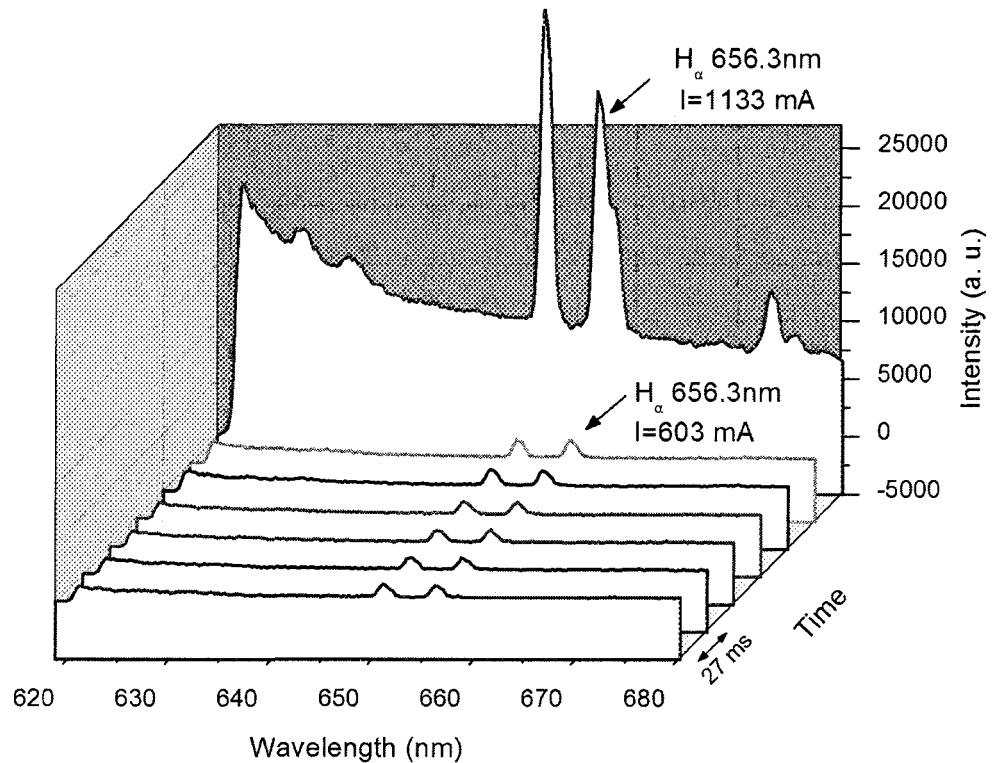


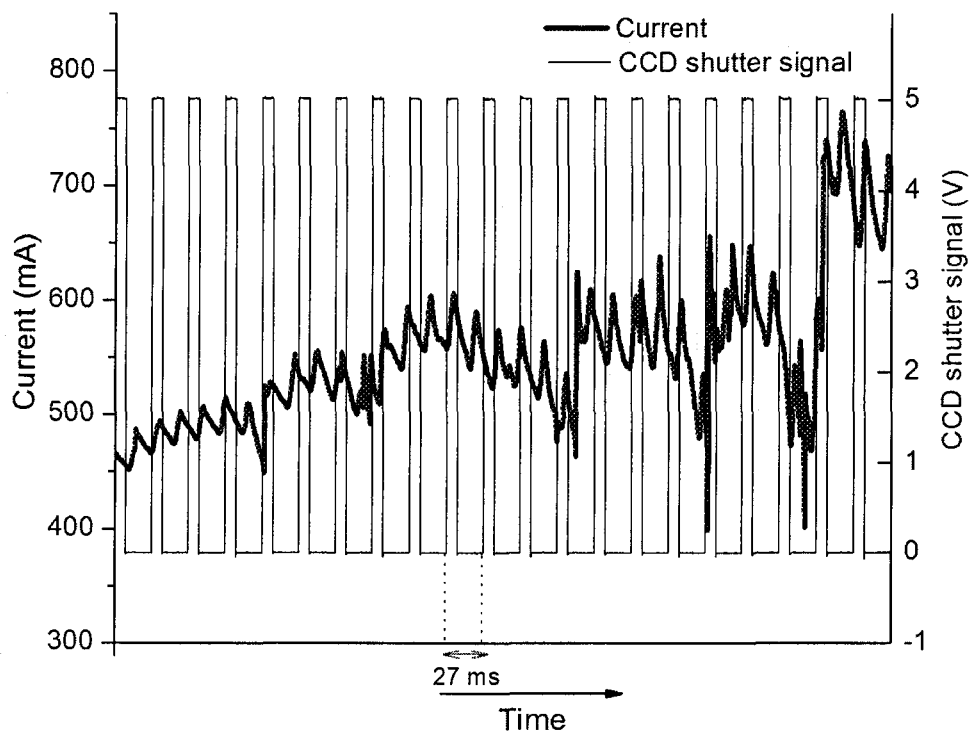**Figure 4.24. Time-resolved spectra during discharge development.**

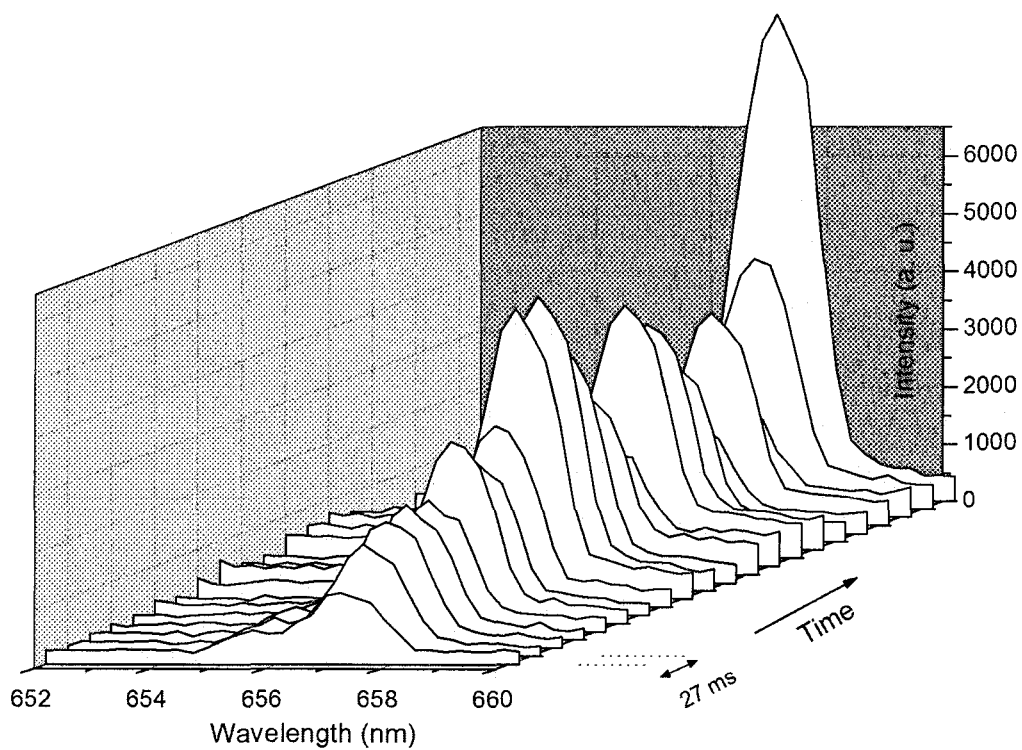**Figure 4.25.   Current variations during discharge development.**



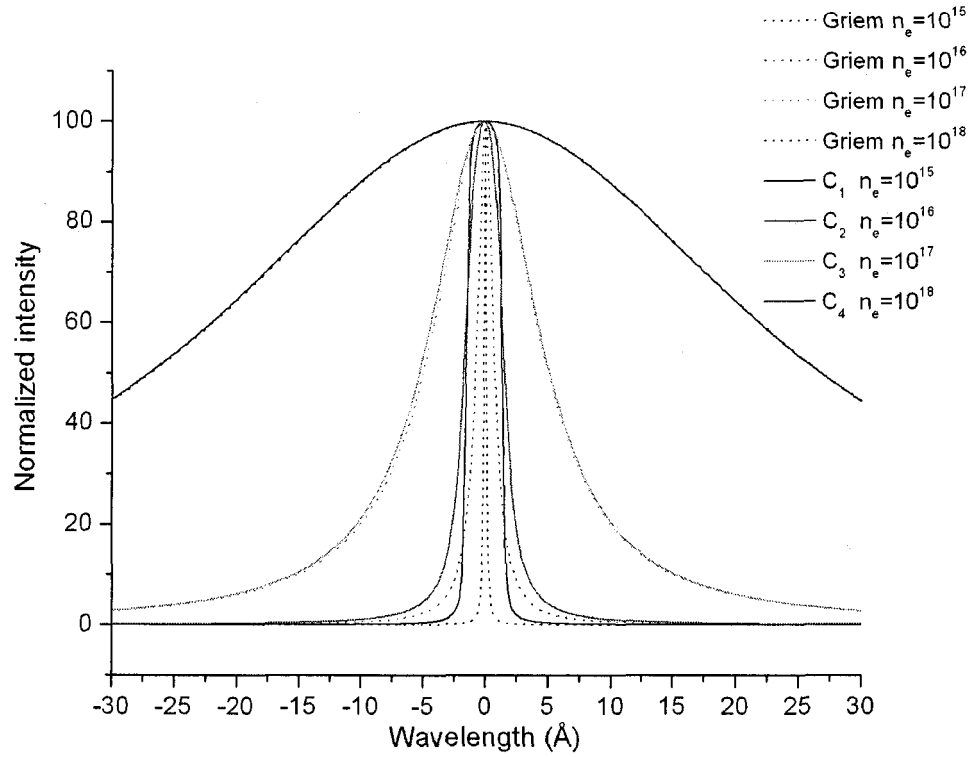**Figure 4.26.   H$_\alpha$ line profiles relative to time.**

101

**Figure 4.27.** Dotted lines: Normalized Stark profiles of $H_\alpha$ lines for different electron densities at $T_e$ =10,000 K, from the data provided by Griem [42]. Solid lines: Results of convolution of Griem data with measured instrumentation function.

In Figure 4.28 the solid line belongs to a recorded spectrum of a 615 mA discharge current. In this part of the spectrum, the $H_\alpha$ line is placed on the background continuum. In order to use the profile for Stark-effect analysis, this background continuum should be subtracted from the original profile. This continuum level and the subtracted profile are also depicted in Figure 4.28.

The experimental points shown in Figure 4.29 were determined after subtraction of continuum and intensity normalization. The measured $H_\alpha$ line profile is in good agreement with the theoretical profile for an electron density of $1.64 \times 10^{17}$ cm$^{-3}$.
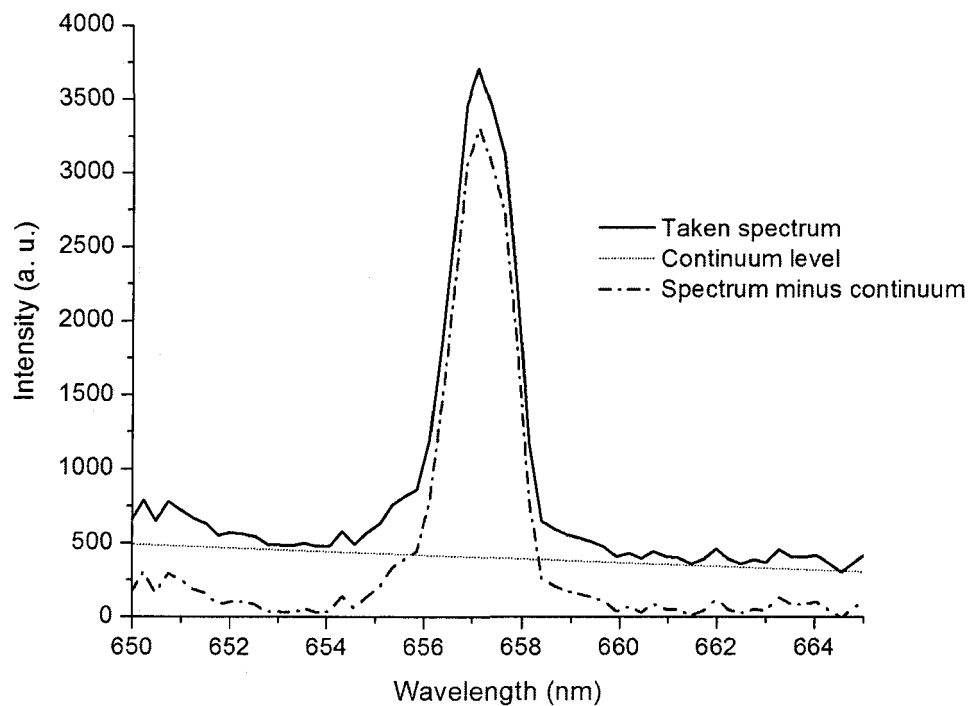
**Figure 4.28. Spectrum at 615 mA, background continuum level and subtracted profile**
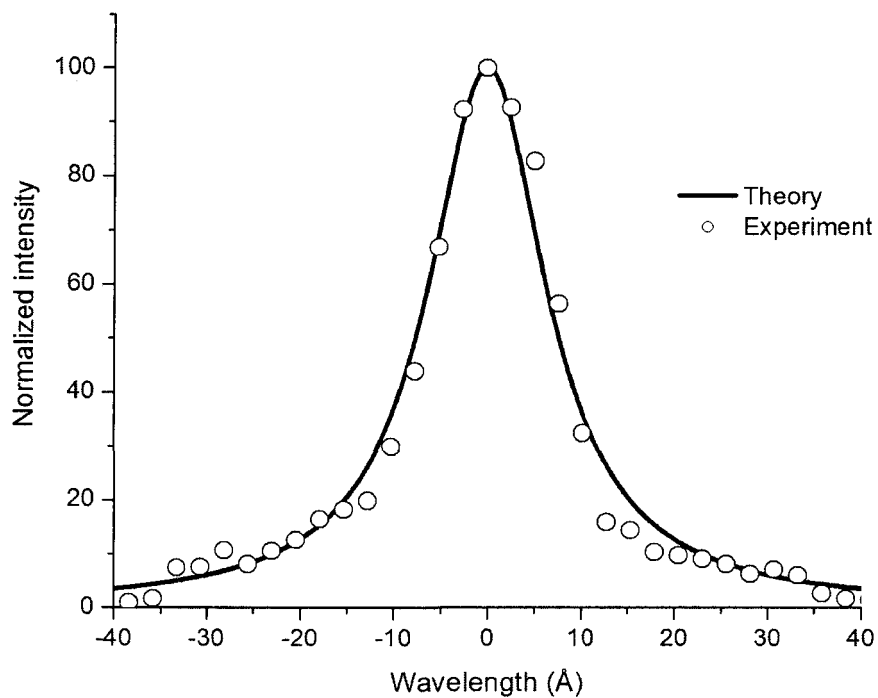


**Figure 4.29. Comparison of the normalized measured and theoretical $H_\alpha$ line profiles at 615 mA. The theoretical profile given by Griem [42] is for an electron density of $1.64 \times 10^{17}$ $cm^{-3}$**

103

Another simple and still precise variation of this method is the application of Full-Width at Half-Maximum (FWHM) of profiles.

The FWHM of profiles for different electron densities and considering instrumentation broadening were measured from Figure 4.27. Figure 4.30 shows the simulation results for the dependence of FWHM on electron density. Fitting the simulation results using an exponential function, an equation giving the electron density as a function of FWHM of $H_\alpha$ lines can be derived:

$$n_e = 6.48 \times 10^{17} e^{FWHM / 56.57} - 6.81 \times 10^{17} \qquad (4.3)$$



Figure 4.30. FWHM of profiles for different electron densities, considering the measured instrumentation broadening

104

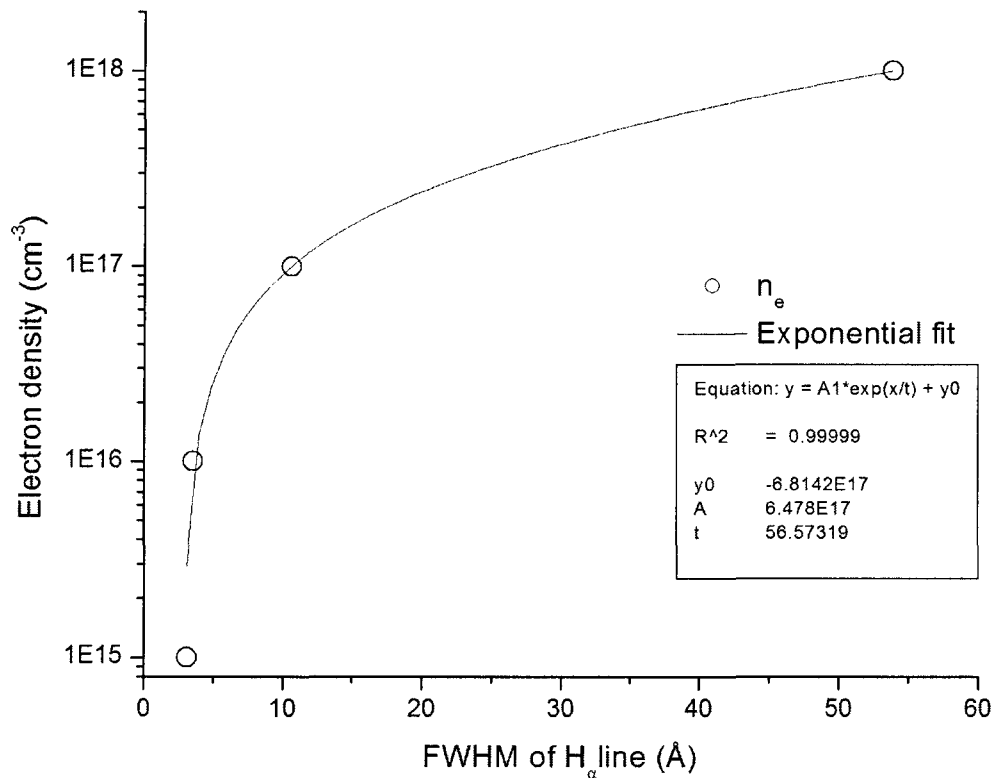Figure 4.31 shows the variation of FWHM with arc current. The data were collected from several experiments performed under the same conditions. Each spectrum the FWHM of $H_\alpha$ line was calculated by subtracting the background level of the adjacent continuum from the profile. The current is the mean value of the arc current measured for each 8 ms exposure time. The last point represents the FWHM from the spectrum taken at the instant of flashover. It turns out that during the first part of propagation time, the $H_\alpha$ profiles have low FWHM, whereas in the last , corresponding to flashover, the FWHM is increased.

Using equation (4.3), electron density can be calculated from FWHM. Figure 4.32 shows the results of applying this equation to the measured data from Figure 4.31.

This figure shows that the average electron density increases during propagation, reaching a very high value at flashover. Increasing electron densities correspond to increases in the degree of ionization.
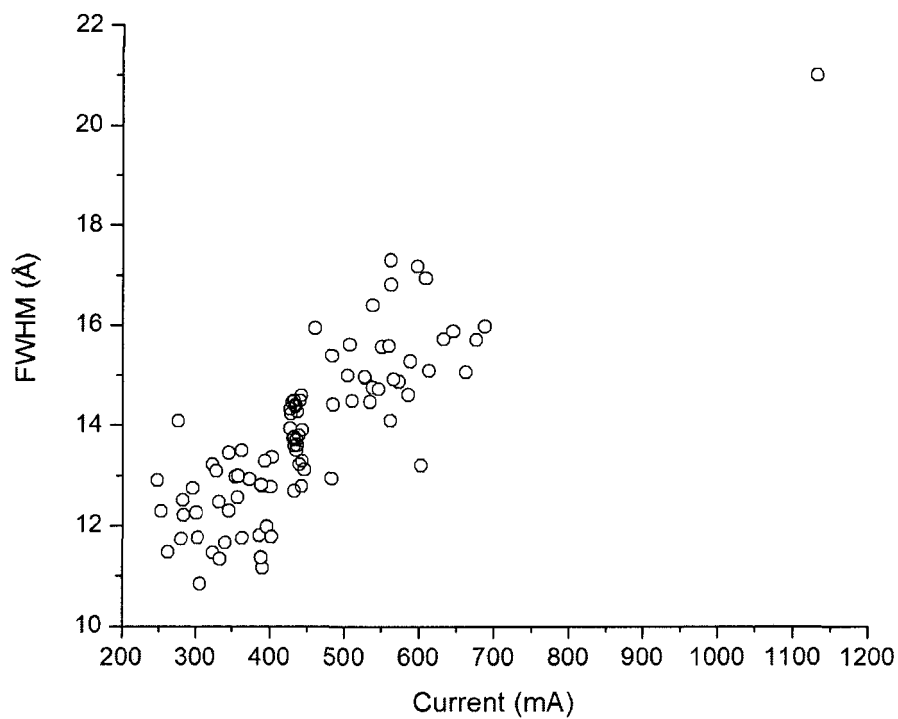
**Figure 4.31.  Variation of FWHM of $H_\alpha$ line with arc current**
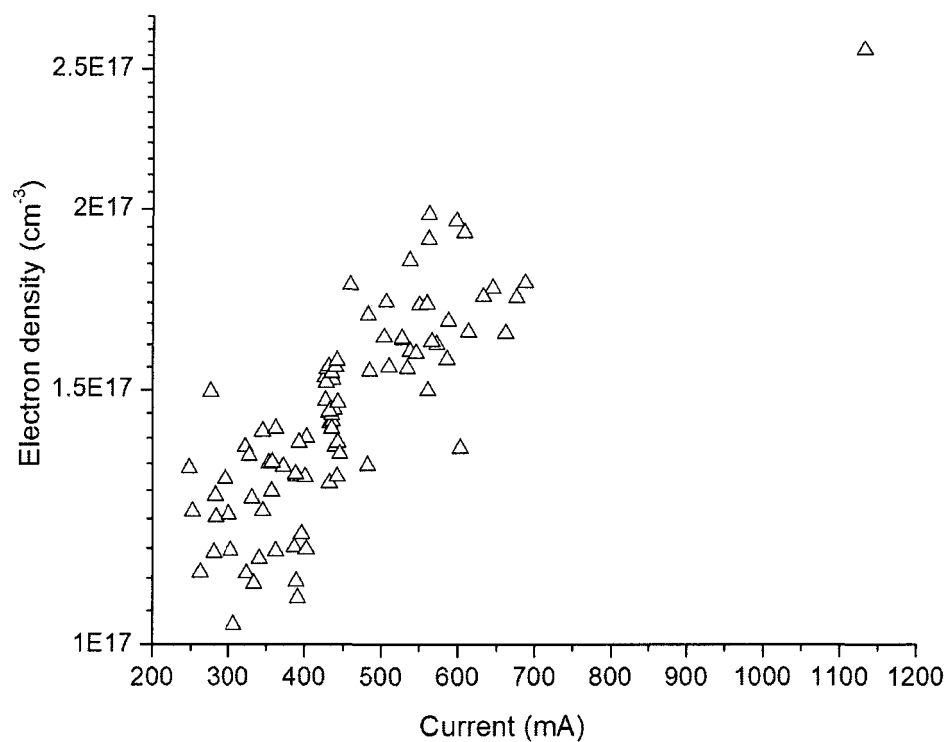


**Figure 4.32.  Variation of electron density with arc current during propagation**

To put these results into context, Orville [11] found values in the order of 28,000 K to 31,000 K for peak temperatures in the lightning return stroke, and an electron density of $8 \times 10^{17}$ $cm^{-3}$. For a 5 m gap under lightning voltage, the measured values for temperature and electron density were 34,000 K and $11 \times 10^{17}$, and almost the same values for a 2.5 m gap [49]. Comtois et al. [76] found that electron densities between $10^{12}$ $cm^{-3}$ and $10^{13}$ $cm^{-3}$ from UV laser pulses was sufficient to guide the development of discharge in a 2.8 m gap using switching surges but not sufficient to reduce the flashover strength.

# CHAPTER 5

# DISCUSSIONS ON RESULTS

# CHAPTER 5

# DISCUSSIONS ON RESULTS

## 5.1 Introduction

Experiments were performed to achieve the objectives of this research, using the methodology described in Chapter 3. In Chapter 4, the experimental results and analyses for of different temperature measurements and electron densities were described. This chapter presents discussions on the experimental results and measurements.

The possible chemical reactions responsible for emitting observed lines and bands are discussed. The effect of voltage type and polarity on arc temperature are studied. The possible sources of error in the measurement results are examined. Finally, based on the results of this research work, the existence of LTE in an arc formed over an ice surface is evaluated.
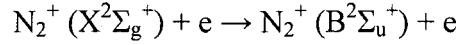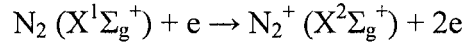
## 5.2 Excitation reactions

### 5.2.1 $N_2^+$ first negative system

Two possible reactions are the most likely for the excitation of the upper state of this system ($B^2\Sigma_u^+$) [20]:

1) Direct ionization and excitation by electron collisions in nitrogen molecules in the ground state.

2) A two stage reaction with the intermediate formation of $N_2^+$ ions in the ground state:

$$N_2 \ (X^1\Sigma_g^+) + e \rightarrow N_2^+ \ (X^2\Sigma_g^+) + 2e$$

$$N_2^+ \ (X^2\Sigma_g^+) + e \rightarrow N_2^+ \ (B^2\Sigma_u^+) + e$$

## 5.2.2 OI lines

This radiation is produced mainly by two excitation reactions [20]:

1) Direct dissociative excitation of oxygen molecules by electron collisions.

2) A two-stage process which starts with dissociation of the oxygen, which can occur through a number of processes:

$$O_2(X^3\Sigma_g^-) + e \rightarrow \qquad O_2(A^3\Sigma_u^+) + e \rightarrow 2 \ O(^3P) + e$$

$$\begin{cases} O_2(B^3\Sigma_u^-) + e \rightarrow O(^3P) + O(^1D) + e \\ O_2^-(^2\Pi_u) \rightarrow O(^3P) + O^-(^2P^0) \end{cases}$$
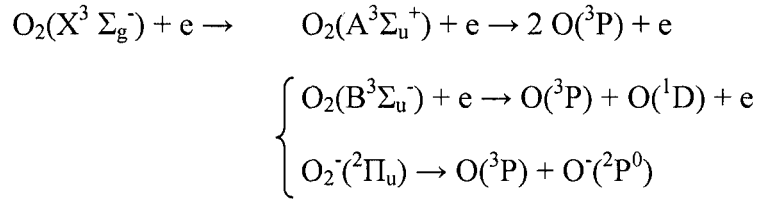
This is followed by direct excitation of the associated products.

Radiation of excited oxygen atoms could be a result of the direct impact of electrons with water molecules:

$$e + H_2O \rightarrow O(3p \ ^3p) + H_2 + e$$

$$e + H_2O \rightarrow O(3p \ ^5p) + H_2 + e$$
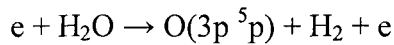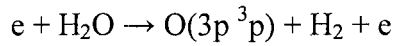
The first equation produces excited oxygen atoms with transition emissions of 844 nm (O 3p $^3$p-3S $^3$S$^0$), while the latter produces oxygen atoms with emissions of 777 nm (O 3p $^5$p-3S $^5$S$^0$) [78].

### 5.2.3 Na –D lines

The dissociation of NaCl does give rise to the emission of all Na lines:

$NaCl \rightarrow Na^+ + Cl^-$

$Na^+ + e \rightarrow Na$
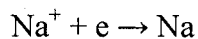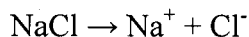
Another possible reaction which results in the emission of only Na-D lines (contrary to the above reactions which emits all Na lines) could be:

$Na^* (^2p) \rightarrow Na(^2s) + h\upsilon$
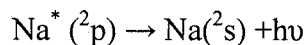
This wavelength corresponds to transition in atomic sodium in which the valence-electron transition from 2p to 2s electronic state takes place [79].

While the dissociation of NaCl could also give rise to Na-D lines, the formation of $Na^*$; these have such a short life that the intensity of these fundamental lines (D-lines) is extraordinarily high relative to the other Na lines.


### 5.2.4 NH band

The NH free radical is an important intermediate reaction in some flames, rocket-engine plasmas, electric discharges, and astronomical emission sources. [80]. The predominant emission spectrum arises from $NH(A^3\Pi - X^3\Sigma^-)$ by electron collisions at electron energies up to 25 eV in the region between 300 nm to 600 nm.

In the case of an arc propagating over an ice surface, the sharp (0,0) band at 336nm from $NH(A^3\Pi - X^3\Sigma^-)$ transition is predominant.

### 5.2.5 OH band

The chemical reactions associated with high-temperature dissociation of water vapor are shown below:

$$H_2O \rightarrow H_2 + \frac{1}{2} O_2$$

$$H_2 \rightarrow 2H$$

$$O_2 \rightarrow 2O$$

$$O + H \rightarrow OH$$
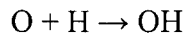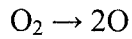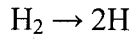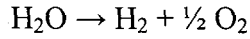
Multiple uses of electrons is made possible by the high rate of negative ion collapses due to electron collisions [81]:

$$e + H_2O \rightarrow H^- + OH$$

$$H^- + e \rightarrow H + 2e$$
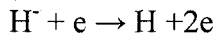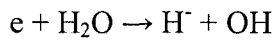
The leading mechanism of OH production in humid air discharges is the dissociation of water caused by electron collisions:

$$e + H_2O \rightarrow OH + H^-$$
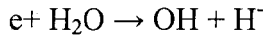
## 5.3 Overall spectral variation of arc

Detailed analyses of the white arc and flashover arc spectra were performed. Figure 5.1 shows the results of one of these analyses. Figure 5.1 (a) is concerned with a white arc over the ice surface showing the spectra between 250 nm and 500 nm, while Figure 5.1 (b) shows the spectra between 500 nm and 725 nm.

Figure 5.1 (c) and Figure 5.1 (d) are the spectra of flashover arcs over the ice surface. Comparison of the overall spectral variation of light from white and flashover

arcs, leads to the conclusion that the white arcs emit light mainly in the ultraviolet region between 300 nm and 310 nm, while flashover arcs emit mostly in the visible region. UV emissions are due to OH band emissions, while the visible emissions originate from the $N_2^+$ $1^{st}$ negative system, which appears at higher excitation levels. This observation is in good agreement with results obtained by Les Renardières [52] and Laux [8].

Figure 5.2 shows the time-resolved spectra of the Na lines. The intensity of these two lines increases constantly during arc development, which is also associated with an increase in current level.

It is also interesting to point out that the intensities of some lines, such as copper, increases constantly between the white arc and flashover occurrence, as shown in Figure 5.3. However, the intensity of some lines, such as $H_\alpha$ and $H_\beta$ and $N_2^+$ first negative, increases suddenly during flashover.

(a)



(b)

114
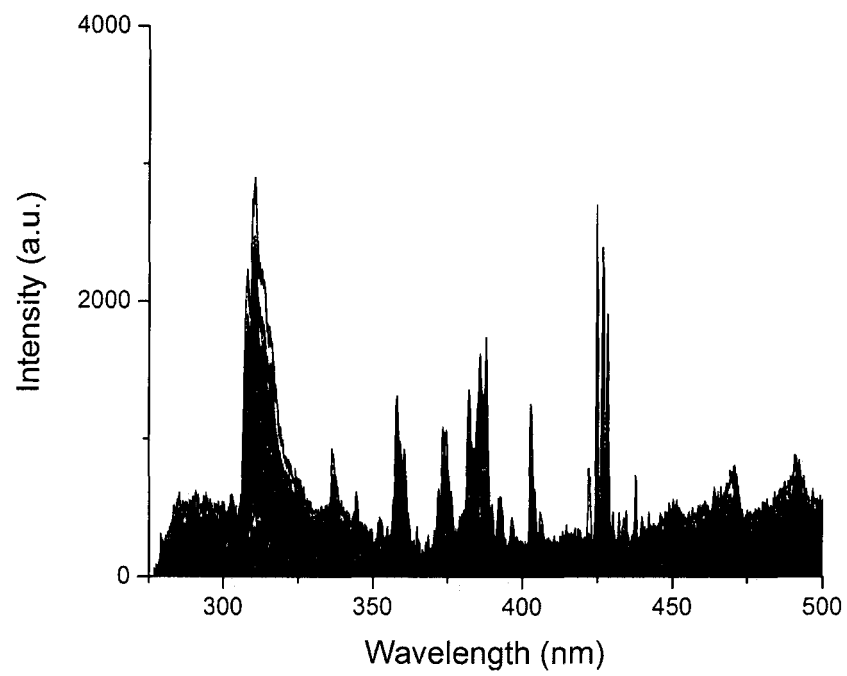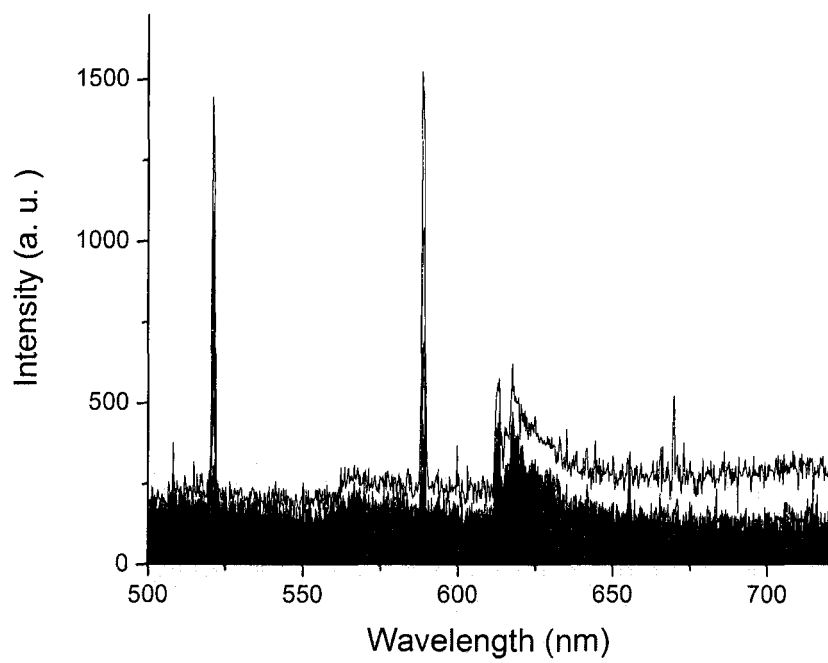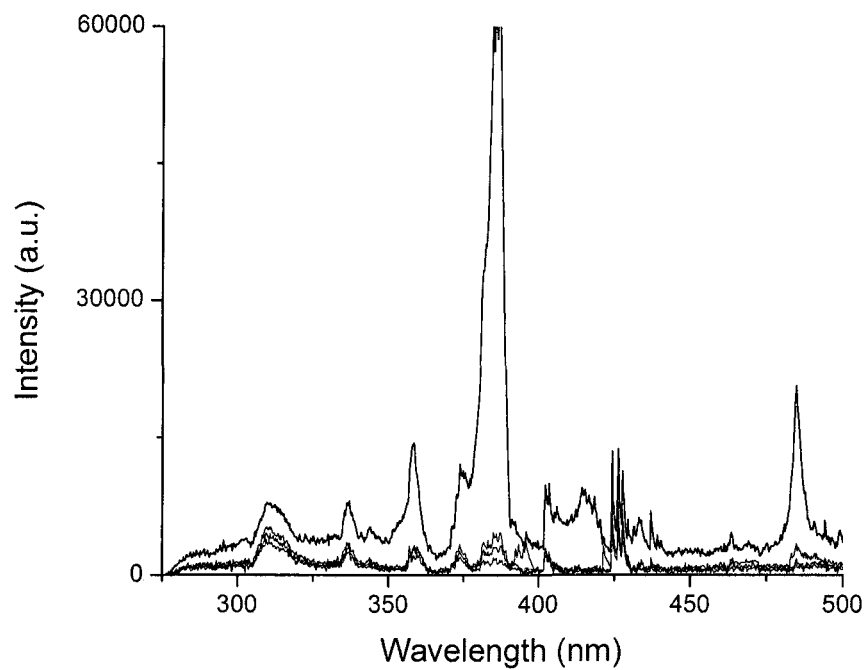
(c)
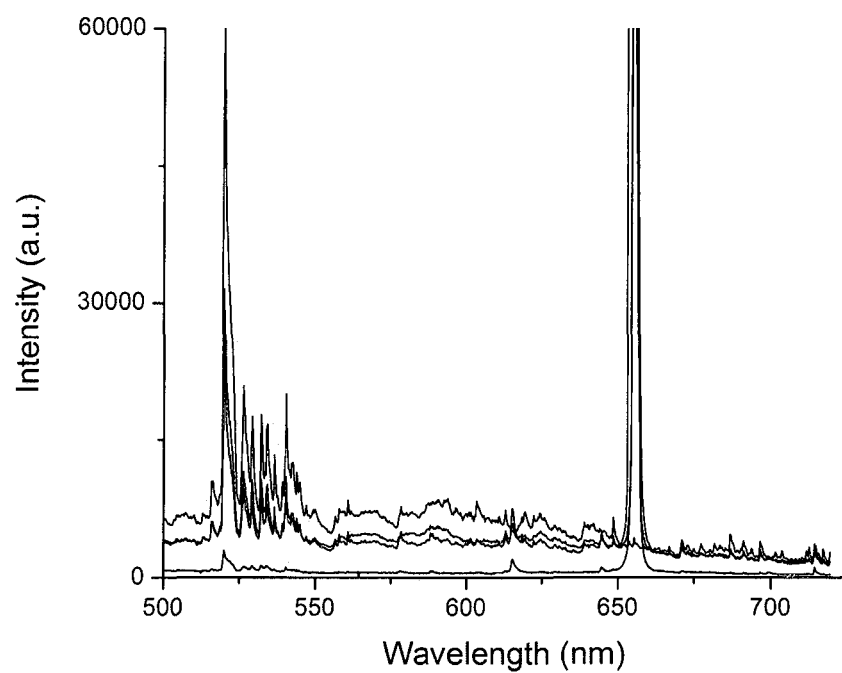


(d)

**Figure 5.1.** Spectra of arc light during (a) white arc 250-500 nm (b) white arc 500-750 nm (c) flashover arc 250-500 nm and (d) flashover arc 500-750nm
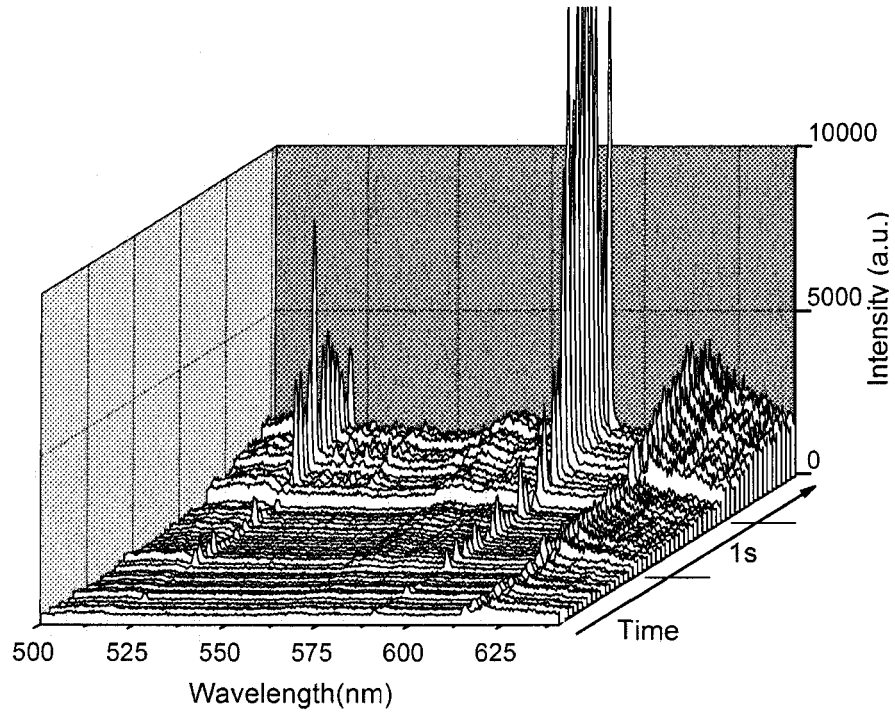
**Figure 5.2.** **Time-resolved spectra of white arc.**
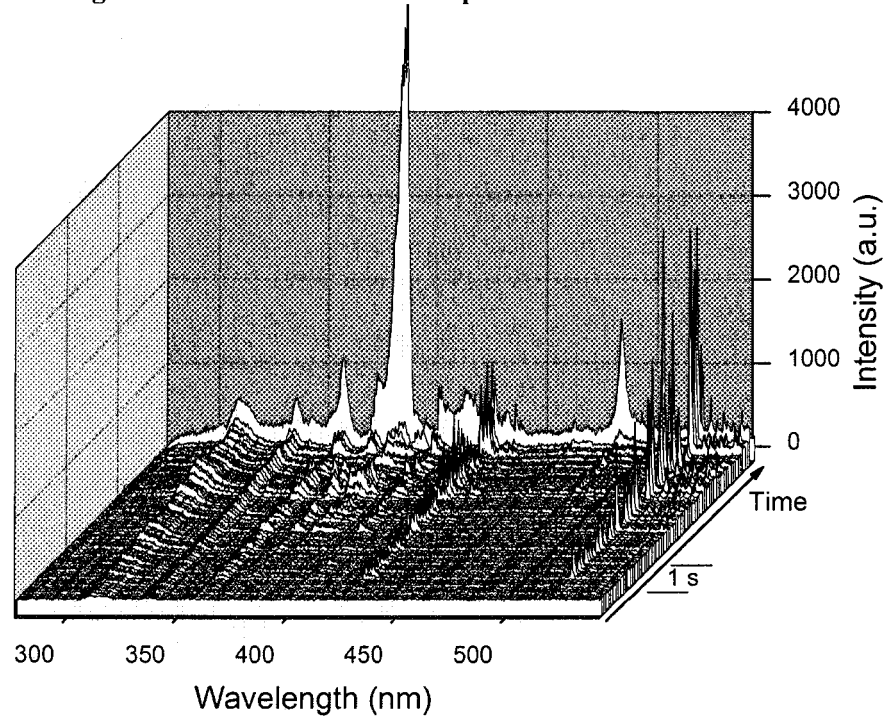


**Figure 5.3.** **Time-resolved spectra of arc at different stages.**

116

## 5.4 Voltage polarity effect

Figure 5.4 shows the effect of voltage type on arc temperatures, with the current variations. It can be seen that, in the shown current range, arc temperatures increase from about 3,500 K to 4,500 K for DC-, and 3,700 K to 5,700 K for DC+ applied voltages. In both cases there is a tendency towards saturation temperatures in higher currents. These results agree with those of Ishii and Ohashi [82]. They performed interferometric investigations on positive and negative arcs propagating over contaminated surfaces. From the differences in the airflow around the partial arc of each polarity, they noticed differences in arc temperatures, i.e. the positive arc is hotter than the negative arc. Arc temperatures under AC voltage is lower than that of DC+ and is close to that of DC-.
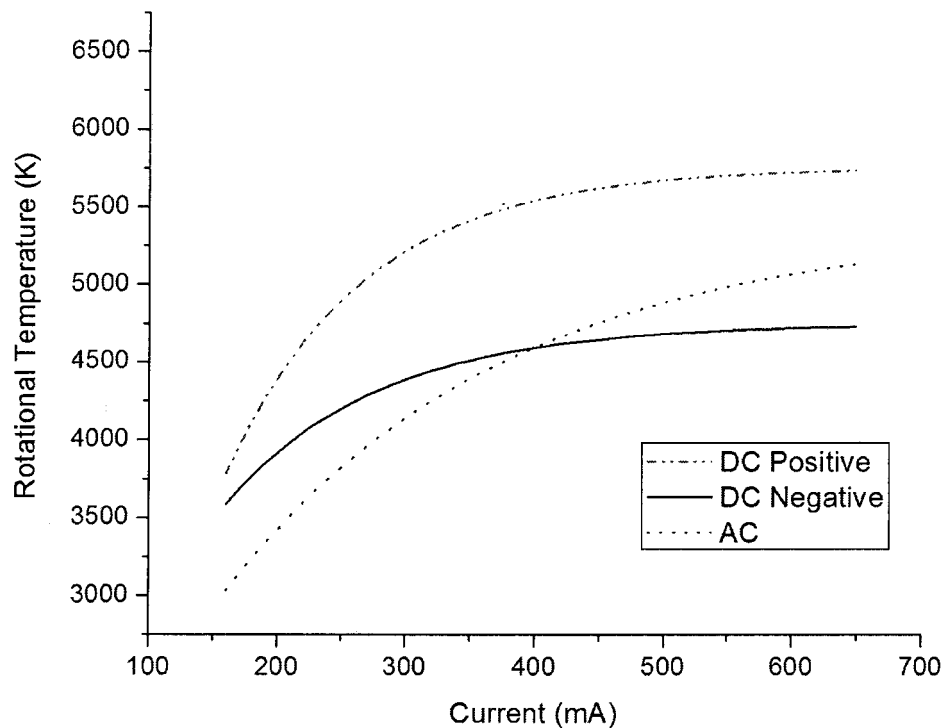


**Figure 5.4.** **Rotational temperatures versus current for different applied voltage types.**

A discharge is normally modeled as an arc in series with a residual resistance consisting of an ice layer that is not bridged by the arc.

$$V = AxI^{-n} + IR_p(x) + V_e$$

(5.1)

Where V is the applied voltage (V), A and n are the arc constants, x is the local arc length (cm), and I is the leakage current (A). $R_p(x)$ is the residual resistance ($\Omega$) of non-bridged ice layer from the arc root at x to the ground electrode. $V_e$ is the electrode voltage drop [18].

V-I characteristic of arc is usually expressed using voltage gradients of arc per unit length (V/cm):

$$E = AI^{-n}$$

(5.2)

Arc constants (A, n) have already been measured using different voltage types [18]. These constants are summarized in Table 5.1.

Figure 5.5 shows the voltage gradient along arc columns for DC+ and DC-applied voltages. Multiplying these voltage gradients by arc current yields the dissipated energy in the arc column. This energy, which is consumed in the ionization activities and compensation for heat losses from outside boundaries of arc column, is an indication of arc column temperature. The dissipated energy in the arc channel is shown in Figure 5.6.

Table 5.1. Typical values[a] of A and n in relation $E=AI^{-n}$ for arcs over an ice surface [83, 84]

|  | A | n |
|---|---|---|
| DC+ | 208.9 | 0.449 |
| DC- | 84.6 | 0.772 |
| AC | 204.7 | 0.5607 |

[a]E in peak V/cm and I in peak amperes

118

Comparing Figure 5.4 with Figure 5.6 shows that the measured arc temperatures correspond with the dissipated energy in the arc channel. The dissipated energy is greater in DC+ than in DC-. The dissipated energy in the case of AC falls between DC+ and DC- and is closer to DC-. This fact can also be observed when comparing their temperatures.
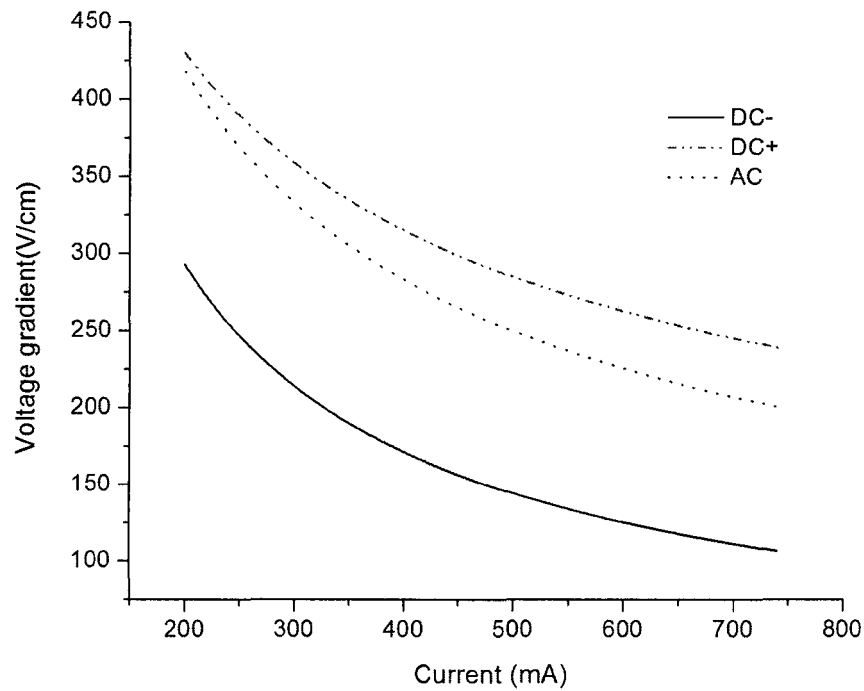


**Figure 5.5.** The voltage gradient along arc column versus current for different applied voltage types (adapted from data of [83,84]).
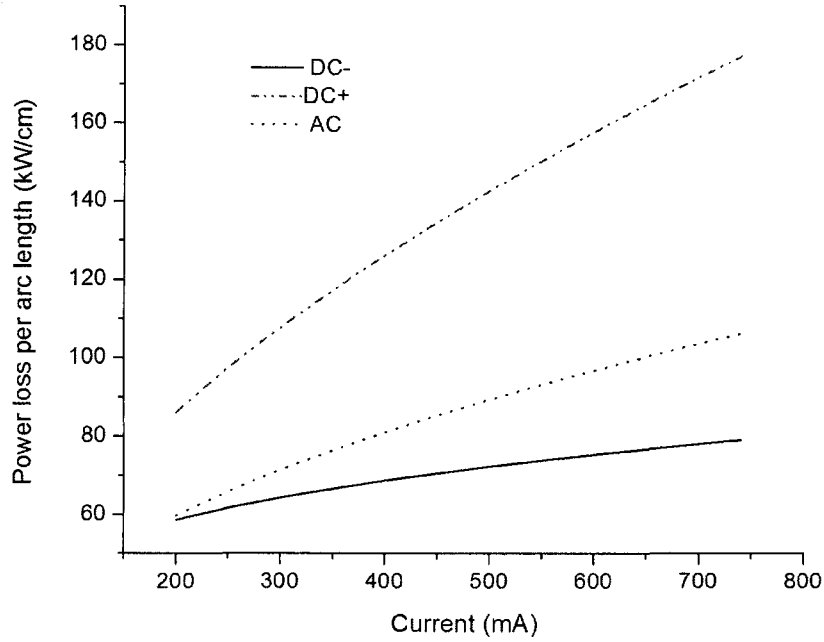
**Figure 5.6.** Power loss per arc length along arc column versus current for different applied voltage types.

## 5.5 Error analysis

When the discharge current varies from 200 mA to 1200mA, the electron temperature $T_e$ increases from 7,500 K to 11,500 K [85]. As the Stark effect depends primarily on charge number densities and is only a weak function of temperature [41], the databases [42] usually only consider the following temperatures: $T_e$ = 5,000 K, 10,000 K and 20,000 K. Considering a constant electron temperature of 10,000 K will result in negligible error in electron density calculations.

Natural broadening arises from the uncertainty in energy of the states involved in the transition. This source of broadening is rarely significant in atomic spectroscopy in atmospheric applications [86]. A typical lifetime for an atomic energy state is about $10^{-8}$

seconds, corresponding to a natural line width of about $6.6 \times 10^{-8}$ eV, which is negligible in our case [87]. FWHM due to Doppler effect could be calculated from [26]:

$$\Delta\lambda = \sqrt{\frac{8\ln 2\, kT}{Mc^2}}\lambda_0 \quad \Delta\lambda = \sqrt{\frac{8\ln 2\, kT}{Mc^2}}\lambda_0 \tag{5.3}$$

Where k is the Boltzmann constant, $T$ and $M$ are radiators' kinetic temperature and mass, $\lambda_0$ is the central wavelength, and $c$ is the light speed. Considering temperatures between 7,500 K and 11,500 K [85], Doppler effects will lead to an FWHM of 0.27 Å to 0.33 Å. This will result in a maximum error of less than 4 % in evaluating electron densities using the Stark effect and neglecting the Doppler effect. Broadening resulting from resonance; Van der Waals and Zeeman effects are also negligible in this type of discharge.

## 5.6 Verifying thermal equilibrium

In optically thin plasma, the processes leading to radiation are those due to spontaneous emission and radiative recombination. Griem deduced a very simple criterion of LTE, expressing that for a given time unit the number of transitions due to electronic collisions between the first excited state and the fundamental level as being ten times greater than the number of transitions due to spontaneous emission [10].

Another criterion to verify the existence of LTE given by McWhirter is [45]:

$$N_e^* \geq 1.6 \times 10^{12}\, T_e^{1/2}\, \chi(p,q)^3 \quad \text{cm}^{-3} \tag{5.4}$$

Where $T_e$ is electron temperature in K and $\chi(p,q)$ is the excitation potential of level $p$ from level $q$ in eV.

The expressions of Wilson and Griem are in good agreement. They only differ in the constants [45]:

Griem $9.2 \times 10^{11}$

Wilson $1.3 \times 10^{12}$

Mcwhirter $1.6 \times 10^{12}$

For the current range of 200 mA to 700 mA, electron density increases from $1 \times 10^{17}$ cm$^{-3}$ to $2 \times 10^{17}$ cm$^{-3}$. Considering the excitation temperature to be about 9,000 K and the following is obtained using Mcwhirter criterion:

$$1.6 \times 10^{12} T_e^{1/2} \chi(p,q)^3 = 1.2 \times 10^{16} \leq 1 - 2 \times 10^{17} \qquad (5.5)$$

The derived criterion value is close to the calculated electron density.

This inequality is a necessary, but not a sufficient condition for plasma to be in LTE.

In atmospheric pressure plasmas, rotational temperatures are close to gas temperature owing to fast collisional relaxation. Rotational temperatures ($T_{rot}$) are relevant to all processes in which molecules, radicals, and their dissociation products are involved, and excitation temperatures ($T_{exc}$) describe the populations of the various energies.

Figure 5.7 shows gas temperatures $T_g$ measured at the centerline of the discharge column, found to vary between 4,000 K and 6,500 K, depending on current. The measured $T_{exc}$ was higher (around 9,000 K) and therefore suggests that the arc is in a state of thermal non-equilibrium.
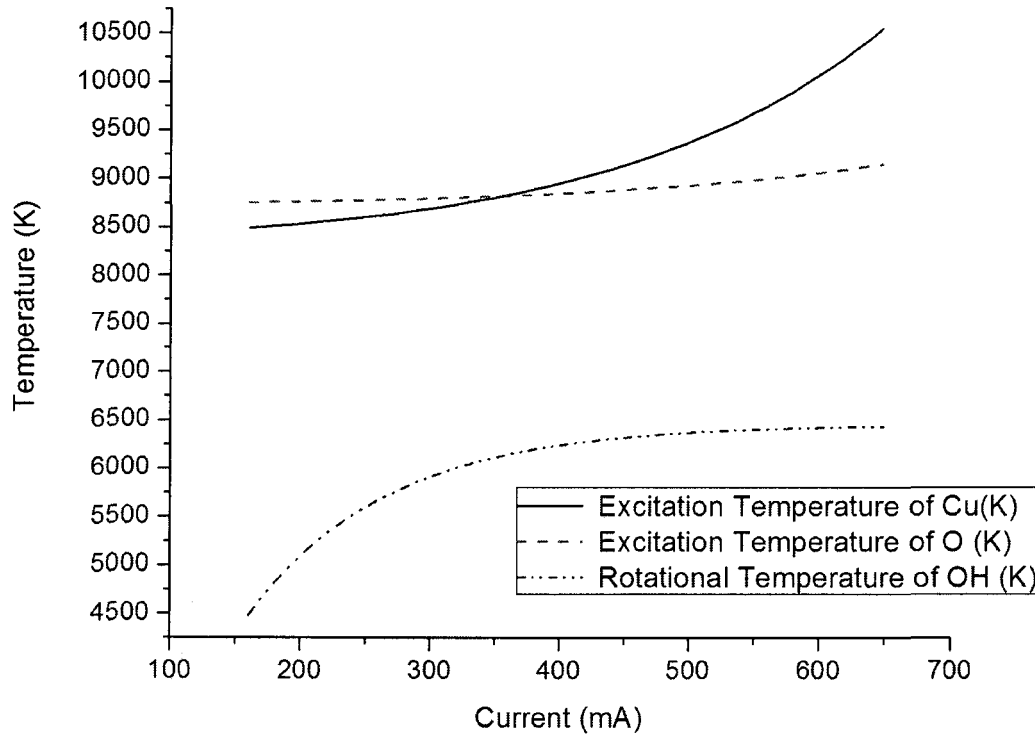
**Figure 5.7.**     **Comparison of excitation and rotational temperatures**

## 5.7  Conclusion

The chemical reactions which could be responsible for emitting the observed lines and bands in arc spectra were discussed. Arc temperatures were found to be higher in DC+ than DC- applied voltages. Arc temperatures were found to be lower in AC than in DC+, and close to DC-. The situation is related to the difference in the dissipated energy per unit length of arc column under different voltage types. Possible sources of uncertainty in the measurements have been discussed. From the analysis of the results, this kind of discharge was found to be in the state of thermal non-equilibrium.

# CHAPTER 6

# CONCLUSIONS AND RECOMMENDATIONS

# CHAPTER 6

# CONCLUSIONS AND RECOMMENDATIONS

This chapter presents concluding remarks as well as recommendations intended to guide further research.

## 6.1 Conclusions

1) An original spectroscopic test setup was developed. The spectra of emitted light from arcs formed over an ice surface were recorded using a triggered spectrometer. The optical measurement was synchronized with the electrical parameters, voltage and current. This was achieved using a gateable charge-coupled device (CCD) camera fed with the output of the spectrometer synchronized with electrical measurements through a data acquisition system.

2) Based on the obtained results, the spectroscopic method seems to be appropriate for the study of arc characteristics on an ice surface. Moreover, results showed that this method is repeatable and reproducible.

3) Detailed analysis of the spectra allowed identifying different atomic lines and molecular bands from the background gases, as well as excited species from polluted ice.

    a) Using the plasma diagnostic method, several lines from ionized O, Na and Cu were observed.

    b) Moreover, emission features of Hydrogen Balmer series $H_\alpha$ and $H_\beta$ were observed and found to be distinctly different from those of singly ionized species.

    c) Strong diatomic molecular bands of OH, $N_2^+$ 1st negative system and NH were observed from the captured spectra.

    d) High-intensity sodium-D lines were observed during the early stages of arc development. From dissolution of NaCl in water, sodium ions appear in the water film that forms over ice surface. Since sodium has low ionization energy and can be ionized easily, high intensity sodium lines were emitted.

    e) Chemical reactions which are responsible for emitting these lines and bands were discussed.

4) Time-resolved spectra were recorded at different stages of arc propagation over an ice surface to gather data on the occurring ionization processes. From comparisons of overall spectra from the white and flashover arcs, it was concluded that a white arc emits light mostly in the ultraviolet region, whereas a flashover arc emits light mostly in the visible region.

5) To determine rotational temperatures, which are similar to gas temperatures, an optical emission spectroscopy (OES) analysis was carried out using the OH (A-X) (0, 0) transition band.

  a) An OH (A-X) transition around 308 nm appeared suitable for rotational temperature measurements due to the strong emissions of this band and its high sensitivity to rotational temperature variations.

  b) Rotational temperatures were determined by measuring the ratio of peak intensities of the OH (0, 0) R to the P branches and comparing them to those of computer-simulated synthetic spectra.

  c) Variation of rotational temperatures, which are similar to gas temperatures, with discharge current were studied. Measured rotational temperatures were found to vary from 4,000 K to 6,500 K, while the current increased from 200 mA to 700 mA.

  d) Rotational temperatures were also evaluated using the $N_2^+$ $1^{st}$ negative system. The rotational temperatures measured using this system were in good agreement with those obtained using OH bands.

  e) Rotational temperatures were calculated versus current variation during discharge propagation over an ice surface using DC-, DC+ and AC applied voltages. It was observed that for different values of arc current, DC- arcs were hotter than DC-. Moreover, arc temperatures under AC voltage is lower than that of DC+ and close to that of DC-. Comparing these results

with the dissipated energy for each type of arc showed that arc temperatures correspond to the dissipated energy per arc unit length.

6) Excitation temperatures were calculated using the ratio of line intensities of different copper and oxygen lines. Inequality between the excitation temperatures of the copper and oxygen indicates deviation from LTE in this kind of discharge. The Burton and Blade correction factor was used to reconstruct the Boltzmann plots. The results revealed that the excitation occurs at about 9,000 K and does not vary significantly with discharge current.

7) Electron densities were calculated based on measuring the broadening of the hydrogen line $H_\alpha$ due to the Stark effect. Based on Griem's theoretical data and taking into account the instrumentation function of the spectroscopic system, an empirical relationship between the FWHM and electron densities was established. Time-resolved spectra were processed to calculate the FWHM of each spectrum after subtraction of the background continuum and intensity normalization.

8) The results showed that as current increases, electron density increases as well. For currents ranging from 200 mA to 700 mA, electron densities increased from 1 to 2 $\times 10^{17}$ $cm^{-3}$. Electron densities increase up to $2.5 \times 10^{17}$ $cm^{-3}$ at the later stage of arc when flashover occurs.

9) Differences between the rotational and excitation temperatures showed that the arc is in a state of thermal non-equilibrium.

## 6.2  Recommendations for future work

1.  The chemical composition of pollution varies by location. The insoluble compounds, $SiO_2$, $Al_2O_3$, $Fe_2O_3$, are the most common. Highly soluble salts causing elevated conductivity and greater risk of flashover include: NaCl, $NaNO_3$, $MgSO_4$, etc. [69]. It is possible to obtain the rotational temperature of OH, in fact the gas temperature, using different salts as the pollution layer. Therefore, it would be helpful to determine the influence of different contamination layers on the gas temperatures of arcs on an ice surface.

2.  In this study, the light was captured from the entire arc column. However, it is suggested to perform spatially resolved spectroscopy with a configuration using a multi-channel detector which captures the arc light from different positions along the channel.

    It is also proposed to use a multi-channel CCD camera and multi-branched fiber-optic cable to bring the light from several arc positions to the spectrometer. It would help to measure gas temperatures at different positions of arc simultaneously, as well as the temperatures of the arc root and column.

3.  According to the dynamic model developed previously [7], knowing the exact values of different variables, such as arc length and temperature, and surface conductivity, is necessary for arc current simulation, otherwise this cannot be carried out at this stage. Thus, it is suggested to incorporate the results of

spectroscopic temperature measurements with the dynamic model of arc propagation over an ice surface to improve it.

4. Measuring arc temperatures under lightning and switching impulse voltages using the method developed in this thesis is recommended.

5. Measuring electric fields via the Stark effect for hydrogen and also highly excited atoms is possible over a wide range of field strengths [15]. Applying this method to measure electric field intensities will not disturb it, unlike some probe measurements that may change the original field pattern. As this is a nondestructive method, using to measure the electrical field intensity along an arc column over an ice surface is recommended.

6. There have been several recent standards and regulations related to the fundamental dangers of arc flash energy: IEEE Standard 1584-2002 [88] NFPA 70E [89] and OSHA Standard 29-CFR, part 1910 [90]. Computer codes (such as ArcPro and PTW) have also been developed to calculate arc temperature. The developed methodology in this research is a practical way to verify and extend the modeling of arc hazards.

# CHAPTER 7

# REFERENCES

# CHAPTER 7

# REFERENCES

[1]  M. Farzaneh, "Ice accretion on high voltage conductors and insulators and related phenomena", *Phil.Trans. of the Royal Soc.*, Vol. 358, No. 1776, pp. 2971-3005, 2000.

[2]  M. Farzaneh and J. Kiernieki "Flashover problems caused by ice build-up on insulators" *IEEE Electrical Insulation Magazine*, Vol. 11, No. 2, pp. 5-17, 1995.

[3]  O. T. Melo, Y. T. Tam and M. Farzaneh "Freezing rain and fog events in southern Ontario: properties and effect on EHV transmission systems" *Proc 4th Int. Wksp. Atm. Icing of Struct*, IWAIS, pp. 70-75, 1988.

[4]  F. Su and S. Hu "Icing on overhead transmission lines in cold mountainous district of southwest China and its protection" *Proc. 4th Int. Wksp. Atm. Icing of Struct*. Pp. 354-357, 1988.

[5]  I. Fofana, C. Tavakoli and M. Farzaneh, "Dynamic modeling of ac iced insulator flashover characteristics" *IEEE Bologna Powertech Conference Proceeding*, Vol. 2, June 2003.

[6]  I. Fofana, M. Farzaneh, "Application of dynamic model to flashover of ice-covered insulators" *IEEE Trans. on Dielectr. And Electr. Insul*, Vol. 14, No. 6, pp. 1410-1417, December 2007.

[7] C. Tavakoli-Zaniani, *Dynamic Modeling of AC Arc Development on Ice Surfaces*, Ph.D. thesis, UQAC, November 2004.

[8] C. O. Laux, T. G. Spence, C. H. Kruger& R. N. Zare "Optical diagnostics of atmospheric pressure air plasmas" , *Plasma Sources Sci. Technol.* No.12, pp.125-138, 2003.

[9] A. Chelouah, E. Marode, G. Hartmann and S. Achat "A new method for temperature evaluation in a nitrogen discharge" *J. Phys. D: Appl. Phys.* No.27, pp.940-945, 1994.

[10] M. Venugopalan, *Reactions under Plasma Conditions*, Vol. 1, Wiley-Interscience 1971.

[11] R.E. Orville, "A high-speed time-resolved spectroscopic study of the lightening return stroke: part II. A quantitative analysis" *J. of Atmospheric Sci.,* Vol. 25, No. 5, pp. 839-851, 1968.

[12] E. E. Kunhardt & L. H. Luessen., *Electrical Breakdown and Discharges in Gases*, Plenum Press, 1981.

[13] CIGRE Task Force 33.04.09, "Influence of ice and snow on the flashover performance of outdoor insulators, part I: Effects of Ice", *Electra*, No. 187, pp. 91-111, Dec. 1999.

[14] M. Kawai, "AC flashover tests at project UHV on ice- coated insulators", *IEEE Transactions on Power Apparatus and Systems*, Vol. PAS-89 , Issue 8, pp. 1800 – 1804, 1970.

[15] H Makkonen, H. Komuro, & K. Takasu, "Withstand voltage characteristics of insulator string covered with snow and ice" *IEEE Transactions on Power Delivery*, Jul 1991, Vol. 6 , Issue 3, pp. 1243- 1250

[16]M. Farzaneh, I. Fofana, "Experimental study and analysis of corona discharge parameters on an ice surface", *Journal of Physics D: Applied Physics*, Vol. 37, No. 5, pp. 721-729, 2004.

[17] I. Ndiaye, M. Farzaneh and I. Fofana, "Study of the Development of Positive Streamers Along an Ice Surface", *IEEE Transactions on Dielectrics and Electrical Insulation*, Special Issue on Ice-Covered Insulators, vol. 14, No. 6, pp. 1436-1445, 2007.

[18] M. Farzaneh & W.A. Chisholm, *Insulators for icing and polluted environments*, IEEE Press series on Power Engineering, IEEE/John Wiley, New York, October 2009.

[19] M.A. Uman, R.E. Orville, "Electron density measurement in lightning from stark-broadening of $H_\alpha$" *Journal of Geophysical Research*, Vol. 96, No. 24, pp. 5151-5154, December 1964.

[20] I Gallimberti, J K Hepworth and R C Klewe, "Spectroscopic investigation of impulse corona discharges", *J. Phys. D: Appl. Phys.* No.7, pp. 880, 1974.

[21] A. A. Fridman, L. A. Kennedy, *Plasma Physics and Engineering*, Taylor & Francis, 2004.

[22] J. L. Delcroix, *Plasma physic*, John Wiley& Sons Ltd, 1965.

[23] J. Inczedy, T. Lengyel, and A.M. Ure, *Compendium on Analytical Nomenclature*, Blackwell Science, 3rd ed 1998.

[24] H. Hegazy, "Oxygen spectral lines for diagnostics of atmospheric laser-induced plasmas", *Applied Physics B: Lasers and Optics*, Vol. 98, No. 2-3 / February, pp. 601-606, 2010.

[25] S. Semenov, B. Cetegen, "Spectroscopic Temperature Measurements in Direct Current Arc Plasma Jets Used in Thermal Spray Processing of Materials" *Journal of Thermal Spray Technology*, Vol. 10(2) pp.326-336, June2001.

[26] H.R. Griem, *Principles of Plasma Spectroscopy*, Cambridge University Press, 1997.

[27] P.W.J.M. Boumans, *Theory of Spectrochemical Excitation*, Hilger& Watts Ltd., London, pp.102-108, 1966.

[28] J. A. C. Broekaert, *Analytical atomic spectrometry with flames and plasmas*, 2nd Ed. Wiley-VCH Verlag GmbH, Weinheim, 2005.

[29] S. Pellerin, J. Koulidiati, O. Motret, M. de Graaf, K. Musiol, B. Pokrzywka & J. Chapelle; "Temperature determination using molecular spectra simulation", *High Temp. Mat. Proc*, No. 1-4 , PP. 493-509, 1997.

[30] S. Pellerin, J.M. Cormier, F. Richard, K. Musioł, J. Chapelle; "A spectroscopic diagnostic method Using UV OH band spectrum", *J. Phys. D*, 1996.

[31] C. O. Laux, R. J. Gessman, C. H. Kruger, F. Roux, F.Michaud and S. P. Davis "Rotational temperature measurements in air and nitrogen plasmas using the first negative system of $N_2^+$" *J. Quant. Spectrosc. Radiat. Transfer* No.68, PP. 473–482, 2001.

[32] C. Parigger, DH. Plemmons, JO. Hornkohl, JWL. Lewis "Temperature measurements from $N_2^+$ first negative spectra produced by laser-induced

multiphoton ionization and optical breakdown of nitrogen" *Applied Optics*, Vol. 34, Issue 18, pp. 3331-3335.

[33] C. Izarra "UV OH spectrum used as a molecular pyrometer" *J. Phys. D: Appl. Phys.* No.33, PP. 1697-1704, 2000.

[34] G. H. Dieke, H. M. Crosswhite "The ultraviolet bands of OH fundamental data" *Journal of Quantitative Spectroscopy and Radiative Transfer*, Vol. 2, Issue 2, PP. 97-199, April-June 1962.

[35] O. Motret, C. Hibert, S. Pellerin and J. M Pouvesle "Rotational temperature measurements in atmospheric pulsed dielectric barrier discharge gas temperature and molecular fraction effects" *J. Phys. D: Appl. Phys.* No. 33 PP. 1493–1498, 2000.

[36] C. O., Laux, "Radiation and Nonequilibrium Collisional-Radiative models" *von Karman Institute Lecture Series 2002-07, Physico-Chemical Modeling of High Enthalpy and Plasma Flows, eds. D. Fletcher, J.-M. Charbonnier, G.S.R. Sarma, and T. Magin, Rhode-Saint-Genèse*, Belgium, 2002.

[37] P.W.J.M. Boumans, *Theory of Spectrochemical Excitation*, Hilger& Watts Ltd., London, pp.102-108, 1966.

[38] N.K. Joshi et al., "Variation of axial temperature in thermal plasma jets", *Journal of Meas. Sci. Technol.* No. 8, pp.1146-1150, 1997.

[39] K. Kano, M. Suzuki, H. Akatsuka, "Spectroscopic measurement of electron temperature and density in argon based on collisional-radiative model" *Journal of Plasma Sources SCi. Technol.* , No. 9, pp.314-322, 2000.

[40] L.L. Burton and M.W. Blades, "A simple method for calculating deviations for local thermodynamic equilibrium in the inductively coupled plasma", *Spectrochim. Acta Part B* No.45, pp. 139–144, 1990.

[41] M.A. Uman, *Lightning*, McGraw-Hill, New York, pp. 156-157, 1984

[42] H.R. Griem, *Spectral line broadening by plasmas*, Academic Press New York and London, pp.282-312, 1974.

[43] M.A. Uman, R.E. Orville, "Electron density measurement in lightning from stark-broadening of $H_\alpha$" *Journal of Geophysical Research*, Vol. 96, No. 24, pp. 5151-5154, December 1964

[44] S.K.Dhali, P.F. Williams, R.J. Crumley and M.A. Gundersen, "Electron densities in Laser-triggered hydrogen spark" *IEEE Trans. On Plasma Science*, Vol. 8, No. 3, pp.164-167, September 1980

[45] R. H. Huddlestone, S. L. Leonard, *Plasma Diagnostic techniques*, Chapter 6, Line broadening by W. L. Wiese, academic press, New York, 1965.

[46] H.R. Griem, *Plasma Spectroscopy*, McGrow -Hill, Inc. 1964.

[47] W. Lochte-Holtgreven, *Plasma Diagnostics*, North Holland (1968), pp. 135–210.

[48] H.R. Griem "Stark Broadening of the Hydrogen Balmer-$\alpha$ Line in. Low and High Density Plasmas" Contributions to Plasma Physics, vol. 40, issue 1-2, pp. 46-56, 2000.

[49] R.E. Orville "Temperature and electron density in long air sparks" *Journal of Applied Physics*, Vol. 38, No. 2, pp. 895-896, February 1967.

[50] Les Renardières Group "Research on long air gap discharges at Les Renardières– 1973 results" *Electra 035*, pp.135-147.

[51] Les Renardières Group "Negative discharges in long air gaps at Les Renardières–1978 results" *Electra 074*, pp.201-212.

[52] Les Renardières Group "Positive discharges in long air gaps at Les Renardières–1975 results and conclusion" *Electra 053*, pp.120-151.

[53] A.Vassy, H.Norinder& E.Vassy, "Étude spectrophotometrique d'étincelles de grande longueur dans l'air". *Compt. rend. Journal*, Vol. 234. *6*:42, pp. 437-50. 1953.

[54] M. A. Uman, R.E. Orville and A.M. Sletten "Four-meter sparks in air" *Journal of Applied Physics*, Vol. 39, No. 11, pp. 5162-5168, October 1968.

[55] D. Staack, B. Farouk, A Fridman, A. Gutsol, "DC normal glow discharges in atmospheric pressure atomic and molecular gases," *Plasma Sources Science & Technology*, vol. 17, No. 2, 2008.

[56]D. Staack, B. Farouk, A. F. Gutsol et al., "Spatially resolved temperature measurements of atmospheric-pressure normal glow microplasmas in air," *IEEE Transactions on Plasma Science*, vol. 35, No. 5, pp. 1448-1455, 2007.

[57]S. Mukasa, S.Nomura, H. Toyota, T. Maehara, F. Abe and A. Kawashima "Temperature distributions of radio-frequency plasma in water by spectroscopic analysis" *Journal of Applied Physics*, Vol. 106, Issue 11, pp. 113302-113302-6 ,2009.

[58] J. Niet-Salazar, N. Bonifaci, A. Denat and O. Lesaint "Characterization and Spectroscopic Study of Positive Streamers in. Water" *Dielectric Liquids. IEEE International* PP. 91-94, July 2005.

[59] X. Zhu et al., "Gas temperature, electron density and electron temperature measurement in a microwave excited microplasma" *J. Phys. D: Appl. Phys.* No. 41, PP. 105212-105218, 2008.

[60] S. Vacquié, *L'arc électrique*, CNRS Editions 2000.

[61] A.*S.* Farghaly, "Calculation of relative oscillator strengths of spectral lines from atomic self-absorption data", *J. Phys. B: Atom. Molec. Phys.*, Vol. 6, July 1973.

[62] F.W.Sears, G.L.Sainger, *Thermodynamics. Kinetic Theory and Statistical Thermodynamics*, 3rd edition, Addison-Wesley Publishing Company, 1975.

[63] A. Shavit, C. Gutfinger, *Thermodynamics: From concepts to applications*, Prentice Hall, 1995.

[64] M. I. Boulos, P. Fauchais, and E. Pfender, *Thermal Plasmas: Fundamentals and Applications*, Vol.1, Plenum, New York, 1994.

[65] M. Mitchner, C.H. Kruger, *Partially Ionized Gases*, Wiley, New York, 1973.

[66] E.M. Bazelyan, Yuri P. Raizer, *Spark Discharge*, CRC Press1998.

[67] P. D. Scholz and T.P . Anderson, "Local thermodynamic equilibrium in an RF argon plasma", *J. Quant . Spectrosc . Radiat . Transfer*, No. 8, 1968.

[68] User manual of TRIAX 320

[69] Z. Machala , M. Janda , K. Hensel , I. Jedlovsky , L. Lestinska , V. Folti et al., "Emission spectroscopy of atmospheric pressure plasmas for bio-medical and environmental applications" *J . Mol Spectrosc*, No. 243, PP. 194–201, 2007.

[70] N. Yoshimura, M. Nishida, and F. Noto "Light emission from tracking discharges on organic insulation *" IEEE Trans. Electr. Insul*, E1-19 No. 2, April 1984.

[71] P. André , J. Ondet , R. Pellet and A. Lefort, "The calculation of monatomic spectral lines' intensities and composition in plasma out of thermal equilibrium; evaluation of thermal disequilibrium in ICP torches", *Journal of Physics D: Applied Physics*, Vol. 30, No. 14, pp. 2043-2055, 1997.

[72] D. Vacher, G. Faure and P. Andre, "Thermodynamic considerations and optical emission diagnostics of a N2/O2 mixture in an inductively coupled air plasma" *Spectrochimica Acta Part B: Atomic Spectroscopy*, Volume 56, Issue 3, 29 March 2001, Pages 309-330

[73] T. Namihira, S. Sakai, M. Matsuda, D. Wang , T. Kiyan , H. Akiyama , K. Okamoto and K. Toda "Temperature and Nitric Oxide Generation in a Pulsed Arc Discharge Plasma", *Plasma Science and Technology*, Vol. 9, No. 6, pp. 747-751.2007.

[74] NIST Atomic Spectra Database. Lines Data, http://physics.nist.gov/cgi-bin/AtData/main-asd

[75] A. NEKAHI & M. FARZANEH, "Electron density measurement of Dc+ arc propagating over an ice surface based on Hα line" *IEEE Transactions on Plasma Science*, vol. 39, no. 4, pp. 1120-1124, 2011.

[76] D. Comtois et al. "Triggering and guiding leader discharges using a plasma channel created by an ultrashort laser pulse" *Applied Physics Letters*, Vol. 76, No. 7, pp.819-821, Feb. 14, 2000.

[77] K. Chrzan "Conductivity of aqueous solutions", *IEEE Transactions on Electrical Insulation* Vol. EI-22 No.3, pp. 241-244, June 1987.

[78] P. Lukeš, M. Člupek , V. Babický , M. Šimek , I. Tothová , V. Janda , T. Moucha, M. Kordač "Role of solution conductivity in the electron impact dissociation of H2O induced by plasma processes in the pulsed corona discharge in water" Proceedings, 19th International Symposium on Plasma Chemistry. Bochum: Wiley-VCH Verlag GmbH & Co. KGaA, 2009

[79] A. N. Srivastava and R. V. Shukla, "Excitation rate of sodium D line in the nightglow", *Astrophysics and Space Science,* Vol. 8, No. 1, PP. 136-139,1970.

[80] K. Fukui, I. Fujita, K. Kuwata, "Formation of the NH ($A^3\Pi$, $C^1\Pi$) radicals by electron impact near threshold", *J. Phys. Chem.*, No. 81 , pp. 1252–1257, 1977.

[81] W.R. Pyle, M.H. Hayes, A.L. Spivak "Direct solar-thermal hydrogen production from water using nozzle/skimmer and glow discharge", *IECEC 96.* Vol. 3, pp. 1753 – 1760, PP. 11-16 Aug 1996.

[82] M. Ishii, H. Ohashi, "Polarity effect in DC withstand voltages of contaminated surfaces", *IEEE Transactions on Electrical Insulation*, Vol. 23 Issue 6, pp. 1033 – 1042, 1988.

[83] M. Farzaneh & J. Zhang, "Modeling of DC Arc Discharge on Ice Surfaces". *IEE Proceedings - Generation, Transmission and Distribution*, Vol. 147, No. 2, pp. 81-86, 2000

[84] J. Zhang & M. Farzaneh, "Computation of AC Critical Flashover Voltage of Insulators Covered with Ice". International Conference on Power System Technology, Beijing, China, Vol. 1, pp. 524-528, 1998.

[85] A. Nekahi and M. Farzaneh, "Excitation temperature determination of an arc formed over an ice surface using optical emission spectroscopy", *IEEE Transaction on Dielectrics and Electrical Insulation*, (submitted).

[86] G. E. Thomas and K. Stamnes, *Radiative Transfer in the Atmosphere and Ocean*, Cambridge University Press, New York, 1999.

[87] H. Haken, H. C. Wolf, *The Physics of Atoms and Quanta*, 5th Ed., Springer-Verlag, 1996.

[88] IEEE Standard 1584-2002 (IEEE Guide for Performing Arc Flash Hazard Calculations)

[89] NFPA 70E: Standard for Electrical Safety in the Workplace

[90] Occupational Safety and Health Administration (OSHA), Standards - 29 CFR, Part 1910.